ESPOO 2004 VTT PUBLICATIONS 551

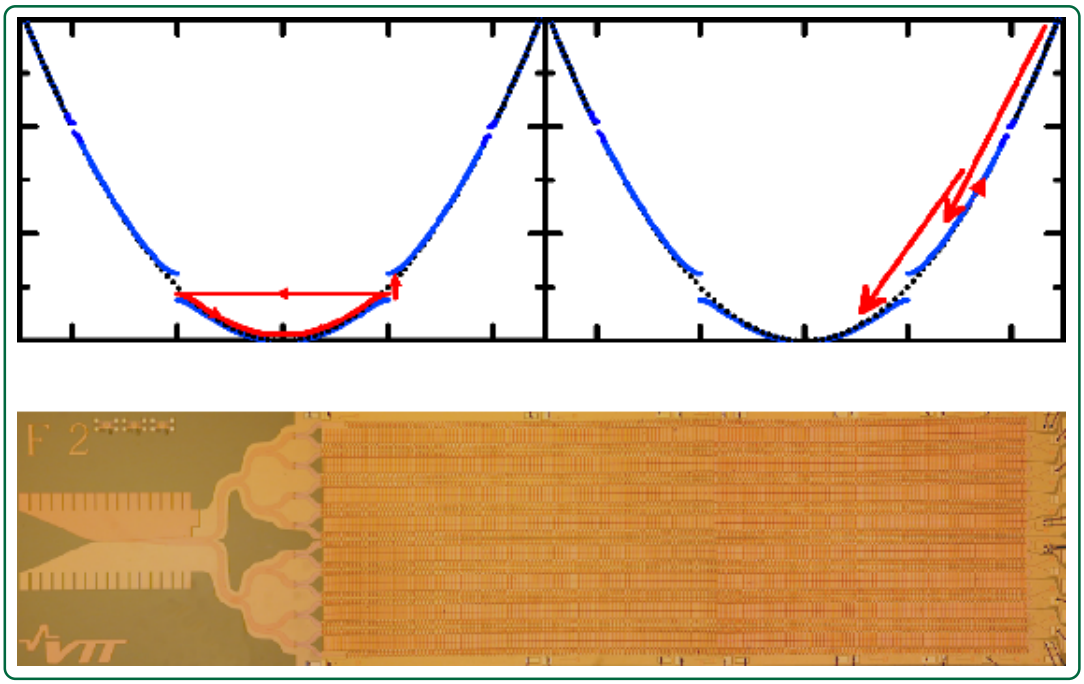

Juha Hassel

Josephson junctions in charge and phase picture

Theory and applications

VTT PUBLICATIONS 551

Josephson junctions in charge and phase picture
Theory and applications

Juha Hassel

VTT Information Technology

Dissertation for the degree of Doctor of Science in Technology to be presented with due permission of the Department of Engineering Physics and Mathematics for public examination and debate in Large Seminar Hall of Micronova at Helsinki University of Technology (Espoo, Finland) on the 9th of November, 2004, at 12 o'clock noon.

ISBN 951–38–6418–9 (soft back ed.)
ISSN 1235–0621 (soft back ed.)

ISBN 951–38–6419–7 (URL: http://www.vtt.fi/inf/pdf/)
ISSN 1455–0849 (URL: http://www.vtt.fi/inf/pdf/)

JULKAISIJA – UTGIVARE – PUBLISHER

VTT, Vuorimiehentie 5, PL 2000, 02044 VTT
puh. vaihde (09) 4561, faksi (09) 456 4374

VTT, Bergsmansvägen 5, PB 2000, 02044 VTT
tel. växel (09) 4561, fax (09) 456 4374

VTT Technical Research Centre of Finland, Vuorimiehentie 5, P.O.Box 2000, FIN–02044 VTT, Finland
phone internat. + 358 9 4561, fax + 358 9 456 4374

VTT Tietotekniikka, Tietotie 3, PL 1207, 02044 VTT
puh. vaihde (09) 4561, faksi (09) 456 7012

VTT Informationsteknik, Datavägen 3, PB 1207, 02044 VTT
tel. växel (09) 4561, fax (09) 456 7012

VTT Information Technology, Tietotie 3, P.O.Box 1207, FIN–02044 VTT, Finland
phone internat. + 358 9 4561, fax + 358 9 456 7012

Technical editing Maini Manninen

Otamedia Oy, Espoo 2004

Hassel, Juha. Josephson junctions in charge and phase picture. Theory and applications. Espoo 2004. VTT Publications 551. 38 p. + app. 40 p.

Keywords Josephson junctions, quantum metrology, mesoscopic tunnel junctions

Abstract

Properties of weak links between two superconductors, or Josephson junctions, make them interesting for fundamental physics research. Since their discovery over four decades ago, they have provided a unique way to study the behavior of the superconducting quantum phase. More recently, ultra small, or mesoscopic, Josephson junctions with substantial single Cooper pair charging energy have gained interest due to their behavior as macroscopic quantum objects.

In addition to the theoretical interest, Josephson junctions can be used as active elements in circuit applications. Particularly, in this Thesis we study two different devices. We develop the required theoretical treatments, derive device properties, and compare the results with experimental data.

The first application is a Josephson voltage standard based on externally damped Superconductor - Insulator - Superconductor junctions. It consists of an array of large Josephson junctions connected in series and irradiated with a 70 GHz microwave signal. Phase locking the Josephson dynamics into the signal leads to the quantization of the voltage. This is utilized in metrology. We introduce a new circuit solution based on frequency dependent damping of the junctions. Optimization and some designs for practical arrays are presented. The purpose is to find such a design that the array is fast, has low power consumption and is as stable as possible. Arrays able to generate DC voltages of order 1 volt with metrological accuracy are demonstrated experimentally and their applicability in AC voltage calibrations is analyzed.

The second application is the Bloch Oscillating Transistor (BOT). The BOT is based on controlling the Cooper pair current in an ultra small Josephson junction by means of quasiparticles tunneling through a normal junction. As part of the thesis work, the principle of operation is first demonstrated computationally. The model is then refined to yield quantitative predictions of the characteristics. Finally, an analytic theory for the device is developed and the properties as an amplifier are derived.

Preface

The research work has been done as a part of the research projects in the Quantronics group and its predecessors at VTT Information Technology and VTT Automation over a time span of about five years. The work has been done in close collaboration with the co-workers. The collaboration with the Low Temperature Laboratory of Helsinki University of Technology, the VTT Microelectronics Centre and the Centre for Metrology and Accreditation (MIKES) has been especially valuable.

First of all, I wish to thank my instructor Prof. Heikki Seppä, whose inexhaustible ideas are mostly behind the work reported here. I also would like to thank the manager of the Quantronics group, Dr. Panu Helistö, whose advice and encouragement has been invaluable. Furthermore, I wish to thank my supervisor, Prof. Pekka Hautojärvi, who has been very helpful about organizing the things with the university.

I have also grately benefited from the help and discussions with our group members, Mikko Kiviranta, Arttu Luukanen, Antti Niskanen, Jari Penttilä, Hannu Sipola and Antti Virtanen. Also all the people working in the Microsensing research field have shown to be very helpful and entertaining to work with. I would especially like to thank Kaisa Falenius, Aija Kaski, Seija Lepistö, Elisa Pylvänäinen and Mia Sarvi for keeping the things running.

The contribution of our collaborators has been very important. The work of Leif Grönberg, Ilkka Suni and Markku Ylilammi in the JVS fabrication has been irreplacable. Jaani Nissilä's, Antti Kemppinen's and Kari Ojasalo's work at MIKES on further development of the JVS setup has also been of crucial value. Experimentalists at the Low Temperature Laboratory, Julien Delahaye, Rene Lindell, Mika Sillanpää, Prof. Pertti Hakonen and Prof. Mikko Paalanen, have made a crucial part of the work related to the BOT.

Finally, I would like to thank my parents for the support during the years.

List of publications

This Thesis is based on the following original publications:

Josephson voltage standard

P1. Hassel, J., Seppä, H., Grönberg, L. and Suni, I. 2001. SIS Junctions with Frequency Dependent Damping for a Programmable Josephson Voltage Standard. IEEE Trans. Instrum. Meas Vol. 50, No. 2, pp. 195–198.

P2. Hassel, J., Seppä, H., Grönberg, L. and Suni, I. 2003. Optimization of a Josephson Voltage Array Based on Frequency Dependently Damped Superconductor - Insulator - Superconductor Junctions. Rev. Sci. Instrum. Vol. 74, No. 7, pp. 3510–3515.

P3. Hassel, J., Grönberg, L., Helistö, P, Seppä, H., Nissilä, J. and Kemppinen, A. 2004. Fast Josephson Arrays for Voltage and Impedance Metrology. Conference of Precision Electromagnetic Measurements. London, 27 June – 2 July 2004, Conference Digest, pp. 154–155.

Bloch oscillating transistor

P4. Hassel, J. and Seppä, H. 2001. Analysis of the Bloch Oscillating Transistor. IEEE Trans. Appl. Supercond. Vol. 11, No. 1, pp. 260–262.

P5. Delahaye, J, Hassel, J., Lindell, Sillanpää R., Paalanen, M. Seppä. H. and Hakonen, P. 2003. Low-Noise Current Amplifier Based On Mesoscopic Josephson Junction. Science, Vol. 299, pp. 1045–1048.

P6. Hassel, J. Seppä, H., Delahaye, J. and Hakonen, P. 2004. Control of Coulomb Blockade in a Mesoscopic Josephson Junction Using Single Electron Tunneling. J. Appl. Phys. Vol. 95, No. 12, pp. 8059–8062.

P7. Hassel, J. and Seppä. H. Theory of the Bloch Oscillating Transistor. Submitted for publication.

The author's own contribution

In publications P1–P3 I did most of the modelling and design work for the devices as well as carried out most of the low-temperature experiments. In publications P4–P7 I took part in testing the ideas about the new device as well as largely did the simulations and the theoretical work to characterize its properties. Publications P1–P4 and P6–P7 are to a large part written by myself. I also participated in the writing process of publication P5.

Table of contents

1. Introduction

Brian Josephson showed theoretically in 1962 that two weakly coupled superconductors can exhibit peculiar phenomena related to Cooper pairs tunneling through the link [1]. He predicted that with a constant voltage V applied across such a link, which was later named Josephson junction (JJ), the current through the junction oscillates with frequency $2eV/h$. He also predicted that a current can flow through the junction without a voltage drop, if the current is smaller than a "critical current". These effects are manifestations of the dynamics of the quantum phase difference Φ across the junction.

Since then, theoretical, experimental and technological understanding on Josephson phenomena and their applications has increased substantially. Especially the development of reliable fabrication techniques has made it possible to create applications for a variety of purposes. These include sensors for magnetic fields, amplifiers, passive and active components for RF and millimeter wave technology, etc. (for an overview see e.g. [2]).

More recently, a new class of phenomena was discovered in small junctions, in which the charging energy of a single charge carrier (a Cooper pair) is comparable to other energy scales in the system [3, 4]. This includes the blockade of charge flow at small voltages (the Coulomb blockade) as well as novel coherent charge oscillations called the Bloch oscillations.

In this Thesis, we first give a brief review of the physics of Josephson junctions starting from the phenomenological description as a single quantum object. Models in the limit of large and mesoscopic junctions are derived. Then they are applied to the devices under study. Finally, theoretical and experimental results from the devices are presented.

2. Physics of Josephson junctions

A. General

The Josephson junction is a macroscopic quantum object described by Hamiltonian [3]

$$H = \frac{Q^2}{2C} - \left(\frac{\Phi_0}{2\pi} I(t)\,\Phi + E_J \cos(\Phi) \right) + H_q, \tag{1}$$

where the first term is the capacitive charging energy, second term is the interaction with an external current source $I(t)$, third term is the Josephson coupling and fourth term is the interaction with the quasiparticle system and the electromagnetic environment. Here Q is the charge operator, C is the junction capacitance, and E_J is the Josephson coupling energy. The superconducting flux quantum is $\Phi_0 = h/2e \approx 2.07 \times 10^{-15}$ Vs. A schematic circuit diagram of a JJ is shown in Fig. 1(a). The cross symbolizes Josephson coupling, the capacitor the capacitive coupling and $\overline{Z}(\omega)$ the electromagnetic environment. The current $I(t)$ is also shown.

The operators for charge Q and phase Φ satisfy the following commutation relation:

$$[\Phi, Q] = 2ei, \tag{2}$$

i.e. they are bound by the Heisenberg uncertainty relation. The charge operator can be written in terms of phase as

$$Q = \frac{2e}{i} \frac{\partial}{\partial \Phi}. \tag{3}$$

From Eqs. (1)-(3) one can draw an analogy to a particle moving in a sinusoidal potential shown in Fig. 1(b). Mathematically this "washboard potential" $U(\Phi, t)$ is given as

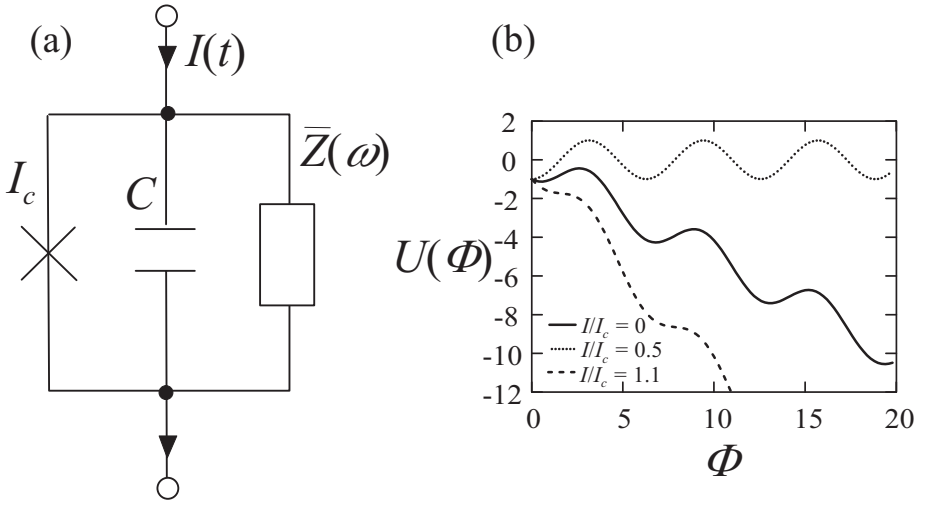

Figure 1. (a) The circuit diagram of a Josephson junction connected parallel to an impedance $\overline{Z}(\omega)$. (b) Washboard potential $U(\Phi)$ as function of the quantum phase difference Φ.

$$U(\Phi,t) = -E_J\left(\frac{I(t)}{I_c}\Phi + \cos\Phi\right), \tag{4}$$

where I_c is the critical current of the junction. The position of the "particle" corresponds to phase difference Φ, and momentum to charge Q. Tilting of the potential depends on $I(t)$, while the amplitude of the "bumps" is E_J. The dissipation of the particle is included in H_q. The Josephson coupling energy is related to the critical current as

$$E_J = \frac{\Phi_0 I_c}{2\pi}. \tag{5}$$

B. Large Josephson junctions

Here we consider the limit, where both the phase Φ and the charge Q are assumed to be classical variables. This is the case, if the quantum energies $\hbar\omega$ of all frequencies ω present in the system are small compared to E_J and the thermal energy k_BT as explained below [5]. Assuming the Hamiltonian in Eq. (1) to be classical and solving the equations of motion $\partial H/\partial Q = (\Phi_0/2\pi)(\partial\Phi/\partial t)$ and $(2\pi/\Phi_0)(\partial H/\partial\Phi) = -\partial Q/\partial t$ one obtains

$$V = \frac{\Phi_0}{2\pi}\frac{\partial\Phi}{\partial t} \tag{6}$$

$$I(t) = C\frac{\partial V}{\partial t} + I_S(t) + I_c\sin\Phi, \tag{7}$$

where we have defined voltage across the junction $V = Q/C$ and marked $I_S(t) = \partial H_q/\partial\Phi$ ("the shunt current"). The displacement current due to junction capacitance is the first term on the right hand side of Eq. (7). The quasiparticle tunnel current as well as the current through circuit elements connected parallel to the junction ($\overline{Z}(\omega)$ in Fig. 1) are accounted for by the second term. In case of externally damped junctions (see Section III), the quasiparticle tunnel current is usually small and it thus can be neglected. If the circuit connected parallel to the junction is linear, I_S is obtained from the linear circuit theory. In general, it includes both a deterministic part and a fluctuation associated with the real part of $\overline{Z}(\omega)$. The Cooper pair tunnel current through the JJ is the third term.

In the simplest case the junction is damped with a linear resistor, i.e. $Z(\omega) = R$, and thus $I_S = V/R + I_n$, where I_n is a random variable, whose spectral density satisfies the Nyquist formula $\langle I_n^2\rangle = 4kT/R$ [6]. Then Eqs. (6) and (7) can be written as

$$\beta_c\frac{d^2\Phi}{d\tau^2} + \frac{d\Phi}{d\tau} + \sin\Phi = i(\tau) + i_n(\tau). \tag{8}$$

This is called the resistively and capacitively shunted junction (RCSJ) model for a Josephson junction. Here the dimensionless time $\tau = (2\pi I_cR/\Phi_0)t$ and the dimensionless current $i(\tau) = I(t)/I_c$. The hysteresis parameter is defined as $\beta_c = \left(2\pi I_cR^2C\right)/\Phi_0$.

To study the range of the applicability of the model, we will first note that an important characteristic frequency of a junction is the plasma frequency f_p, i.e. the frequency of the oscillation within a minimum in the washboard potential. From the circuit picture of Fig. 1(a) this can also be interpreted as the L_JC oscillation in the junction capacitance and the Josephson inductance L_J. For small bias currents and phase variations the linearized tunnel element behaves as an inductance $L_J = \Phi_0/2\pi I_c$. The angular plasma frequency $\omega_p = 1/\sqrt{L_JC}$ can then be written as

$$\omega_p = \sqrt{\frac{2\pi}{\Phi_0}\frac{I_c}{C}}. \tag{9}$$

Using the definition of E_J in Eq. (5) and defining the single electron charging energy

$$E_C = \frac{e^2}{2C}, \tag{10}$$

the energy levels of the plasma oscillation can be written as

$$E_p = \hbar\omega_p\left(N + \frac{1}{2}\right) = \sqrt{8E_JE_C}\left(N + \frac{1}{2}\right) \tag{11}$$

with N as an integer. A sufficient requirement for the classical approximation to hold is that the spacing of the levels $\Delta E_p = \sqrt{8E_JE_c}$ is small compared to E_J and k_BT i.e.

$$\frac{E_J}{E_C} \gg 8 \tag{12}$$

$$\frac{(kT)^2}{E_CE_J} \gg 8. \tag{13}$$

Typical tunnel junction fabrication techniques (see e.g. Section III) produce junctions with critical current densities J_c above 10^5 A/m^2 and specific capacitance $C_s \approx 0.05$ F/m^2. For junctions having dimensions above 1 μm this leads to $E_J/E_C \gtrsim 100$. If measurements are performed at the liquid helium temperature, $T = 4.2$ K, then $(k_BT)^2/E_CE_J \gtrsim 400$.

In principle, also other frequencies present at the system (driving signals, characteristic frequencies of the system consisting of the junction and the rest of the circuit) should be studied to prove the applicability of the model. However, these are typically not substantially above f_p. Thus the treatment above is sufficient to state that devices fabricated with optical litography and measured at liquid He can be handled classically. As the temperature is lowered, it is sometimes necessary to apply quantum corrections, especially if the fluctuations of the system are studied [7].

C. Ultrasmall junctions

With electron beam litography one can fabricate junctions having lateral dimensions from 10 nm to 100 nm. In this case the condition of Eq. (12) fails. With cooling techniques such as dilution

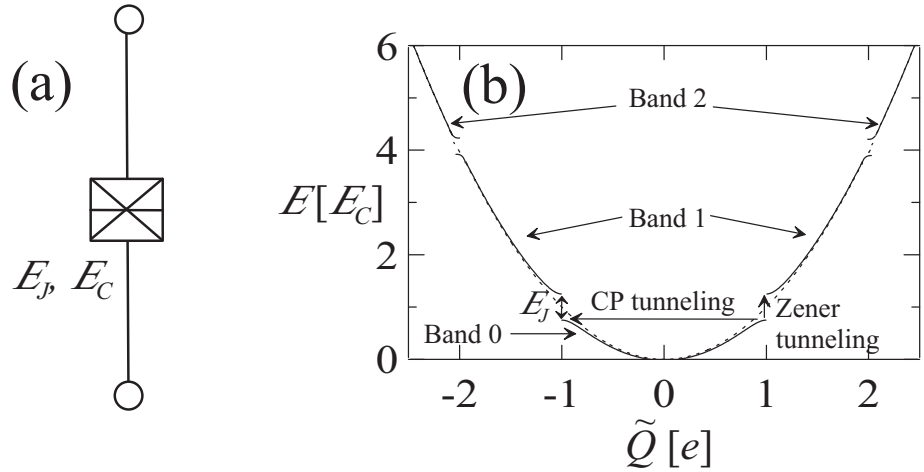

Figure 2. (a) The drawing symbol of a mesoscopic Josephson junction and (b) the band diagram in the "weak binding limit". Possible transitions, i.e. Cooper pair tunneling and Zener tunneling, are indicated with arrows.

refrigeration or adiabatic demagnetization, temperatures below 100 mK can be reached. In this case also the condition of Eq. (13) fails.

To understand the dynamics of ultra small junctions, we will again start from the Hamiltonian in Eq. (1), but assume that $E_J \lesssim E_C$ and $E_J, E_C \gg kT$. The drawing symbol for a mesoscopic junction is shown in Fig. 2(a). We will further assume that the bias source and the environment are small perturbations in the system [3]. For the unperturbed Hamiltonian (using appropriate terms in Eq. (1) and Eq. (3)) we get

$$H_0 = -\left(E_C \frac{\partial^2}{\partial \left(\Phi/2\right)^2} + E_J \cos\Phi\right). \tag{14}$$

Physically, the difference as compared to the previous section is, that the state of the junction can no longer be described with a single value of Φ. Overlap of wavefunctions corresponding to different minima in the washboard potential cause splitting of energy levels. In the infinite periodic potential this leads to formation of energy bands. This is in analogy to an electron in a solid-state crystal, where the periodic lattice forms the potential [8].

The time-independent Schrödinger equation $H_0\Psi = E\Psi$ is in this case mathematically a Mathieu differential equation. The energy eigenvalues are best represented in the basis of "quasicharge" $\widetilde{Q}$, a quantity analogous to crystal momentum in solid-state systems. In Fig. 2(b) we show the band structure in the limit $E_J \ll E_C$, the so-called weak-binding limit. In this Thesis we are using the extended band picture, where the lowest band is represented by $\left|\widetilde{Q}\right| < e$, the second band with $e < \left|\widetilde{Q}\right| < 2e$, etc. The voltage across the junction is given as

$$V = \frac{\partial E}{\partial \widetilde{Q}}, \tag{15}$$

and the expectation value of real charge is $Q = CV$. Thus the quasicharge $\widetilde{Q}$ agrees with Q at the

points, where the dashed parabola $E = \widetilde{Q}^2/2C$ coincides with the solid lines in Fig. 2(b). At $\widetilde{Q} = ne$ (with n an integer) the expectation value of Q is zero.

To understand the junction dynamics, let us first assume that the junction is initially at the lowest energy band at $\widetilde{Q} = 0$, and the junction is connected to an ideal constant current source with $I(t) = I_0$. If $I_0 \ll I_z \equiv \pi e E_J^2/8\hbar E_C$ (the criterion for adiabaticity), the quasicharge will increase up to $\widetilde{Q} = e$, return to $\widetilde{Q} = -e$ and finally back to $\widetilde{Q} = 0$. Repeating this cycle leads to coherent charge oscillation, i.e. the Bloch oscillation. The physical interpretation is that at $\widetilde{Q} = e$ a Cooper pair tunnels through the junction.

If I_0 is comparable to I_z, the criterion for adiabaticity is violated. Then interband tunneling at $\widetilde{Q} = ne$ (the Zener tunneling) becomes possible. The probability from band $n-1$ to band n is given as [9, 10]

$$P_{n-1 \rightleftharpoons n}^{Z} \approx \exp\left(-\frac{\pi}{8}\frac{1}{n^{2n-1}}\left(\frac{E_J}{E_C}\right)^{2n}\frac{eE_C}{\hbar I_0}\right). \tag{16}$$

In a realistic situation there are also mechanisms through which the system can return down to lower bands [11]. A way to provide controlled downwards relaxation is discussed in Section IV.

D. Electromagnetic environment

In this section we discuss the effect of ohmic dissipation for Cooper pair tunneling in mesoscopic Josephson junctions. We will be considering the circuit in Fig. 3(a), i.e. a junction voltage biased across a resistor R. We will now express the Hamiltonian of Eq. (1) as

$$H = H_J + H_{\text{env}}, \tag{17}$$

where H_J now represents the Josephson coupling and H_{env} now includes the contribution of both the capacitance of the junction as well as the circuit $\overline{Z}(\omega)$ parallel to the junction. In this case it is simply the resistor R. The environmental Hamiltonian can be represented as an infinite number of harmonic oscillators [12]. Josephson coupling H_J is now considered as a perturbation in the system. The tunneling through the junction is calculated by using the Fermi golden rule [13, 14, 15], where the rate between initial and final states ($|R>$ and $|R'>$, respectively) is given as $\Gamma_{R\rightarrow R'} = (2\pi/\hbar)\left|\langle R'|H_J|R\rangle\right|^2 \delta(E_R - E'_R)$, where $\langle R'|H_J|R\rangle$ is the matrix element describing the transition, and E_R and E'_R are the energies corresponding to initial and final states. We get the total rate by summing over all possible initial and final states, i.e.

$$\Gamma(V) = \frac{2\pi}{\hbar}\sum_{R,R'}\left|\langle R'|H_J|R\rangle\right|^2 P_\beta(R)\,\delta\left(E_R - E'_R\right), \tag{18}$$

where $P_\beta(R)$ is the probability of finding the system initially at state R. By assuming that the environment is at thermal equilibrium (i.e. that $P_\beta(R) = \langle R|\rho_B|R\rangle$, where ρ_B is the equilibrium density matrix), it can be shown that [15]

$$\Gamma(V) = \frac{\pi E_J^2}{2\hbar} P'(2eV), \tag{19}$$

where the direction of tunneling is taken towards positive voltage in Fig. 3(a). The rate to the opposite direction is obtained by reversing the bias voltage. The function $P'(E)$ is given as

$$P'(E) = \frac{1}{2\pi\hbar} \int_{-\infty}^{\infty} dt \exp\left[J(t) + \frac{i}{\hbar} Et\right]. \tag{20}$$

Here $J(t) = \langle [\Phi(t) - \Phi(0)] |\Phi(0)\rangle$ is the phase-correlation function. It can be shown to be [15]

$$J(t) = 2 \int_0^{\infty} \frac{d\omega}{\omega} \frac{R/R_Q}{1 + (\omega RC)^2} \left[\coth\left(\frac{1}{2}\frac{\hbar\omega}{k_B T}\right)(\cos(\omega t) - 1) - i\sin(\omega t)\right], \tag{21}$$

where $R_Q = h/4e^2$ is the quantum resistance for Cooper pairs.

If the charge relaxation time RC in the circuit of Fig. 3(a) is small compared to the average time between consecutive tunneling events, a current-voltage curve is simply $I(V) = 2e(\Gamma(V) - \Gamma(-V))$. However, in many cases this is not the situation. In this Thesis we have adopted an approach, where we integrate the charge across junction electrodes as function of time from

$$\frac{dQ}{dt} = \frac{1}{R}\left(V - \frac{Q}{C}\right) + \left(\frac{dQ}{dt}\right)_{CP}, \tag{22}$$

where the first term is the current through R. Here we have assumed that the voltage across the junction is Q/C. It is equivalent to assume that the quasicharge is the real charge at all times (see Eq. 15). This is approximately true in the limit of small E_J/E_C, where the junction energy roughly follows the parabolic dependence at almost all values of quasicharge (see Fig. 2(b)). The second term changes the charge by $2e$ every time a Cooper pair tunnels through the junction. The corresponding time dependent tunneling rate is obtained from Eq. (19) by setting $V = Q/C$.

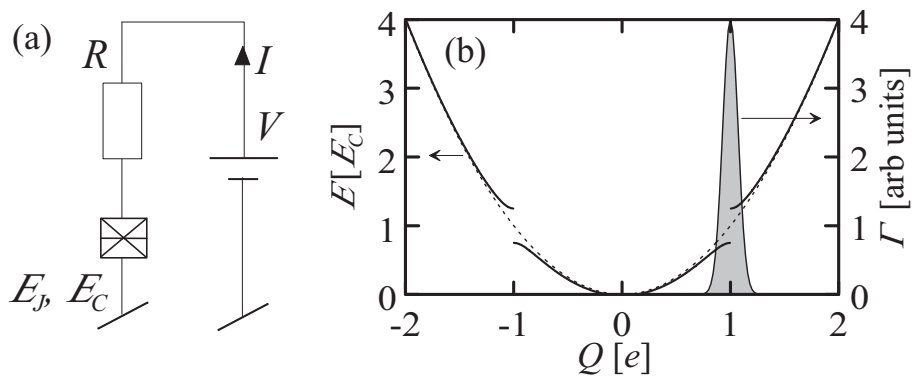

Figure 3. (a) A mesoscopic Josephson junction voltage biased across resistance R. (b) The peaked tunneling probability for large R shown on top of the band diagram.

It is useful to discuss the relation between the band model derived in the previous section and the model derived here. In the limit of large impedance ($R/R_Q \gg E_C/kT$), function $P'(E)$ can be calculated analytically, and stands

$$P'(E) = \frac{1}{\sqrt{16\pi kTE_C}} \exp\left(-\frac{E_C}{16kT}\left(\frac{E}{E_C} - 4\right)^2\right), \tag{23}$$

i.e. it is a Gaussian distribution centered at $E = 4E_C$. The width is determined by the thermal energy kT. The tunneling rate from Eqs. (19) and (23) is shown in Fig. 3(b). It is peaked at $Q = e$. If the bias voltage is set to $V \gtrsim e/C$, the charge relaxes towards $Q = CV$. As the state passes through $Q \approx e$ it is likely that a Cooper pair tunnels through the junction returning the state back to $Q \approx -e$. We have thus recovered the picture of Bloch oscillations by interpreting $|Q| \lesssim e$ as the lowest band. The difference is that now the Cooper pairs do not tunnel strictly at $Q = e$, which is due to fluctuations of R. The oscillations are no longer strictly coherent, but have a finite bandwidth.

If we further simplify Eq. (23) by assuming that $E_C/kT \gg 1$ and use Eq. (19) we get

$$\Gamma'(Q) = \frac{\pi e E_J^2}{8\hbar E_C}\delta(Q - e) \tag{24}$$

by expressing the rate in terms of charge (i.e. $\Gamma(V) = \Gamma'(Q)$). During a period of Bloch oscillations the tunneling rate is thus $\Gamma = \left(\pi e E_J^2/8\hbar E_C\right)/\Delta Q$ for a very short time Δt, i.e. while $e - \Delta Q/2 < Q < e + \Delta Q/2$. If the current at $Q = e$ is I_0, we can write $\Delta Q = I_0 \Delta t$, so $\Gamma = \left(\pi e E_J^2/8\hbar E_C I_0\right)/\Delta t$. The probability distribution of tunneling is exponential $\Gamma \exp(-\Gamma t)$. The total probability of Cooper pair tunneling during the period is thus

$$P_{CP} = \int_0^{\Delta t} \Gamma \exp(-\Gamma t)\, dt = 1 - \exp\left(-\frac{\pi}{8}\left(\frac{E_J}{E_C}\right)^2 \frac{eE_C}{\hbar I_0}\right). \tag{25}$$

Zener tunneling is complementary to Cooper pair tunneling, i.e. $P^Z_{0\rightleftharpoons 1} = 1 - P_{CP}$. Thus, for the two lowest bands ($n = 1$) the result of Eq. (16) is recovered. Cooper pair tunneling at upper bands is not included. This is justified for small E_J/E_C, since $P^Z_{n-1\rightleftharpoons n}$ is very close to unity for $n > 1$.

In conclusion, for large resistances R, low temperatures, and small Josephson coupling the dynamic model derived in this section is equivalent to the band model of the previous section. As an extension it takes into account environmental fluctuations due to R.

3. Josephson voltage standards

A. Background

In the original article by Josephson [1] it was predicted that a junction, when irradiated by microwaves having frequency f (the pump frequency), would exhibit a constant average voltage

$$V_{ave} = n \times f/K_J \tag{26}$$

over a range of DC bias currents determined by the amplitude of the irradiation. Here n is an integer and $K_J = 2e/h \approx 4.83 \times 10^5$ GHz/V is the Josephson constant.

The phenomenon is understood in terms of phase locking the Josephson oscillation with the external microwave signal. In reference to the dynamical model in Section IIB and Fig. 1(b) the phase-locking corresponds to a situation, where the washboard potential is periodically tilted with frequency f. If the bias parameters and the parameters of the junction are properly selected, the phase advances exactly $2\pi n$ during one microwave period $1/f$. From Eq. (6) this leads to average voltage

$$V_{ave} = \frac{1}{1/f}\int_0^{1/f} \frac{\Phi_0}{2\pi}\frac{d\Phi}{dt}dt = f\int_0^{2\pi n}\frac{\Phi_0}{2\pi}d\Phi, \tag{27}$$

which reproduces Eq. (26). Solutions of dynamic equations (Eqs. (6) and (7)) of this type are called harmonic. Other possible solutions are subharmonic, where during m microwave periods the phase advances $2\pi n$, i.e. $V_{ave} = (n/m)\, f/K_J$, or chaotic, where the dynamics is completely aperiodic. The conditions for harmonic phase locking are widely studied theoretically in case of the simple resistively shunted junction [6],[16]-[19]. In section IIIB we will study the conditions for the circuit of another realization.

Constant voltage steps were first experimentally measured by Shapiro in 1963 [20]. In 1967 Parker et. al. measured the value of K_J with uncertainty of about 6 parts per million (ppm) using many different types of weak links [21]. The largest source of error was the inaccuracy of the realization of the absolute volt at the time. Within the measurement uncertainty of the experiment (2 ppm) the values of K_J were reproduced for both superconductor-oxide-superconductor and point contact weak links fabricated from various materials. This suggests that the frequency-to-voltage conversion is highly independent on the experimental details. Therefore the phenomenon has been adopted to use in metrology, and today the Josephson voltage is the most commonly used practical realization of the volt.

The problem with a single junction is the low voltage it produces at realistic frequencies. This causes several problems. It is difficult to calibrate out possible error voltages, e.g. thermal voltages in the measurement leads. Practical calibrations are also often done at 1 - 10 V level, and the required voltage dividers cause additional uncertainty. For a single junction voltage standard together with a divider calibrated by means of a cryogenic current comparator the relative uncertainty at 1 V level has been brought down to 10^{-8} [22].

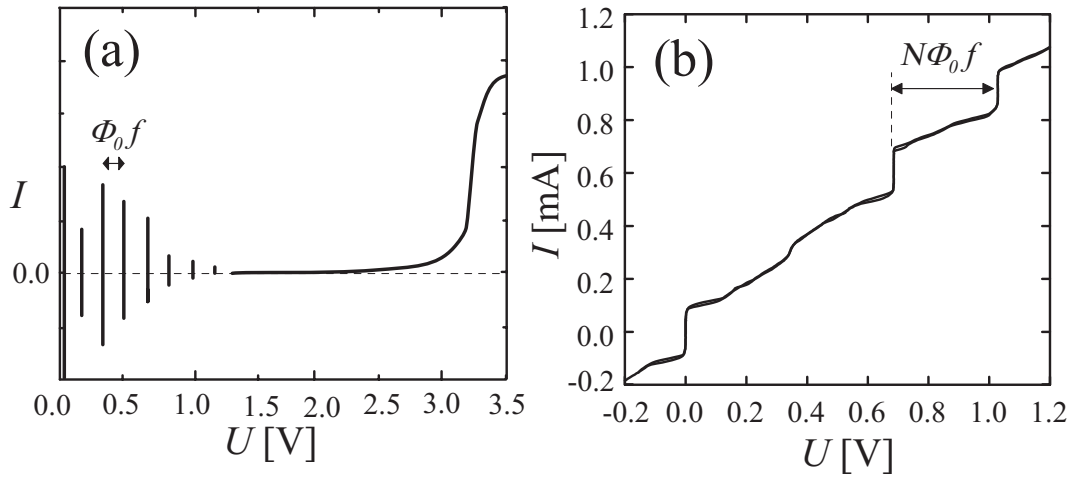

Figure 4. (a) A schematic IV curve of a conventional Josephson voltage standard irradiated with frequency f. The spacing of different voltage levels is exaggerated for clarity. (b) A measured IV curve from a VTT programmable Josephson standard.

The development of junction fabrication techniques has made it possible to increase the voltage by connecting several junctions in series. Today practical 1 - 10 V DC references are based on arrays of typically 2000 - 20000 series connected junctions irradiated with $f \approx 70$ GHz [23]-[25]. Thus they directly produce the required output voltage. The junctions are undamped superconductor - insulator - superconductor (SIS) junctions. An IV curve of an undamped Josephson array under microwave irradiation is schematically shown in Fig. 4(a). It is highly hysteretic, since for high quality junctinons the subgap leakage resistance is very high. This increases the hysteresis parameter β_c (see Eq. 8). The quantized voltage across the junction can exist without DC bias current. The steps are thus called zero-crossing steps.

The zero-crossing steps have some advantages. The absence of bias current makes the output voltage insensitive to possible additional series resistance. In case of arrays it also alleviates the fabrication criteria, since the variation of damping resistance does not cause problems. They have some disadvantages as well. They are very sensitive to environmental interference. The output voltage is not a single-valued function of bias parameters, but rather depends on the initial conditions of the dynamic equations (Eq. (8)). Therefore the interference can cause transitions between different voltage steps making the requirement of electromagnetic shielding strict. Low damping also makes the selection of the desired output voltage slow and tricky, which makes it more difficult to automate measurements. It also prevents the direct use of the Josephson voltage in AC calibrations.

The drawbacks of zero-crossing voltage standards has lead to development of programmable Josephson arrays based on damped junctions [26]. They are both faster and more stable than the conventional arrays. Working programmable voltage standards at 1 volt level have been fabricated using intrinsically damped junctions. In them the damping is provided by a dissipative material in the junction barrier. Suitable junctions are superconductor - normal- superconductor (SNS) [27] or superconductor - insulator - normal - insulator - superconductor (SINIS) junctions [28] .

In this thesis we discuss another approach, where SIS junctions are damped with external shunt resistors. A one volt programmable Josephson voltage standard has been developed as part of the thesis. An example IV curve from such an array is shown in Fig. 4(b).

B. VTT programmable voltage standard

In this Section we present design and experiments of the VTT arrays. In addition, we present a general optimization procedure for programmable arrays based on externally damped SIS junctions. The aim is to answer the question of how to design an array for a given voltage level, which is stable against external fluctuations, has low power consumption, and is fast.

A photograph of a one volt VTT Josephson voltage array chip is shown in Fig. 5(a). The main parts are generally similar to those used in conventional zero-crossing voltage arrays (see e.g. [29]). The fin-line taper provides a transition from a waveguide into on-chip superconducting microstriplines, which are used to guide the 70 GHz microwave signal into the Josephson junctions. The off-chip waveguide is in this case a rectangular E-band waveguide (WR-12). After the fin-line taper the microstriplines form a power distribution network, which guides the signal into parallel paths connected to junction chains. The power distribution network is formed by a cascade of matched T-junctions, where each junction divides the incoming signal into two outgoing signals of equal power. The junctions are also in a microstripline configuration, where the hotline is formed by the junction chain and the groundplane is a superconducting plate (Fig. 5(b)). The JJ chains are organized in branches, which are parallel with respect to the incoming microwave power. After the chains the microwave is guided into terminations. They are also microstriplines, but with normal conducting hotlines. They are long enough to dissipate most of the incoming power. This is to prevent standing waves due to reflections, which guarantees homogeneous microwave power for all junctions. At low frequencies the junction chains are connected in series to sum the voltages from different branches. The frequency separation is provided by filtering, i.e. DC block capacitors to isolate the power distribution network from low-frequency signals and low-pass filters to prevent microwave signals to couple from one branch to another.

The fabrication process is the VTT niobium trilayer process, which with some modifications has been successfully used to fabricate SQUIDs [30] for over a decade [31]-[35]. The devices are fabricated on 100 mm silicon wafers. Patterning is done by photolitography and either by reactive ion etching (Nb layers) or wet-etching (SiO_2 and Mo layers). The layer structure is visualized in Fig. 5(b), where the junction structures as well as other superconducting and insulating layers are shown. The lowest layer, sputtered Nb, forms the superconducting groundplane. The next layer is an insulator, which forms the dielectric for the microstriplines. It is SiO_2 grown with plasma enhanced chemical vapor deposition (PECVD). On top of this there is the trilayer, a Nb-Al-AlO_x-Nb -layer containing the Josephson junctions. It is formed by sputtering the base Nb, on top of which a thin ($\sim$5 nm) Al-layer is deposited. The tunnel barrier AlO_x ($\sim$2nm) is then formed by exposing the aluminium to oxygen for a given time at a constant pressure. On top of the oxide, a Nb counter electrode is grown . The junctions are then defined by anodizing the area around the junctions forming a zone of Nb_2O_5 around them. The counter electrode is

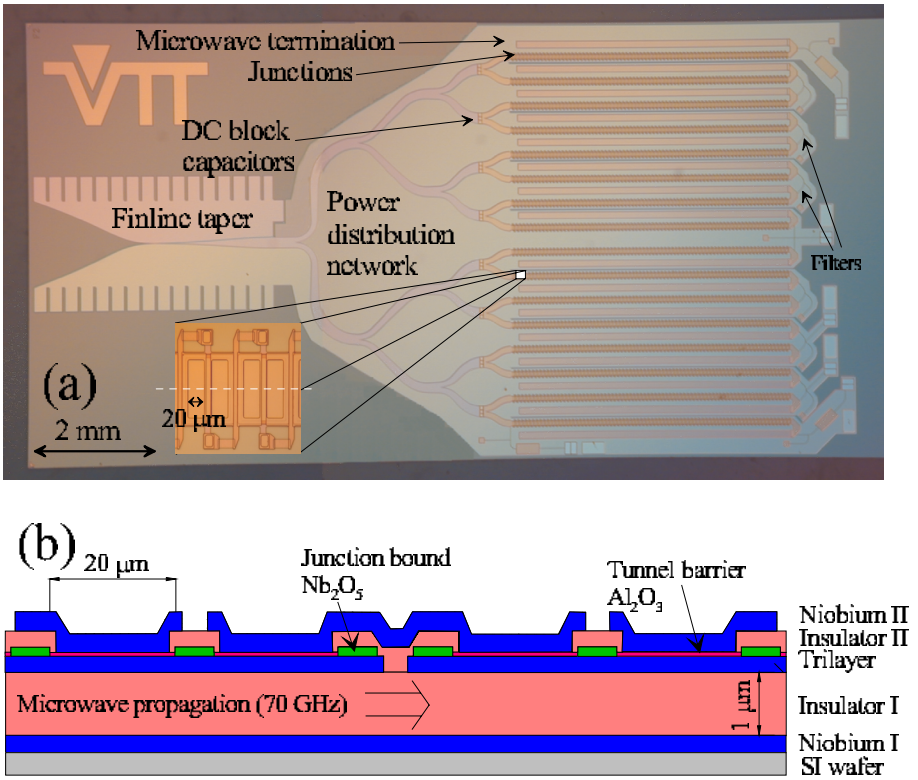

Figure 5. (a) An optical microscope photograph of a VTT programmable voltage standard (design 1(a)). Main parts of the circuit are indicated. The magnification shows a part of a junction chain. (b) A cross section from the junction chain. The aspect ratio is altered for clarity.

then removed excluding the junction areas. For the wiring, additional layers of SiO_2 and Nb are deposited. The last layers (not shown in the figure) are the resistor layer (sputtered molybdenum forming the shunt resistors and microwave terminations) and the passivation layer SiO_2 to protect the on-chip components.

In order to produce a stable quantized voltage, the microwave distribution along the branches must be sufficiently homogeneous. To achieve this, our approach is to minimize the attenuation of the shunt resistors by blocking the microwave signal from the resistor by an inductor L. The circuit is shown schematically in Fig. 6(a) and the realization in 6(b). We first study the intrinsic stability criteria. By intrinsic stability we mean here that a quantized voltage (Eq. (26)) appears as a single-valued function of bias current for as large a range of bias currents as possible. For a junction, which satisfies the simple RCSJ-model (Eq. (8)), the step amplitude (i.e. the range ΔI_n of bias current I_0, at which the quantized voltage state can appear) is [17]

$$\Delta I_n = 2I_c \left| J_n \left(\frac{I_1}{2\pi\Phi_0 f^2 C} \right) \right|, \tag{28}$$

where I_1 is the amplitude of the pump current. Here it has been assumed $(\omega C)^{-1} \ll R$, where $\omega = 2\pi f$ is the angular pump frequency. This is typically always satisfied for SIS junctions. The index n corresponds to the step index n in Eq. (26).

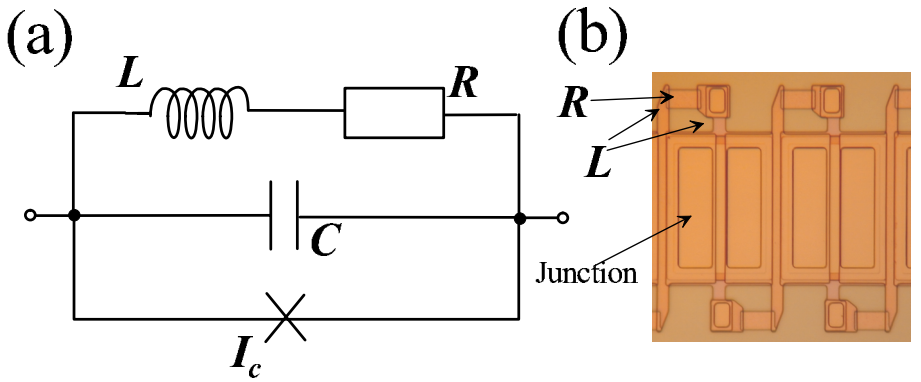

Figure 6. (a) The circuit with frequency dependent damping (schematically) and (b) the realization.

We quantify the criterion for intrinsic stability so that the effective step amplitude of our circuit in Fig. 6 is not substantially suppressed from the value of Eq. (28). The method to analyze the problem is solving Eqs. (6) and (7) numerically as in Ref. P2. The parameter space to be mapped is defined by the hysteresis parameter β_c (see Section IIB), the dimensionless inductance $\beta_L = 2\pi L I_c/\Phi_0$, and the dimensionless angular frequency $\Omega = (\Phi_0/2\pi I_c R)\,\omega$.

The data from such simulations is collected in Fig. 7. In Fig. 7(a) each triangle represents a result from a simulated IV curve. The triangles pointing upwards indicate points, where the simulated step amplitude satisfies Eq. (28). The triangles pointing downwards indicate points, where the simulated step amplitude is suppressed from this value. The main objective was to find a criterion for β_L. Therefore especially the boundary, where the increasing inductance begins to cause decreased stability, was mapped. Each pair of triangles thus illustrates the boundary of stable (below) and unstable (above) region. The resulting certainly stable region is shown grey in Fig. 7(a), where also the conventional criterion, that the pump frequency exceeds the plasma frequency [17]

$$\Omega\sqrt{\beta_c} \gtrsim 3 \tag{29}$$

was adopted. Although it was originally derived for undamped junctions, it was found to apply here as well.

Even though the stable region of Fig. 7(a) guarantees the existense of the quantized voltage state with a wide range of bias currents, it does not yet guarantee, that the voltage is a single valued function of current. To avoid constant voltage steps with different indices n to become overlapping (in the same sense as in zero-crossing steps, see Fig. 4(a)), the criterion is (see e.g. Ref. [27])

$$\Omega \gtrsim 1. \tag{30}$$

On the other hand, a resistive solution can coexist with the quantized voltage state (see e.g. the insets of Fig. 7). To avoid this, a set of simulations was executed to find out how this affects the effective step amlitude. The data is summarized in Fig. 7(b). It can be seen, that sufficient

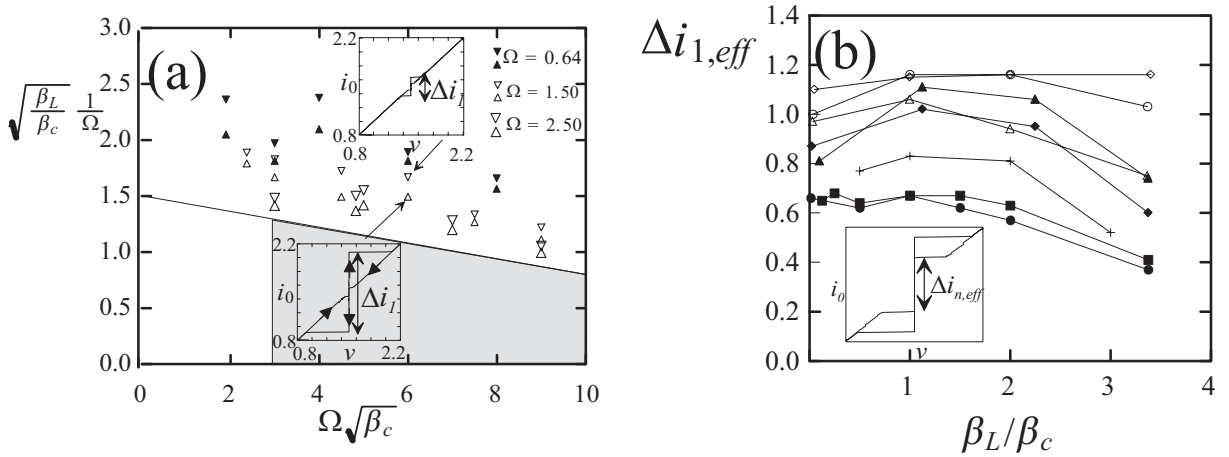

Figure 7. Stability data from numerical simulations. (a) Triangles pointing upwards mark IV curves with large step amplitudes ΔI_1 (the lower inset). Those pointing downwards mark IV curves with suppressed amplitudes due to chaotic behavior (the upper inset). The insets are examples of simulated IV curves. The arrows of the lower inset also shows the trajectory as the current is swept up and down. The area shown in gray is the certainly stable region of parameters. (b) The effective step amplitude (see the inset for the definition) for different parameters and step $n = 1$. Parameters for open diamond: $\Omega = 1.5$, $\beta_c = 2.0$, open circle: $\Omega = 1.5$, $\beta_c = 3.0$, solid triangle: $\Omega = 1.5$, $\beta_c = 4.0$, cross: $\Omega = 1.5$, $\beta_c = 6.0$, solid square: $\Omega = 1.5$, $\beta_c = 8.0$, open triangle: $\Omega = 2.5$, $\beta_c = 3.0$, solid diamond: $\Omega = 2.5$, $\beta_c = 4.0$ and solid circle $\Omega = 2.5$, $\beta_c = 8.0$.

criteria in practice are

$$\beta_c \lesssim 4 \tag{31}$$

$$\beta_L \lesssim 2\beta_c, . \tag{32}$$

The criterion of Eq. (31) together with Eqs. (29) and (30) also in practice guarantees that the stable region of Fig. 7(a) is reached.

To study the homogeneity of the pump current, analysis of the circuit in Fig. 8(a) (see Ref. P2) gives for the pump signal attenuation

$$\alpha = \alpha_c \left(\frac{sl_0}{L}\right)^2 + \alpha_d, \tag{33}$$

where $\alpha_c = (1/2)\, R/Z_0$ is the attenuation in the absence of frequency separation, s is the length of the microstripline occupied by one junction, l_0 is the microstripline inductance per unit length and α_d is the dielectric attenuation of the microstripline.

The optimization is performed assuming the simplified geometry shown in Fig. 8(b). The figures of merit are the output voltage U_{out}, the required microwave power P_{in}, the speed described by the time constant of the array τ_{RC}, and the step width ΔI_n. The speed is essential in precise AC voltage generation and the step width is a measure of stability against external fluctuations due to the environment and the measurement circuitry. Demanding that the intrinsic stability criteria (Eqs. (29)-(32)) apply, and that the attenuation (Eq. (33)) does not significantly suppress the step width, we can write the figures of merit in terms of design parameters. These are junction

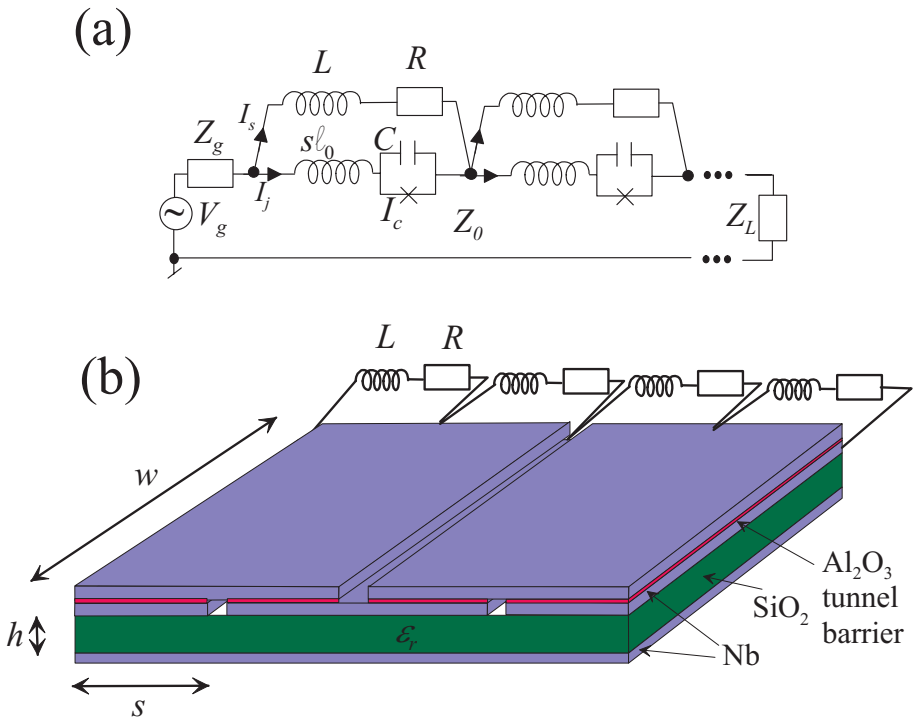

Figure 8. (a) The circuit diagram of the junctions embedded in the transmission line. (b) The simplified geometry assumed in the optimization procedure.

and microstripline dimensions w, s, h (see Fig. 8(b)), number of branches M, number of junctions N, and the step number n. It follows

$$U_{out} = Nn\Phi_0 f \tag{34}$$

$$\Delta I_n = \frac{4}{\pi}\frac{j_c w s}{\sqrt[3]{n}} \tag{35}$$

$$P_{in} = M\rho\left(1+n\right)^2 hws^2 \tag{36}$$

$$\tau_{RC} = N^2\gamma\frac{1}{h} \tag{37}$$

$$\frac{N}{M}\left(\kappa h s^3 + \alpha_d s\right) \lesssim \ln\left(1+\frac{1}{n}\right), \tag{38}$$

where the last line is the remaining criterion for the attenuation, which needs to be satisfied. Here j_c is the critical current density, which should be maximized while keeping Eq. (29) valid. In physical units this leads to $j_c = 2\pi\Phi_0 c_s \left(f/3\right)^2$, which is nearly constant for a given pump frequency and a fabrication process. The junction capacitance per unit area c_s is nearly constant for a given tunnel barrier material. Other constants are $\gamma = \left(2/3\pi^2\right)\Phi_0 f\varepsilon_0\varepsilon_r/j_c$, $\rho = 2\sqrt{\mu_0/\varepsilon_0\varepsilon_r}\pi^2\Phi_0^2 f^4 c_s^2$ and $\kappa = \left(3j_c/4\Phi_0 f\right)^3\sqrt{\mu_0^3\varepsilon_0\varepsilon_r}/c_s^2$.

Approximating $\ln\left(1+1/n\right) \approx 1/n$, and assuming that $\alpha_d \approx 0$, we can find the general trade-off for the optimized design as

$$\tau_{RC} \propto \frac{n+1}{n^{7/6}} \frac{1}{f^5} \frac{(U_{out}\Delta I_n)^{5/2}}{\sqrt{P_{in}}}, \tag{39}$$

which indicates that an array cannot be speeded up beyond a limit without either using more input power, or dropping the output voltage. The situation can be slightly improved with increasing the step number n, but the dependence is very weak. However, operating the device at higher steps has the practical advantage of decreasing the number of junctions needed.

In addition to the design, the devices set strict criteria to the fabrication process. For example, a one volt array pumped with $f = 70$ GHz needs about 2300 series connected Josephson junctions. Each of these needs to be fabricated flawlessly. In other words the yield of Josephson junctions needs to be at least 99.96% for an array to work. The critical current spread needs to be at a tolerable value, since at metrological measurements the smallest critical current determines the step amplitude and thus the stability against external fluctuations. Also the scatter in the shunt resistance needs to be very small. In the presence of resistance scatter the quantized voltage state is obtained at different bias currents for different junctions, which decreases the effective step amplitude (see Ref. P1).

As part of this Thesis, two main versions of arrays aimed to work at about 1 V level were designed and tested at DC. The first design (Ref. P1) is aimed to produce the voltage of 1 V (design 1a) or 1.5 V (design 1b) at step $n = 3$. A photograph of an array with design 1a is shown in Fig. 5(a). The second design (design 2) (Ref. P3) has two identical arrays integrated on the same chip with a single microwave input. Both subarrays produce an output of about 1.5 V at step $n = 3$. A photograph and a schematic circuit arrangement are shown in Fig. 9. Design 1 was made before the optimization procedure above was developed, while in design 2 the optimization was utilized.

The room temperature electronics of the experimental setup consisted of 70 GHz electronics, a DC bias source (typically Fluke 5700 calibrator in series with resistance of 5 - 50 kΩ) and a voltmeter. In high precision measurements, HP 3458A digital voltmeter was used to verify the step flatness with a resolution of ∼100 nV. A cryoprobe was designed for cooling the chip down to 4.2 K. For the pump signal, the probe has a waveguide transition from WR-12 waveguide into an oversized circular waveguide at the room temperature end. At the cold end there is

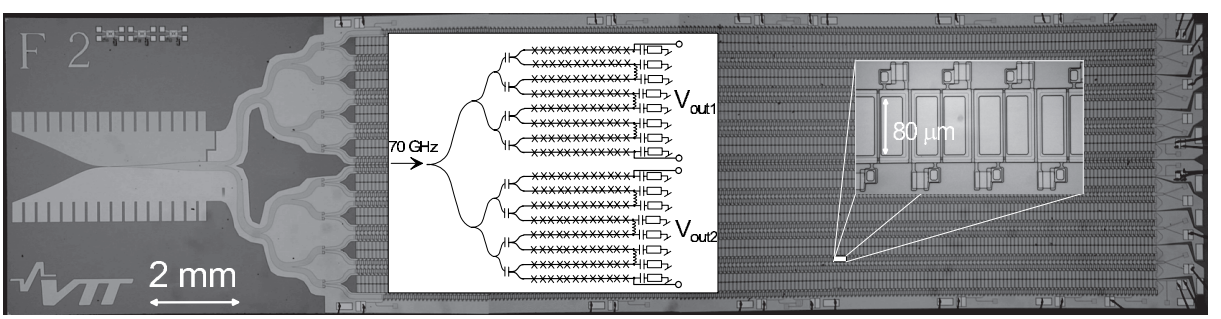

Figure 9. A microscope photograph of an array with design 2. Insets show the wiring arrangement with two independent output voltages and a magnification from a junction chain.

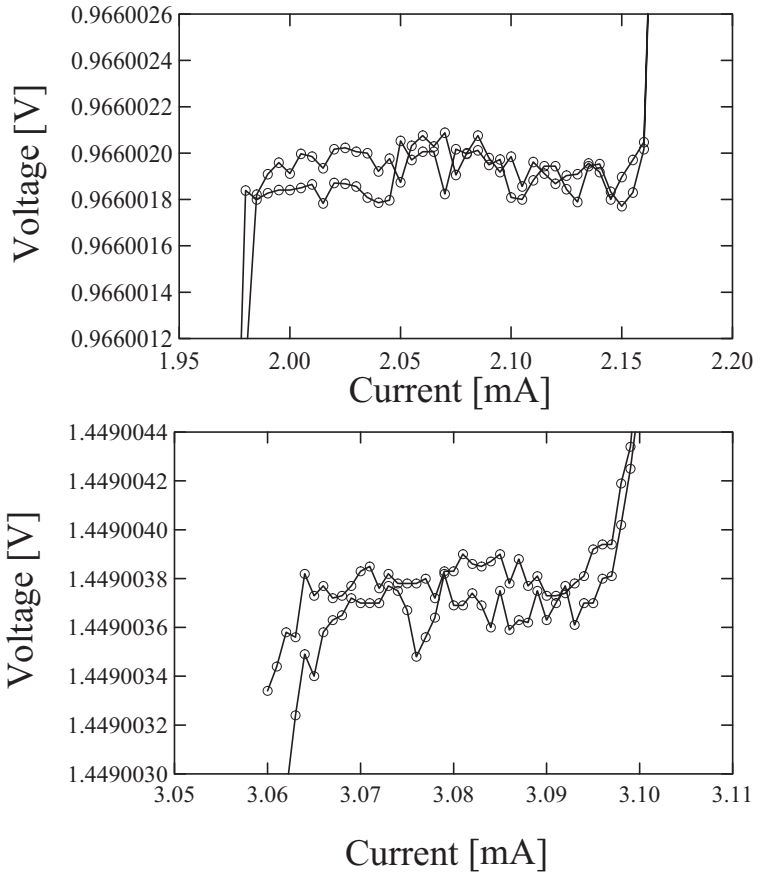

Figure 10. Quantized voltage states measured with an array of design 2. (a) Step $n = 2$ and (b) Step $n = 3$.

another transition from the oversized waveguide back to WR-12 guide, which has a slot for the finline taper of the chip. The DC lines (twisted copper pairs) were filtered with *RLC*-filters at room temperature. The 70 GHz electronics was a part of the standard JVS calibration setup of the Centre for Metrology and Accreditation and (MIKES). It consists of a Gunn diode as the microwave source. It is operated in a phase-locked loop consisting of an EIP-578B frequency counter with a 110 GHz extension. The frequency reference is traceable back to the Cs atomic clock of MIKES.

An IV curve from a chip with design 1a is shown in Fig. 4(b) at a rough voltage scale. At more accurate measurements the constant voltage steps with $n = 1$ and $n = 2$ showed flat steps. The one volt steps with arrays of design 1b and $n = 2$ showed effective step amplitudes typically between 60 – 100 μA. The third constant voltage step, however, has not been found flat in measurements having a resolution below 1 μV. An array with design 1b also took part in an international intercomparison measurement (Euromet project 626 [36]), where the array output at about 0.5 V and 1 V levels were compared against conventional SIS-arrays. In direct comparisons an agreement better than 0.4 nV was achieved.

The optimization algorithm presented above was utilized in design 2. The problem of degrading step amplitude with increasing step index n is possibly due to the variation in the shunt resistance.

An attempt to decrease the scatter was made by sputtering the resistor films in a mode, where the sample stage was oscillating. The aim of this was to decrease thickness variations of the resistor film. The resistors were characterized by measuring a large quantity of room temperature test structures aiming to clarify both the contribution of the film thickness and the line width. From the set of experiments an estimate was made, that ΔR should be below 4%.

Resulting IV curves are shown in Fig. 10. Shown are the steps $n = 2$ and $n = 3$ taken from measurements having resolution of about 200 nV. Flat constant voltage steps are obtained in both cases. With $n = 2$, the effective step amplitude at 1 V level is about twice the value obtained from design 1, even though the power consumption per subarray is about one half, and the rise time is of the same order as in design 1. The step $n = 3$ shows flat steps for this design as well. However, a practical problem has been the low yield of arrays, and by the date only one working array has been found to produce flat voltage steps at a metrological accuracy. A probable reason is the variation of critical current density between different arrays. It was also later found, that an additional design criterion is imposed to prevent the self-generated power of the junctions from causing pump signal inhomogenity [37]. This makes the criterion for the scatter more restrictive.

The main application of the arrays is a calibration setup for tracing an AC voltage back to the Josephson voltage. This can be done in a more direct way than with conventional methods. A possible method for doing this is introduced in Ref. [38] and the practical setup is being developed as collaboration of MIKES and VTT. Two arrays in a bridge configuration can also be utilized in arbitrary impedance intercomparisons (Ref. P3). In this case the array with two independent outputs (design 2) is useful. The main requirement for AC applications is the speed. For an AC waveform of frequency f_s, the error due to transients as limited by the array is (Ref. P2)

$$\frac{\Delta U}{U} = 2\pi^2 \left(\tau_{RC} f_s\right)^2 . \tag{40}$$

For $f_s = 1$ kHz both designs should enable an uncertainty as low as about 0.1 ppm. An additional challenge is whether the array tolerates the level of noise introduced by the fast bias electronics. Experiments made with arrays of design 1 have confirmed that $\tau_{RC} \lesssim 250$ ns, which is still likely to be limited by the setup [39, 40]. Preliminary experiments with AC generation suggest that also the steps remain flat at least within 1 ppm with the fast bias electronics.

4. The Bloch oscillating transistor

A. Amplifiers based on mesoscopic tunnel junctions

Development of nanofabrication techniques has led to a new family of devices, in which the charging energy $\sim e^2/2C$ of a single charge carrier (either an electron in a normal conductor or a Cooper pair in a superconductor) is an important energy scale. The one most extensively studied is the single electron transistor (SET), which consists of two normal tunnel junctions connected to a normal conducting island having small capacitance C such that $e^2/2C \gg kT$ [41] -[43]. The Coulomb blockade of the island is tuned by an additional gate electrode, which in turn changes the current through the junctions. The SET has been found to be a highly sensitive electrometer [42, 44]. Also its superconducting counterpart, the single Cooper pair transistor (SCPT) provides comparable sensitivity [45]. Both devices have a gate-controlled island, which causes sensitivity to background charge fluctuations. This is seen as a high level of $1/f$ noise. To enhance the band (usually limited by the wiring of the cryostat in low-frequency applications) beyond the $1/f$-corner, varous RF readout techniques have been developed for the two-junction devices [46, 47], or a single junction embedded in a tank circuit [48].

In the gate-controlled devices the input signal is coupled capacitively to the device. In this sense they resemble the field effect transistor (FET) among semiconducting devices. The properties of FETs are crucially different from the bipolar junction transistors (BJTs), which have a resistive input and which essentially detect current. Among devices based on mesoscopic tunnel junctions, the resistively coupled SET (R-SET) has a resistive input impedance, though its performance has been found to suffer strongly from thermal fluctuations [49]. In this Thesis we analyze a new device, the Bloch Oscillating Transistor (BOT). It is based on controlling Cooper pair current in a single mesoscopic Josephson junction by means of quasiparticle current through a normal tunnel junction. Instead of controlling the static charge on the island, the tunneling quasiparticles induce interlevel transitions, which in turn affect the strength of the Coulomb blockade.

B. Principle of operation

The circuit of the Bloch oscillating transistor is schematically shown in Fig. 11(a). In addition to the basic mesoscopic Josephson junction voltage biased across a large resistor (see Section IID) there is an additional tunnel junction connecting a superconducting "island" to the base electrode (B). The base electrode is normal conducting, i.e. the base junction is a NIS or a NIN junction depending on the realization. The other two electrodes are named the collector (C) and the emitter (E). In the basic mode of operation the BOT is biased to a voltage $V_C \gtrsim e/C$, which makes the Bloch oscillations possible. They lead to a net charge flow through the collector-emitter circuit. The Bloch-oscillations are occasionally interrupted by Zener tunneling causing the transition into the second band, where the Cooper pair flow is blocked. We assume further that Cooper pairs tunnel only at the lowest band. This is justified in case of small Josephson coupling since the Zener tunneling probability between the upper bands is close to unity (see Eq. 16). We will thus refer to the system as a two-level system, and refer to the Bloch-oscillating

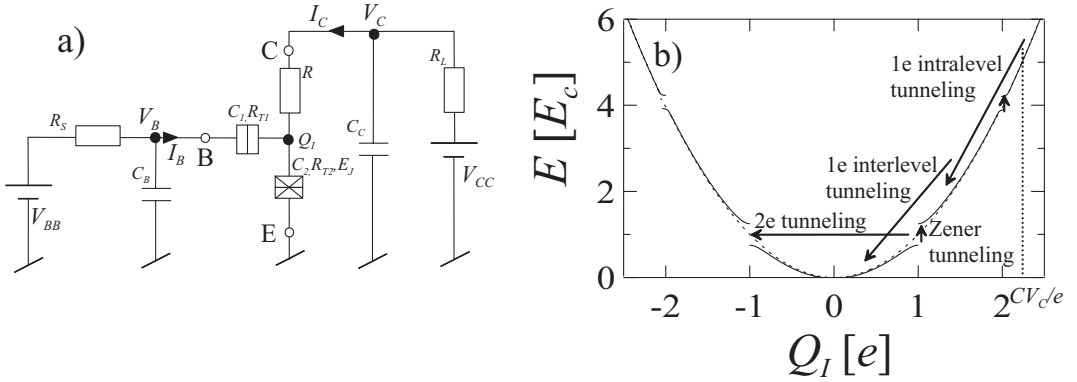

Figure 11. (a) The circuit of the Bloch oscillating transistor connected to source and load resistances R_S and R_L. Shown are also the lead capacitances C_B and C_C. (b) The band structure with possible transitions. The quasiparticle tunneling events through the base junction are shown in addition to transition mechanisms present in a bare mesoscopic JJ as well.

state (the lowest band) as the first level and the upper bands as the second level.

The transition from the second level down to the first one occurs via quasiparticle tunneling through the base junction. If the charge is initially $Q < 2e$, one quasiparticle always suffices to cause an interlevel transition. For $Q > 2e$ at least two electrons are needed, which leads to intralevel transitions within the second level (see Fig. 11(b)). The quasiparticle tunneling probability can be adjusted by changing the bias voltage (or current) of the base electrode. Thus the share of time the system spends at the first level is also adjusted. Therefore the current at the collector-emitter circuit (or collector current I_C) is controlled from the base electrode leading to transistor-like characteristics and signal amplification.

C. Computational modelling

The principle of operation was first shown computationally using a model similar to that described in Section IIC (Ref. P4). Originally the impedance at the collector electrode was assumed to be an LR-circuit instead of the simple resistor as in Fig. 11(a). The charge dynamics of the Josephson junction were described by adiabatic charge flow within the lowest band occasionally interrupted by Zener tunneling, the probability of which was evaluated from Eq. (16). The quasiparticle tunneling rate through the base junction was obtained from the orthodox theory of single electron tunneling [47]. The model did not, however, include inelastic Cooper pair tunneling which is possible in case of finite temperature and/or finite impedance at the collector electrode. It was still possible to predict charge dynamics essentially similar to those described above. Qualitatively correct characteristic curves were predicted and the device was shown to have gain.

Due to realization issues the practical devices were fabricated without the extra inductance at the collector. To predict the device characteristics quantitatively, the effect of fluctuations due to the collector resistor needs to be accounted for. The solution was to use the model introduced in Section IID, i.e. the time dependent phase-correlation theory, which gives correct charge dynamics

also in case of finite collector resistance R_C and finite temperature. The model is extended to account for the quasiparticle tunneling as well (Ref. P6). It is summarized as follows. The "island" charge $Q_I = Q_2 - Q_1$ is integrated in the time domain as

$$\frac{dQ_I}{dt} = \frac{V_C - V_2}{R_c} - \left(\frac{dQ_I}{dt}\right)_{QP1} - \left(\frac{dQ_I}{dt}\right)_{QP2} - \left(\frac{dQ_I}{dt}\right)_{CP}, \tag{41}$$

where the first term describes the charge flow through the collector resistor, the second and third terms describe the effect of quasiparticle tunneling through the base junction and the JJ, respectively, and the last term is the Cooper pair tunneling through the Josephson junction. Tunneling rates for both quasiparticles and Cooper pairs are obtained from the $P(E)$-theory [15].

D. Comparison of experiments and simulations

The experimental BOT samples were fabricated and measured in the Low Temperature Laboratory of Helsinki University of Technology. They were fabricated using electron beam lithography and four-angle shadow evaporation technique. The JJ was an Al/AlO_x/Al -junction ($\sim$ 100nm $\times$ 100 nm), and the base junction had Al/AlO_x/Cu structure. The collector resistor was a narrow strip ($\sim$100 nm $\times$ 20 μm) made of a thin ($\sim$10 nm) layer of chromium. In some samples the JJ was fabricated in the SQUID geometry, which enables tuning of the Josephson coupling by an external magnetic field. The measurements were done in a dilution refrigerator at temperatures of about 100 mK.

Sets of computed collector current - collector voltage ($I_C - V_C$) curves together with corresponding experimental results are shown in Fig. 12. The sample parameters are presented in Ref. P6. Quantitative agreement is reasonably good. Differences appear particularly, when the Josephson coupling is large. This is the case especially with the sample in Fig. 12(b), where $E_J/E_C \approx 1.7$ as estimated from the experimental data. The computed peaks are at lower voltages and currents than the experimental ones. In this case Zener tunneling probability between the higher bands is below unity (Eq. (16) with $n > 1$). This indicates that Cooper pair tunneling at higher bands may have an impact to the experimental result. Also the assumption that quasicharge equals real charge is somewhat violated with $E_J/E_C \gtrsim 1$.

The computed dynamics of different samples at different points of operation are illustrated in Fig. 13. The corresponding points of operation are indicated in Fig 12. Regular BOT operation, i.e. the operation essentially similar to the original idea of BOT, is shown in Fig. 13(A1), where the quasiparticle current clearly enhances Cooper pair current. The inverted BOT-operation is shown in Fig. 13(A2), where quasiparticle tunneling tends to drive the Josephson junction out of the lowest band. The single-electron current thus suppresses Cooper pair current in this case. The nonsymmetric nature of the dynamics explains why $I_C - V_C$ curves are not symmetrical as the sign of V_C is reversed. It has been shown that substantial current gain is obtained for both regular and inverted operation.

The IV-curves of Fig. 12(b) are slightly hysteretic both in the experimental and the computational datasets. The time-domain plots of Fig. 13(B1) and (B2) illustrate the dynamics in

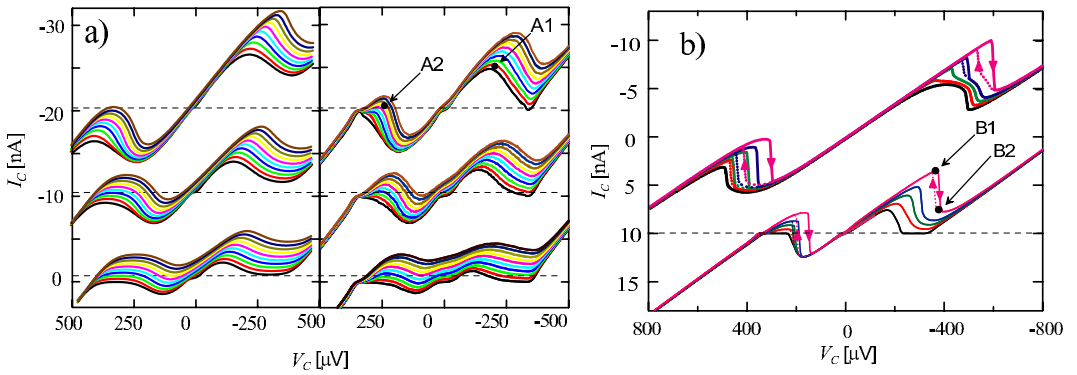

Figure 12. Simulated and experimental $I_C - V_C$ curves for two samples. The arrows denote points of operation, the dynamics of which are plotted in Fig. 13. (a) The sample has a SQUID geometry, and is measured with three different Josephson couplings (sets from down to top E_J/E_C=0.35, 0.7, 1.2). The upper sets are offset by -10 nA and -20 nA, respectively, for clarity. The data in the left frame is experimental and the right frame computational. (b) The sample has a constant Josephson coupling E_J/E_C=1.7. The upper set is experimental and the lower set (offset by 10 nA) is computational. Both in (a) and in (b), different curves in each dataset are measured with different base currents.

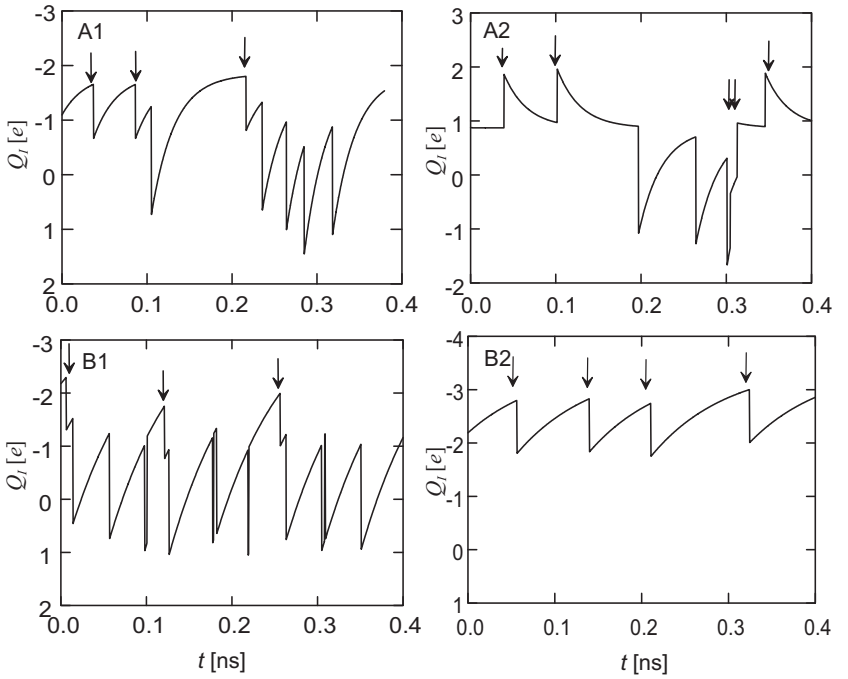

Figure 13. The island charge as function of time at different operating points for two different devices (see Fig. 12). Arrows mark quasiparticle tunneling events.

both branches. It is shown that at the upper branch there is a substantial Cooper pair current, whereas the lower branch consists of quasiparticle leakage only. In simulations the IV curves become more hysteretic as either Josephson coupling or the ratio of resistances R_c/R_{T1} is increased. The transition from hysteretic to nonhysteretic behavior is studied more quantitatively in the next section.

E. Analytic theory and noise properties

In this section we develop an analytic theory based on the assumption of the two-level system [11],[50]. At the first level the current through the JJ (the saturation current) is $I_S = 2ef_B$, where f_B is the frequency of Bloch oscillations. Therefore we may write the average collector current as

$$I_C = \frac{1/\Gamma_\uparrow}{1/\Gamma_\uparrow + 1/\Gamma_\downarrow} I_S - I_B, \tag{42}$$

where the prefactor of the first term is the share of time the system spends in the first level. The transition rates between the states are $\Gamma_\uparrow$ and $\Gamma_\downarrow$. The second term is the quasiparticle current from the base electrode, which leaks to the ground via the collector resistor. The base current is given as

$$I_B = -\frac{\langle N_e \rangle \, e}{1/\Gamma_\uparrow + 1/\Gamma_\downarrow}, \tag{43}$$

where $\langle N_e \rangle$ is the average number of electrons needed to cause a downwards transition. Here it is assumed that quasiparticles do not tunnel while the system is in the first level. If $\langle N_e \rangle$ differs from unity, it means that intralevel transitions are possible.

In Ref. P7 we give estimates for $\Gamma_\uparrow$, $\Gamma_\downarrow$, I_S, $\langle N \rangle$ and $\langle N_e \rangle$ in the limit of large resistance and low temperatures. Knowing them, it is possible to calculate IV curves of the BOT analytically. Comparisons to the simulations show reasonable agreement, though finite-temperature and impedance somewhat modify the properties. It is possible to calculate the small-signal response as well. It can be given by a conductance matrix

$$\begin{bmatrix} i_C \\ i_B \end{bmatrix} = \begin{bmatrix} G_{out} & g_m \\ g_x & G_{in} \end{bmatrix} \begin{bmatrix} v_C \\ v_B \end{bmatrix}, \tag{44}$$

where i_C, i_B, v_C and v_B are the small-signal components of collector and base currents and voltages, i.e. small variations around I_C, I_B, V_C and V_B. The small signal parameters are defined as $G_{out} = (\partial I_C/\partial V_C)_{V_B}$, $g_m = (\partial I_C/\partial V_B)_{V_C}$, $g_x = (\partial I_B/\partial V_C)_{V_B}$ and $G_{in} = (\partial I_B/\partial V_B)_{V_C}$.

It is possible to arrange the measurement so that V_C is kept constant at all times. This is the case for a small input impedance postamplifier, e.g. dc SQUID, whose inductive input impedance is close to zero at small frequencies. Even a large impedance of a voltage postamplifier can be dropped by applying current feedback. This renders output conductance G_{out} and intrinsic feedback transconductance g_x irrelevant. For this case the small signal model is graphically illustrated in the equivalent circuit of Fig. 14. The BOT is described with input impedance $R_{in} = 1/G_{in}$, and the current generator βi_B at the output driving the load resistance R_L, which is assumed small. The current gain is defined as

$$\beta = -\left(\frac{\partial I_C}{\partial I_B}\right)_{V_C} = -\frac{g_m}{G_{in}}. \tag{45}$$

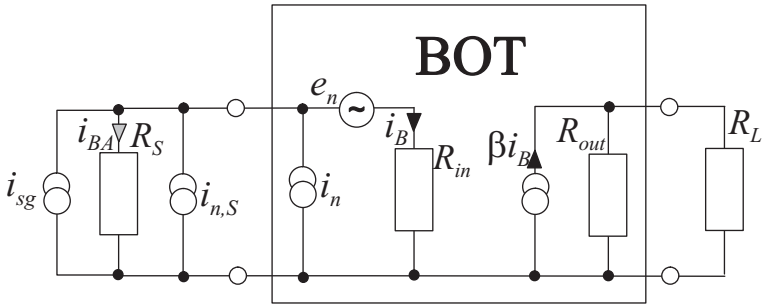

Figure 14. A small-signal model and equivalent noise sources of the BOT.

The signal source is described as Norton's equivalent, i.e. current generator i_{sg} in parallel with the source resistance R_S. The noise from the source is represented by generator $i_{n,S}$.

The noise added by the BOT is shown as equivalent voltage and current generators e_n and i_n, respectively, at the input. We assume that the dominant noise at the output is the two-level switching (telegraph) noise [51] inherent to the dynamics described above. In this case the equivalent sources can be shown to be fully correlated with spectral densities

$$S_{en}^{1/2} = \frac{2I_S}{-g_m}\sqrt{\frac{\Gamma_\downarrow\Gamma_\uparrow}{(\Gamma_\uparrow+\Gamma_\downarrow)^3}} \tag{46}$$

$$S_{in}^{1/2} = \frac{2I_S}{\beta}\sqrt{\frac{\Gamma_\downarrow\Gamma_\uparrow}{(\Gamma_\uparrow+\Gamma_\downarrow)^3}}. \tag{47}$$

This differs from the estimates given in Ref. P4, which assumes uncorrelated sources. However, it was later found that the correlations play a crucial role.

We next apply standard noise theory [52] to calculate the optimum noise resistance R_{opt} and minimum noise temperature T_n. Optimum noise resistance is the value of the source resistance R_S (see Fig. 14) with which the minimum noise temperature is obtained. These can be shown to be

$$R_{opt} = \sqrt{\frac{S_{en}}{S_{in}}} = R_{in} \tag{48}$$

$$T_n = \frac{1}{k_B}\sqrt{S_{en}S_{in}} = \frac{1}{k_B}R_{in}S_{in}. \tag{49}$$

In principle one can now calculate the small signal and noise parameters for a given device at a given bias point. This is, however, somewhat laborious, so in order to get an order of magnitude estimate and an idea about interdependencies, we next make some further simplifications. Two limits have to be considered separately, since for $V_C < 2V_Q \equiv 2e/C$ and $V_C > 2V_Q$ the dynamics is qualitatively different. In the first case $\langle N_e\rangle = 1$. In Ref. P7 we give approximations of some noise

properties. Here we further assume a typical point of operation ($V_C = (3/2)\,V_Q$ and $V_B = -V_Q$). It follows

$$\beta \approx 2\exp\left(\frac{\pi R e^2}{8\hbar}\left(\frac{E_J}{E_C}\right)^2\right) \tag{50}$$

$$g_m \approx -\frac{\beta}{R_T}\frac{1}{\left(1+(\ln 5)/4\,(R/R_T)\,\beta\right)^2} \tag{51}$$

$$S_{in}^{1/2} \approx \sqrt{\frac{4E_C}{R_T}\left(1+\frac{1}{4}\frac{R}{R_T}\ln(5)\,\beta\right)^{-3}} \tag{52}$$

$$S_{en}^{1/2} \approx \sqrt{4E_C R_T\left(1+\frac{\ln 5}{4}\left(\frac{R}{R_T}\right)\beta\right)} \tag{53}$$

$$R_{opt} \approx R_T\left(1+\frac{\ln 5}{4}\frac{R}{R_T}\beta\right)^2 \tag{54}$$

$$T_n \approx \frac{4E_C}{k_B}\left(1+\frac{\ln 5}{4}\frac{R}{R_T}\beta\right)^{-1}. \tag{55}$$

In this mode the BOT acts as a simple $e-2e\,\langle N\rangle$ -charge multiplier. Thus the current gain in Eq. (50) is actually $2\,\langle N\rangle$, i.e. the number of Cooper pairs in one "sequence" of Bloch oscillations. The current noise can also be given as $S_{in}^{1/2} = 2\sqrt{eI_B}\,(1+\Gamma_\downarrow/\Gamma_\uparrow)^{-1}$, i.e. it is essentially the shot noise of the input current times a suppression factor $(1+\Gamma_\downarrow/\Gamma_\uparrow)^{-1}$. A closer study of the dynamics shows that with large $\Gamma_\downarrow/\Gamma_\uparrow$ the noise at the output becomes fully anticorrelated with the noise at the input, which explains the reduction of the equivalent noise. Increasing the Josephson coupling E_J both increases the current gain and decreases the equivalent current noise and noise temperature. However, the transconductance gain drops and the optimum resistance increases simultaneously. The Josephson coupling cannot be increased beyond $E_J/E_C \approx 1$ for the assumptions of the model to hold. At finite temperature there will also be spontaneous downwards transitions due to incoherent Cooper pair tunneling which decreases the current gain [50]. This effect was excluded in this simplified model.

For $V_C > 2V_Q$ intralevel transitions become possible. This strongly modifies the dynamics yielding (see Ref. P7)

$$\beta \approx 1.2\,(1-\beta_B)^{-1} \tag{56}$$

$$g_m \approx -\frac{2}{R} \tag{57}$$

$$S_{in}^{1/2} \approx \frac{12e}{\sqrt{RC}}\left(\frac{R_T}{R}\right)\beta^{-1} \tag{58}$$

$$S_{en}^{1/2} \approx \frac{2e}{\sqrt{RC}}R_T \tag{59}$$

$$R_{opt} \approx \frac{R}{2}\beta \tag{60}$$

$$T_n \approx \frac{50E_C}{k_B}\left(\frac{R_T}{R}\right)^2\beta^{-1}. \tag{61}$$

This approximation is valid at $\beta_B \approx 1$. The hysteresis parameter of BOT, β_B, is defined as

$$\beta_B = -\frac{\Gamma_\downarrow (\Gamma_\uparrow + \Gamma_\downarrow)}{\Gamma_\uparrow \langle N_e \rangle} \left(\frac{\partial \langle N_e \rangle}{\partial V_B} / \frac{\partial \Gamma_\downarrow}{\partial V_B} \right), \tag{62}$$

and an estimate is given as

$$\beta_B \approx 0.02 \left(\frac{R}{R_T} \right)^2 \exp \left(\frac{\pi e^2 R}{16\hbar} \left(\frac{E_J}{E_c} \right)^2 \right). \tag{63}$$

The striking feature is the very strong dependence on β_B, which indicates that intraband transitions play an important role, since the sole effect of them was embedded in its definition (Eq. (62)). The value $\beta_B = 1$ leads to zero input conductance, which is due to the fact that changing V_B causes two competing effects. Firstly, it changes $\Gamma_\downarrow$, which leads to positive input conductance. Secondly, it changes $\langle N_e \rangle$, which leads to negative input conductance. If $\beta_B = 1$ these exactly cancel each other. This means that a small change in the input current causes a large change in the input voltage, and thus also the output current, and the current gain becomes large. Since the noise at the output remains finite, the effect also leads to decreasing equivalent noise.

The effect of increasing β_B is illustrated in the computed $I_C - I_B$ and $I_B - V_B$ plots in Fig. 15(a) and 15(b)). The Josephson coupling is varied. As β_B approaches unity the curves become hysteretic, indicating that the input conductance is negative. The increase of the gain and the

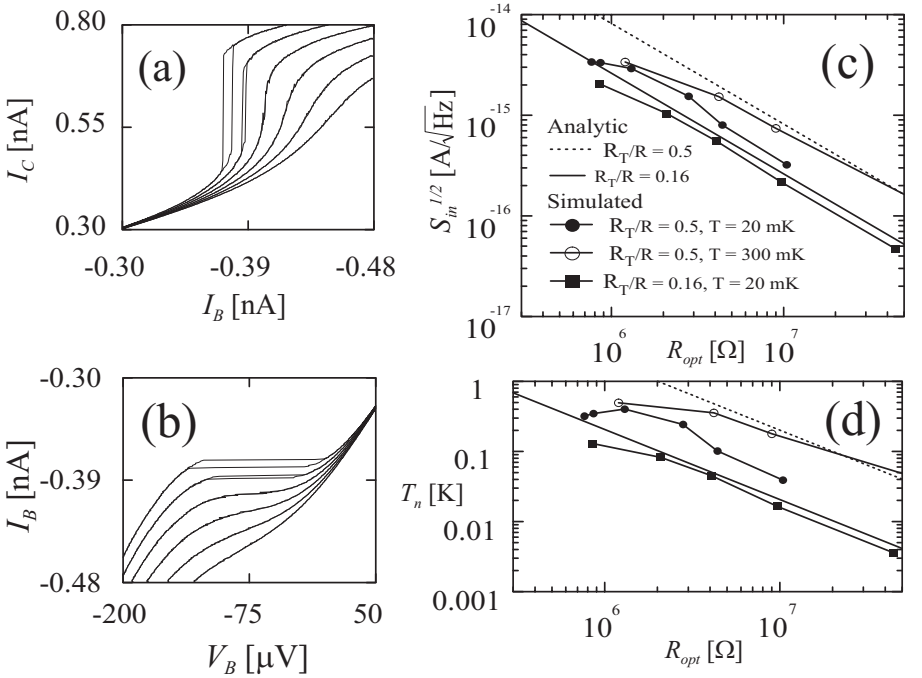

Figure 15. (a) and (b) Simulated characteristic curves with varying Josephson coupling. The base is current biased, so the negative input conductance appears as hysteresis. See Ref. P7 for the parameters used in the simulation. (c) and (d) The spectral current noise density and minimum noise temperature as function of the optimum noise resistance. Markers denote simulated and lines analytic results.

input impedance without a limit is also visible. In Fig. 15(c) and (d) equivalent current noise and noise temperature obtained from the simulations, together with the theoretical predictions from Eqs. (58), (60) and (61) are shown. Reasonable agreement is obtained despite the simplifying assumptions made along the derivation. This also indicates the improvement of noise properties as the optimum impedance increases. It suggests that BOT is a potential low noise amplifier for reading out sources with relatively large (of order 1 MΩ or more) impedances.

5. Summary

We have shown that the rich dynamics of Josephson junctions is of both theoretical and technological interest. Starting from the very basic description of a JJ, Eq. (1), we have derived models useful in realistic applications. The theoretical models were successfully tested in comparison with the experiments on the two devices under study. In both cases it was shown that the modelling techniques are sufficiently accurate for quantitative prediction of device properties as well as for optimizing them for practical purposes.

The new circuit solution for a programmable Josephson voltage standard was developed and optimized. Stable operation at about 1 V DC level with metrological accuracy was demonstrated experimentally. Characterization of the device together with preliminary experiments in AC generation suggest that it is also applicable in AC voltage metrology. A design with two independent outputs is potentially applicable in arbitrary impedance intercomparisons as well.

The principle of operation of the Bloch oscillating transistor was first demonstrated computationally. After the first experiments, the comparison to refined models showed that the device properties are quantitatively understood. Finally, an analytic theory was developed creating more tools for gaining insight into the device dynamics as well as for the device optimization. It was also shown that BOT can serve as a low-noise preamplifier in cryogenic circuits having an equivalent current noise spectral density below 1 $\mathrm{fA}/\sqrt{\mathrm{Hz}}$ and a noise temperature below 0.1 K.

References

[1] B.D. Josephson, Phys. Lett. 1, 251 (1962).

[2] T. van Duzer, Principles of Superconducting Devices and Circuits, Prentice Hall PTR, New Jersey (1999).

[3] K.K. Likharev, J. Low Temp. Phys. 59, 347 (1985).

[4] D.B. Haviland, L.S. Kuzmin, P. Delsing, and T. Claeson, Europhys. Lett. 16, 103 (1991).

[5] K.K Likharev, Dynamics of Josephson Junctions and Circuits, Gordon & Breach, New York (1986).

[6] R.L. Kauz, J. Appl. Phys. 58, 424 (1985).

[7] R.H. Koch, D.J. Van Harlingen, and J. Clarke, Phys. Rev. Lett. 45, 2132 (1980).

[8] J. Ziman, Principles of the Theory of Solids (Cambridge University Press, Campridge, 1972).

[9] U. Geigenmüller, and G. Schön, Phys. B 152, 186 (1988).

[10] G. Schön, and A.D. Zaikin, Phys. Rep. 198, 237 (1990).

[11] A.D. Zaikin, and D.S. Golubev, Phys. Lett. A 164, 337 (1992).

[12] A.O. Caldeira, and A.J. Legget, Phys. Rev. Lett. 46, 211 (1981).

[13] M.H. Devoret, D. Esteve, H. Grabert, G.-L. Ingold, H. Pothier, and C. Urbina, Phys. Rev. Lett. 64, 1824 (1990).

[14] G.-L. Inglold, and H. Grabert, Europhys. Lett. 14, 371 (1991).

[15] G.-L. Ingold, and Yu. V. Nazarov, in *Single Charge Tunneling*, eds. H. Grabert, and M.H. Devoret, Plenum Press, New York, pp. 21 - 107 (1992).

[16] R.L. Kauz, J. Appl. Phys. 52, 3528 (1981).

[17] R.L. Kauz, and R. Monaco, J. Appl. Phys. 57, 875 (1985).

[18] R.L. Kauz, J. Appl. Phys. 62, 424 (1987).

[19] R.L. Kauz, J. Appl. Phys. 76, 5538 (1994).

[20] S. Shapiro, Phys. Rev. Lett. 11, 80 (1963).

[21] W.H. Parker, B.N. Taylor, D.N. Langenberg, Phys. Rev. Lett. 18, 287 (1967).

[22] H. Seppä, P. Immonen, and J. Räihä, IEEE Trans. Instrum. Meas. 37, 2 (1988).

[23] F.L. Lloyd, C.A. Hamilton, J.A. Beall, D. Go, R.H. Ono, and R.E. Harris, IEEE Electron Dev. Lett. 8, 449 (1987).

[24] C.A. Hamilton, C. Burroughs, and K. Chieh, J. Res. Natl. Inst. Stand. Technol. 95, 219 (1990).

[25] R. Pöpel, Metrologia 29, 154 (1992).

[26] C.A. Hamilton, C. Burroughs, and R.L. Kautz, IEEE Trans. Instrum. Meas. 44, 223 (1995).

[27] S.P. Benz, C.A. Hamilton, C.J. Burroughs, and T.E. Harvey, Appl. Phys. Lett. 71, 1866 (1997).

[28] H. Schulze, F. Müller, R. Behr, J. Kohlmann, and J. Niemayer, and, D. Balashow, IEEE Trans. Appl. Supercond. 9, 4241 (1999).

[29] J. Kohlmann, F. Müller, P. Gutmann, R. Pöpel. L. Grimm, F.-W. Dünschende, W. Meier, and J. Niemeyer, IEEE Trans. Appl. Supercond. 7, 3411 (1997).

[30] T. Ryhänen, H. Seppä, R. Ilmoniemi, and J. Knuutila, J. Low Temp. Phys. 76, 287 (1989).

[31] L. Grönberg, H. Seppä, R. Cantor, M. Kiviranta, T. Ryhänen, J. Salmi, and I. Suni, Proceedings of the 4th International Conference SQUID'91, Berlin, 18 - 21 June 1991, 281 (1991).

[32] H. Seppä, M. Kiviranta, A. Satrapinski, L. Grönberg, J. Salmi and I. Suni, IEEE Trans. Appl. Supercond 3, 1816 (1993).

[33] H. Seppä, M. Kiviranta, and L. Grönberg, IEEE Trans. Appl. Supercond. 5, 3248 (1995).

[34] H. Seppä, M. Kiviranta, V. Virkki, L. Grönberg, J. Salonen, P. Majander, I. Suni, J. Simola, and A. Oittinen, Extended Abstracts of 6th International Superconductive Electronics Conference (ISEC'97), Braunschweig, Germany, 20 June 1997 (1997).

[35] M. Kiviranta, J.S. Penttilä, J. Hassel, A. Virtanen, and H. Seppä, Supercond. Sci. Technol. 17, 285 (2004).

[36] R. Behr, J. Kohlmann, J.-T.B.M Janssen, P. Kleinschmidt, J.M. Williams, S. Djordjevic, J.-P. Lo-Hive, F. Piquemal, P.-O. Hetland, D. Reymann, G. Eklund, C. Hof, C., B. Jeanneret, O. Chevtchenko, E. Houtzager, H.E. van den Brom, A. Sosso, D. Andreone, J. Nissila, and P. Helistö, IEEE Trans. Instrum. Meas. 52, 524 (2003).

[37] J. Hassel, P. Helistö, L. Grönberg, H. Seppä, J. Nissilä, and A. Kemppinen, "Stimulated Power Generation in es-SIS Junction Arrays", Submitted to IEEE Trans. Instrum. Meas.

[38] P. Helistö, J. Nissilä, K. Ojasalo, J.S. Penttilä, and H. Seppä, IEEE Trans. Instrum. Meas. 52, 533 (2003).

[39] J. Nissilä, K. Ojasalo, A. Kemppinen, A. Manninen, J. Hassel, P. Helistö, and H. Seppä, Conference of Precision Electromagnetic Measurement, London, 27. June - 2. July 2004, Conference Digest, 158 (2004).

[40] A. Kemppinen, Masters Thesis, Helsinki University of Technology (2004).

[41] D.V. Averin, and K.K. Likharev, J. Low Temp. Phys. 62, 345 (1986).

[42] D.V. Averin, and K. K. Likharev, in Mesoscopic Phenomena in Solids, eds. B.L. Altshuler, P.A. Lee, and R.A. Webb, Elsevier, Amsterdam, 173 (1991).

[43] T.A. Fulton, G.J. Dolan, Phys. Rev. Lett. 59, 109 (1987).

[44] A.N. Korotkov, and M. Paalanen, Appl. Phys. Lett. 74, 4052 (1999).

[45] A.B. Zorin, Phys. Rev. Lett. 76, 4408 (1996).

[46] R.J. Schoelkopf, P. Wahlgren, A.A. Kozhenikov, P. Delsing, and D.E. Prober, Science 280, 1238 (1998).

[47] M.A. Sillanpää, L. Roschier, and P. Hakonen, cond-mat/0402045 (2004).

[48] H. Seppä, Phys. B 284-288, 1804 (2000).

[49] A.N. Korotkov, Appl. Phys. Lett. 72, 3226 (1998).

[50] J. Delahaye, J. Hassel, R. Lindell, M. Sillanpää, M. Paalanen, H. Seppä, and P. Hakonen, Phys. E 18, 15 (2003).

[51] Sh. Kogan, Electronic Noise and Fluctuations in Solids, Cambridge University Press, Cambridge (1996).

[52] J. Engberg, and T. Larsen, Noise Theory of Linear and Nonlinear Circuits, John Wiley & Sons, New York (1995).

Errata

In the published versions of articles following misprints have been found.

P2

1. Section IIB: "$1/2\pi fC \gg 2\pi fL_J$" should be "$1/2\pi fC \ll 2\pi fL_J$".

2. Section IIB: "...transmission line inductance for the length of one junction is larger than the capacitive reactance, i.e. $s\ell_0 \gg 1/2\pi fC$, where ..."
should be
"...transmission line inductive reactance for the length of one junction is larger than the capacitive reactance, i.e. $2\pi fs\ell_0 \gg 1/2\pi fC$, where ...".

3. Section IIC: "...the initial and boundary conditions are $I(x,0) = 0$ for $0 < x < L$ and $I(0,t) = I(0,L) = I_0$."
should be
"...the initial and boundary conditions are $I(x,0) = 0$ for $0 < x < L$ and $I(0,t) = I(L,t) = I_0$."

4. Section IIC: Eq. (10) should stand

$$I(x,t) = I_0 \left(1 - \sum_{n=0}^{\infty} \frac{4}{(2n+1)\,\pi} \sin \frac{(2n+1)\,\pi x}{L} \exp\left(-(2n+1)^2 \frac{t}{\tau_{RC}}\right)\right)$$

5. SectionIID: In the last sentence ($j_c^{-4} f^{-1}$) should stand ($j_c^{-2} f^{-1}$).

P3

Eq. (1) should stand

$$\frac{\tau P^{1/2}}{(U\Delta I_n)^{5/2}} \propto f^{-5}$$

Reprinted with permission from the publisher. PUBLICATION 1
In: IEEE Transactions on Instrumentation and Measurement 2001. Vol. 50, No. 2, pp. 195–198.

SIS Junctions with Frequency Dependent Damping for a Programmable Josephson Voltage Standard

Juha Hassel, Heikki Seppä, Leif Grönberg, *Member, IEEE,* and Ilkka Suni

***Abstract*—Experimental and computational results on programmable Josephson junction array (JJA) chips based on superconductor-insulator-superconductor (SIS) junctions are presented. Implications of circuit design and fabrication process on the performance are discussed. We introduce a method to decrease the attenuation of the pump microwave. Different designs are compared, suggesting that 1 V chips operating at the third constant voltage step with 70 GHz pump frequency can be produced with our process.**

***Index Terms*—Josephson arrays, programmable voltage standard, superconductor-insulator-superconductor (SIS) junctions.**

I. Introduction

TO GENERATE ac voltage with a Josephson voltage standard rapid switching between constant voltage steps is required. This is possible only when the junctions are damped. Programmable Josephson junction arrays (JJAs) are often based on intrinsically damped superconductor-normal conductor-superconductor (SNS) or superconductor-insulator-normal conductor-insulator-superconductor (SINIS) junctions [1], [2]. A problem is the high attenuation of the pump signal, which limits the length of the array branch. It also makes it difficult to use voltage steps $V = nf/K_J$ with $n > 1$. Therefore, longer arrays are needed. In this paper, we present a solution based on externally shunted SIS junctions, which can overcome this problem.

The basic idea is to shunt junctions in a frequency dependent way so that damping is provided at the plasma frequency (typically about 25 GHz) and at lower frequencies to enable rapid transitions between steps but not at the pump frequency. A solution is to use a notch filter at the pump frequency in series with the shunt resistor [3], [4]. This was found, however, too cumbersome to realize. A simpler solution is to use an inductance in series with the resistor. This may degrade the stability of constant voltage steps, so a compromise has to be found.

Based on our earlier studies, we believe that a programmable voltage standard can be used as a precise ac reference at low frequencies at least up to 1 kHz, if the bias system and the signal filtering are optimized [3].

II. Circuit Design and Fabrication

The process used in circuit fabrication is modified from the one used in SQUID processing [5]. The conductors are 250 nm to 450 nm thick sputtered niobium layers and the dielectric material is SiO_2 grown with Plasma Enhanced Chemical Vapor Deposition (PECVD) method. The resistor material is molybdenum. The Josephson junctions are Nb/Al/AlO_x/Nb-sandwiches bounded with Nb_2O_5 formed by anodization. By varying the oxidization pressure, critical current densities from 10 A/cm^2 to 100 A/cm^2 have been obtained. With the junction size of (20 μm) $\times$ (50 μm) critical currents can be varied from 100 μA to 1000 μA.

III. Experimental Results

The design of the test components is shown in Fig. 1(a). The junctions on different wafers had critical currents of about 100 μA, 200 μA, and 800 μA. The capacitance is about 45 pF and the shunt resistance is about 0.25 Ω. The junctions form a microstripline and they are connected to the resistors via Nb strips. The strips and the resistor have an inductance of about 3 pH per junction.

The measurements with one or a few series connected junctions showed that stable constant voltage steps were obtained for components having $I_c \lesssim 200$ μA. The step amplitudes also followed the Bessel-function dependence $\Delta I_n = 2I_c|J_n(AI_1)|$, where I_1 is proportional to the pump current and A is a constant depending on the shunt impedance and the frequency. The components with $I_c \approx 800$ μA, showed voltage steps, the amplitudes of which were suppressed with small pump amplitudes. With larger amplitudes stable steps were obtained also in this case. The measurements with arrays having a larger number of junctions showed, however, that the voltage steps are rounded (Fig. 2).

To determine the attenuation of the pump signal, the step amplitudes of the first and last junctions in a series of 260 junctions were measured as a function of the input pump power. The result was fitted to the function $\Delta I_n = 2I_c|J_n(B\sqrt{P_{\rm in}})|$. The attenuation was then determined from the ratio of constants B for the first and the last junction. An example of the measured step amplitudes is shown in Fig. 3(a) for a shunted array and in Fig. 3(b) for an unshunted array. The attenuation of the former varied between 13 dB and 14 dB, i.e., about 0.05 dB per junction (15 dB/cm). For the latter, it was between 2.3 dB and 2.7 dB, i.e., about 0.01 dB per junction (3 dB/cm).The damping of a shunted 308 junction branch is therefore about 15 dB, which explains the rounding of the steps.

IV. Linear Circuit Model

To study the pump attenuation, a linear model was constructed, as shown in Fig. 4(a). The circuit simulation software

Manuscript received May 14, 2000; revised October 30, 2000.

J. Hassel and H. Seppä are with VTT Automation, Measurement Technology, 02044 VTT, Finland.

L. Grönberg and I. Suni are with VTT Electronics, Microelectronics, 02044 VTT, Finland.

Publisher Item Identifier S 0018-9456(01)02612-2.

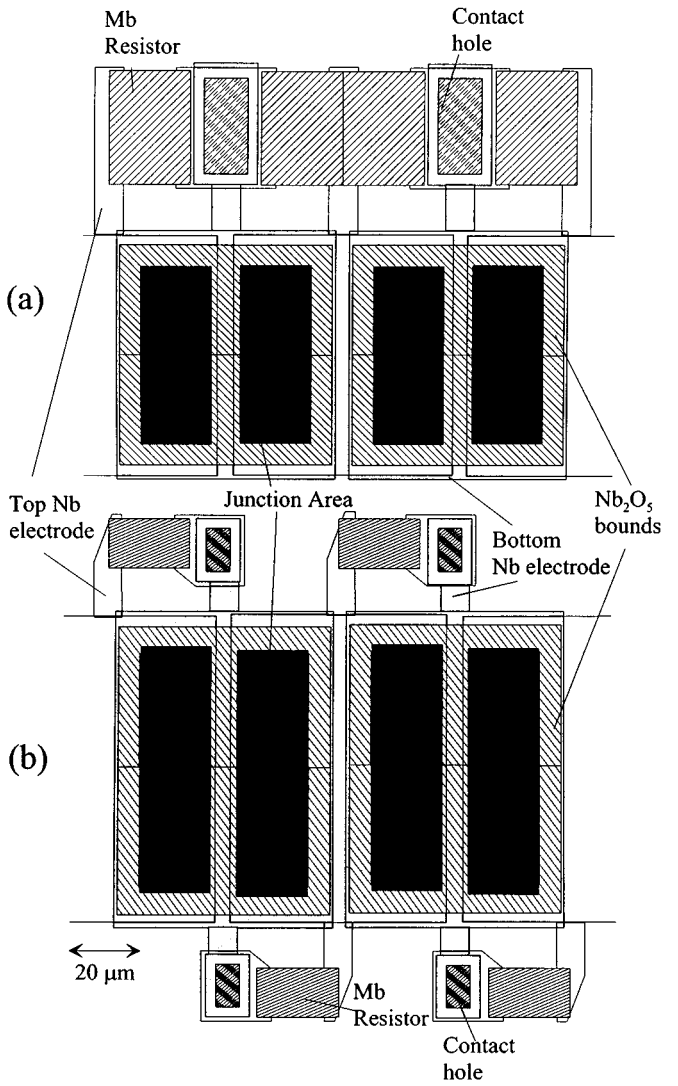

Fig. 1. Piece of microstripline including Josephson junctions. (a) Design of test structures. Parameters: $I_c = (100 - 800)\ \mu$A, $C = 45$ pF, $R = 0.25\ \Omega$, $L = 3$ pH. (b) Design used to minimize the pump microwave attenuation. $I_c = (200 - 500)\ \mu$A, $C = 63$ pF, $R = 0.31\ \Omega$, $L = 4$ pH. For both (a) and (b) the dielectric thickness of the microstripline is about 1 μm.

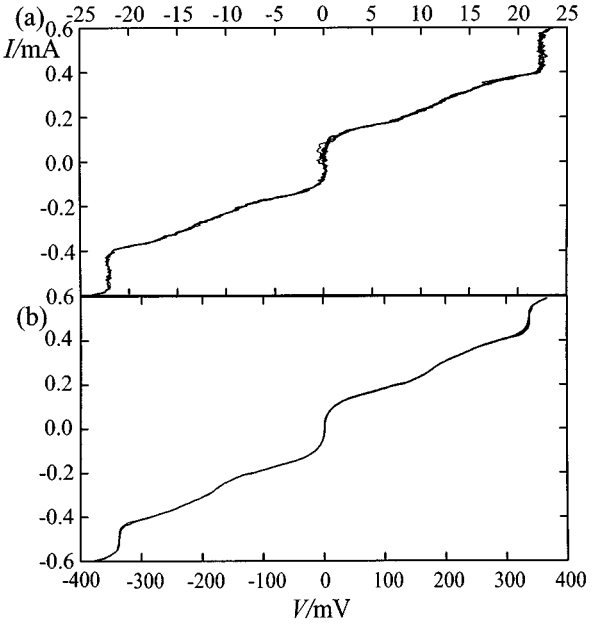

Fig. 2. Current–voltage characteristics with 70 GHz pump. (a) Branch of 154 junctions. (b) 2310 junctions divided in eight branches.

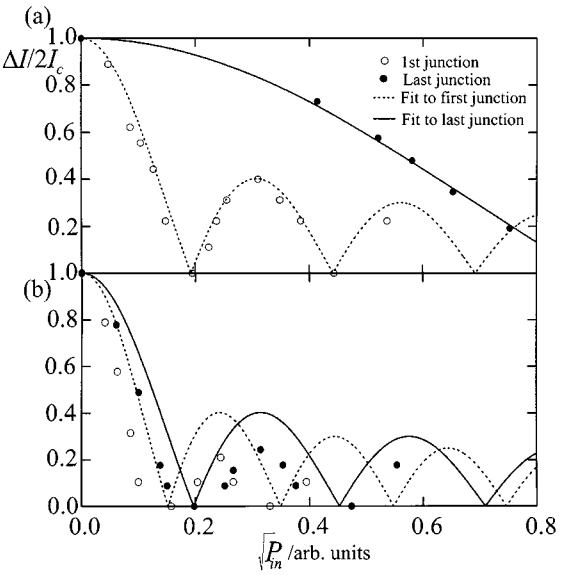

Fig. 3. Amplitudes of the zeroth constant voltage steps as a function of pump power for (a) shunted array branch and (b) unshunted array branch. Both have 260 junctions. According to the Bessel fit the attenuation of the line is about 0.05 dB per junction in (a) and 0.01 dB per junction in (b). In (b), the step amplitudes are suppressed from the theoretical values probably due to the external noise.

Aplac was used to compute the propagating amplitude at different points of the transmission line. The Josephson junctions were described as capacitors and the Josephson coupling was neglected in this analysis. The transmission line sections were described with the built-in model of Aplac. The model of [6] was used in calculating the parameters of superconducting microstriplines. In Fig. 5(a) it is shown the voltage amplitude against the ground plane at the first and last junctions computed with the parameters of the system of Fig. 4(a). The resulting attenuation is then found to be about 13 dB, which is in good agreement with the measured value (about 12 dB excluding the attenuation independent of the shunt circuits).

V. Decreasing the Attenuation

An alternative design is shown in Fig. 1(b). The linearized model of it is shown in Fig. 4(b). The most important difference is that the shunts of sequential junctions are at the opposite sides of the microstripline. With this arrangement the shunt resistors do not form a transmission line, and the series inductance blocks the pump signal from the resistor more efficiently. It was also found essential to maximize Z_2/Z_0 in Fig. 4(b). Making the resistor narrower by decreasing the sheet resistance of molybdenum increases Z_2. Increasing the width of the junction decreases Z_0.

The resulting voltage amplitudes at different junctions in an array branch of 154 junctions are shown in Fig. 5(b). Owing to the extra circuits the characteristic impedance of the transmission line is frequency-dependent. By varying the input and

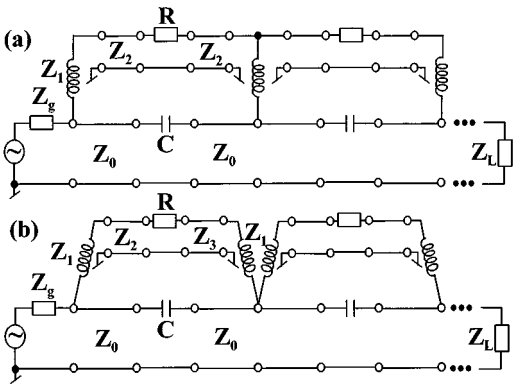

Fig. 4. Linearized models used in pump attenuation computation. (a) The circuit of Fig. 1(a). The parameters used in analysis are $Z_0 = 2.6\ \Omega$, $Z_1 = 17.2\ \Omega$, $Z_2 = 6.0\ \Omega$, $C = 45$ pF, $R = 0.25\ \Omega$ and $Z_g = Z_L = 2.6\ \Omega$. (b) The circuit of Fig. 1(b). The parameters are $Z_0 = 2.0\ \Omega$, $Z_1 = 17.2\ \Omega$, $Z_2 = 13.5\ \Omega$, $Z_3 = 7.3\ \Omega$, $C = 63$ pF, $R = 0.31\ \Omega$ and $Z_g = Z_L = 1.6\ \Omega$. The strips connecting the junctions and shunts are drawn as inductors for clarity, but they are also modeled as microstriplines.

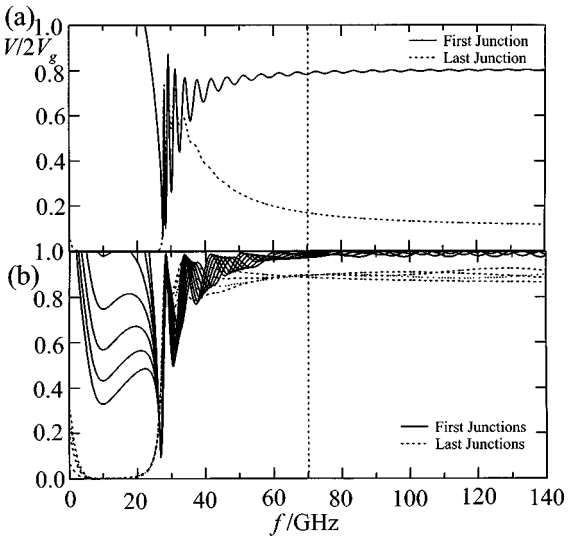

Fig. 5. The propagating amplitude at the beginning and the end of a transmission line. (a) Model 4(a), 308 junctions. (b) Model 4(b), 154 junctions. In (b), the voltage at different points of the transmission line is shown. The ripple indicates standing wave, which has been minimized at 70 GHz.

output impedances $Z_g = Z_L$, an optimum was found and thus no standing wave occurs at 70 GHz. The attenuation due to shunt resistors is then found to be about 1.0 dB for 154 junctions. If the shunt-independent part of the attenuation is 0.01 dB per junction (the measured value), the total attenuation of 154 junctions is about 2.5 dB and 218 junctions about 3.6 dB. Using 15 branches of 154 (218) junctions the output voltage is 1.00 V (1.42 V) if the pump frequency is 70 GHz.

We suppose that the pump attenuation in the unshunted circuits follows mainly from the dielectric loss of the microstripline. PECVD SiO_2 layers deposited at low temperatures can contain up to a few percent hydrogen. Vibrational modes of Si-H bonds are known to produce strong absorption bands in the infrared regime. They are also likely to cause excess losses at microwave frequencies. Processing SiO_2 at a higher temperature may therefore decrease the attenuation.

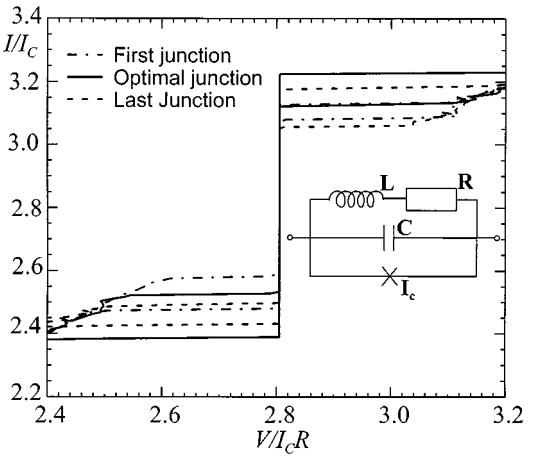

Fig. 6. Simulated I–V curves of junctions at different positions of the transmission line, when its total attenuation is 3.6 dB. The junction is described with the lumped model shown in the inset, the parameters of which are those given in Fig. 1(b). Here $I_c = 500\ \mu$A. The effective step amplitude without the resistance scatter is found to be about $0.4I_c = 200\ \mu$A.

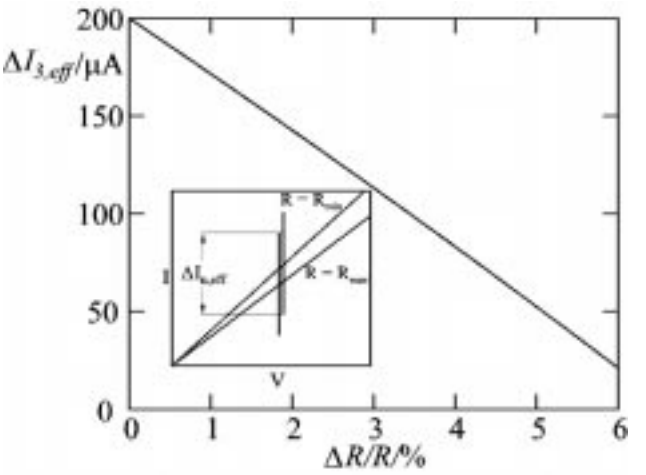

Fig. 7. Effective step amplitude of the third step as a function of resistance scatter. It is assumed that $R = 0.31\ \Omega$, $\Delta I_{3,0} = 200\ \mu$A, and $V_0 = 434\ \mu$V in (1).

VI. Simulations

To find the I–V curve of the system, simulations including the nonlinear effects were executed. The lumped model is shown in the inset of Fig. 6. The value $L = 4$ pH was found by fitting the impedance parallel to the Josephson tunnel element to the value obtained numerically from the linearized model of Fig. 4(b). The effective amplitude $\Delta I_{n,\,\mathrm{eff}}$ of the nth constant voltage step is defined so that all the junctions in the array are biased at the step simultaneously, if the bias current $I_b = I_m \pm (1/2)\Delta I_{n,\,\mathrm{eff}}$. Here $I_m = (nf)/(K_J R)$ is the center of the step. The amplitude depends on the critical current, the attenuation and the resistance scatter. Also hysteresis decreases $\Delta I_{n,\,\mathrm{eff}}$, since a junction may be at the resistive branch of the I–V curve if it is biased so that the voltage is not unambiguous. In Fig. 6 it is shown an I–V curve of the third voltage step for different junctions in the same junction branch assuming that the attenuation is 3.6 dB. It is shown that the step amplitude is in this case $0.4I_c \approx 200\ \mu$A. To include the resistance scatter,

simple geometrical analysis (see inset of Fig. 7) shows that the effective amplitude is obtained from

$$\Delta I_{n,\mathrm{eff}} = \Delta I_{n,0} - \frac{2V_0 \Delta R}{R^2} \tag{1}$$

where V_0 is the voltage of the step (in this case about 434 μV) and $\Delta I_{n,0}$ is the amplitude if the scatter is zero. The error is defined as $\Delta R = (R_{\max} - R_{\min})/2$. Fig. 7 shows $\Delta I_{3,\mathrm{eff}}$ as a function of $\Delta R/R$ in this case.

Too large a critical current or an inductance may destroy the stability of constant voltage steps. To find tolerances for the design, simulations with $L = 4$ pH and different values of I_c were executed. Stable constant voltage steps appeared at least if $I_c \lesssim 1$ mA. To estimate the effect of inductance, simulations with $I_c = 500$ μA were executed as a function of L. Stable steps were obtained at least if $L \lesssim 20$ pH.

VII. Conclusions

We have shown that with appropriate circuit design and fabrication it is possible to realize a programmable voltage standard based on SIS junctions, which works at the third constant voltage step with 70 GHz pump frequency. With the linearized model,we were able to predict the measured attenuation caused by the shunt circuits. A proper way to damp junctions frequency-dependently was found to enable both rapid switching between constant voltage steps and low pump signal attenuation.

References

[1] C. A. Hamilton, S. P. Benz, C. J. Burroughs, and T. E. Harvey, "SNS programmable voltage standard," *IEEE Trans. Appl. Superconduct.*, vol. 7, pp. 2472–2475, June 1997.

[2] H. Schulze, R. Behr, F. Mueller, and J. Niemeyer, "Nb/Al/AlO_x/AlO_x/Al/Nb Josephson junctions for programmable voltage standards," *Appl. Phys. Lett.*, vol. 73, pp. 996–998, Aug. 1998.

[3] J. Hassel, H. Seppä, and M. Kiviranta, "A new way to realize a programmable voltage standard," *Physica B*, vol. 284–288, pp. 2073–2074, June 2000.

[4] J. Hassel, H. Seppä, L. Grönberg, I. Suni, and P. Helistö, "Progress in Josephson voltage standard development," in *Conf. Dig., CPEM 2000*, Sydney, Australia, May 2000, pp. 399–400.

[5] H. Seppä, M. Kiviranta, A. Satrapinski, L. Grönberg, J. Salmi, and I. Suni, "Coupled dc SQUID with low 1/f noise," *IEEE Trans. Appl. Superconduct.*, vol. 3, pp. 1816–1819, Mar. 1993.

[6] W. H. Chang, "The inductance of a superconducting microstripline," *J. Appl. Phys.*, vol. 50, pp. 8129–8134, Dec. 1985.

Reprinted with permission from the publisher.
In: Review of Scientific Instruments 2003. Vol. 74, No. 7, pp. 3510–3515.

Optimization of a Josephson voltage array based on frequency dependently damped superconductor–insulator–superconductor junctions

Juha Hassel[a] and Heikki Seppä
VTT Information Technology, Microsensing, P.O. Box 1207, 02044 VTT, Finland

Leif Grönberg and Ilkka Suni
VTT Information Technology, Microelectronics, P.O. Box 1208, 02044 VTT, Finland

(Received 10 September 2002; accepted 9 April 2003)

We have developed a programmable Josephson voltage standard based on an array of superconductor–insulator–superconductor junctions. The junctions are damped by an external frequency-dependent shunt circuit, which allows operation at Shapiro steps with $n>1$. We derive optimization criteria for the design parameters for a fast and stable array with low power consumption. An array able to generate $1.0\,V_{RMS}$ ac voltage signal with sub-ppm accuracy is experimentally demonstrated. Theoretically it is also shown that a fast programmable 10 V array can be realized. © *2003 American Institute of Physics.* [DOI: 10.1063/1.1582381]

I. INTRODUCTION

The programmable Josephson voltage standards have been a subject of extensive research recently. From the circuit technologies the intrinsically damped junctions, superconductor–normal conductor–superconductor (SNS)[1,2] or superconductor–insulator–normal conductor–insulator–superconductor (SINIS),[3,4] have been found appropriate for the purpose. We have studied the applicability of superconductor–insulator–superconductor (SIS) junctions. Although the low damping of SIS junctions introduces some difficulties and limitations, we show that they can be overcome and that the junction properties can even be utilized. For SNS and SINIS standards it has been found difficult to use constant voltage steps $V_n=nf/K_J$, with $n>1$ in long arrays due to large microwave attenuation. We show that this is not the case with SIS junctions and a proper circuit design. The basic idea is to damp the junction dynamics with an external frequency dependent shunt circuit in such a way that the pump signal is not attenuated, but the lower frequencies up to the plasma frequency are. In our case the pump signal f is blocked from the shunt resistor by an inductance thus preventing the attenuation.

We derive theoretically optimal design parameters for an externally shunted SIS (es-SIS) array producing a desired output voltage. The properties of interest are stability, power consumption and speed of an array, the last one of which determines the accuracy of ac voltage generation. We consider here especially the limitations in a binary type bias setup.[5–8] We also demonstrate experimentally that an es-SIS Josephson junction array (JJA) generates 1 V output using only 2310 junctions and the step $n=3$.

[a]Author to whom correspondence should be addressed; electronic mail: juha.hassel@vtt.fi

II. THEORY

A. Voltage step quality

For stable operation and immunity to extrinsic noise it is preferable to have large step amplitudes (i.e., the range of low-frequency bias current Δi_n, with which a quantized voltage is reproduced). In this section we derive design criteria for a junction so that the step amplitudes would not be suppressed from the theoretical maximum. For SIS junctions, in which the impedance parallel to the tunnel element is essentially capacitive reactance at the pump frequency f, this can be written as[9]

$$\Delta i_n = 2\left| J_n\left(\frac{i_1}{\beta_c\Omega^2}\right)\right|, \tag{1}$$

where i_1 is the pump amplitude in units of critical current, $\beta_c=2\pi I_c R^2 C/\Phi_0$ is the Stewart–McCumber parameter, and $\Omega=(\Phi_0/I_cR)f$ is the dimensionless angular pump frequency, and J_n is the Bessel function of the first kind. A requirement for Eq. (1) to hold is that the pump frequency needs to exceed the plasma frequency of the junction, which is conventionally given as[9]

$$\Omega\sqrt{\beta_c}\gtrsim 3. \tag{2}$$

To find the effect of the external shunt circuit, simulations using the resistively shunted junction model were executed assuming that the circuit is a linear LR circuit parallel to the tunnel element and its capacitance C. The system of differential equations describing the circuit is

$$\begin{aligned}\beta_c\frac{d^2\Phi}{d\tau^2}+i_s+\sin\Phi &= i_0+i_1\sin\Omega\tau,\\ \beta_L\frac{di_s}{d\tau} &= \frac{d\Phi}{d\tau}-i_s,\end{aligned} \tag{3}$$

where Φ is the superconducting phase difference across the junction, $\tau=(2\pi I_cR/\Phi_0)t$ the dimensionless time, β_L

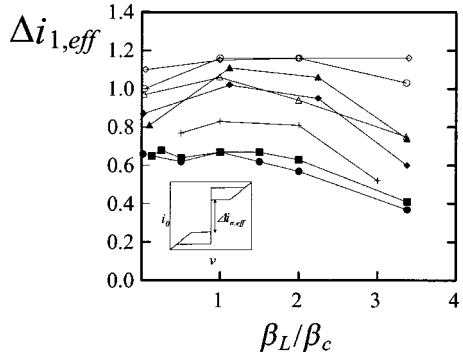

FIG. 1. The effective step height as function of β_L/β_c for different β_c and Ω. The definition is given in the inset. Parameters for: (open diamond) $\Omega=1.5$, $\beta_c=2.0$, (open circle) $\Omega=1.5$, $\beta_c=3.0$, (solid triangle) $\Omega=1.5$, $\beta_c=4.0$, (cross) $\Omega=1.5$, $\beta_c=6.0$; (solid square) $\Omega=1.5$, $\beta_c=8.0$, (open triangle) $\Omega=2.5$, $\beta_c=3.0$, (solid diamond) $\Omega=2.5$, $\beta_c=4.0$, and (solid circle) $\Omega=2.5$, $\beta_c=8.0$. Effective step amplitude is not more than about 25% smaller than the maximum amplitude if $\beta_c \lesssim 4$ and $\beta_L \lesssim 2\beta_c$.

$=2\pi LI_c/\Phi_0$ the dimensionless inductance, i_0 the low frequency bias current, i_1 the amplitude of the microwave pump, and i_s the current flowing through the shunt resistor. All currents are scaled to the critical current I_c. The flux quantum is $\Phi_0=h/2e$.

A series of simulations was executed varying β_c, β_L, and Ω. The pump amplitude was selected so that the step amplitude was maximized according to Eq. (1). It was found that, if Eq. (2) is roughly valid, the step amplitudes follow Eq. (1) as long as β_L is not too large. With large β_L the amplitudes were found to be suppressed. However, the reduced step amplitude was not found to be the upper limit of β_L, but rather the increased hysteresis within the step due to reduced damping. By hysteresis we mean here that for a given bias current i_0 there coexist two solutions. One reproduces the quantized voltage, and another one has ohmic current–voltage ($I-V$) characteristics. This is not acceptable, since it limits the ability to select a desired quantized output voltage by tuning i_0. We can require that the effective step amplitude (i.e., the range of constant voltage step, where the voltage is a single-valued function of i_0) is at least about 75% of the total step amplitude. The data from simulated $I-V$ curves for the first constant voltage step indicates that sufficient criteria are (see Fig. 1)

$$\beta_c \lesssim 4, \tag{4}$$

$$\beta_L \lesssim 2\beta_c. \tag{5}$$

These were found to be sufficient criteria for higher steps as well.

In addition, second kind of hysteresis appears if the steps become overlapping. This is prevented if (see, e.g., Ref. 1)

$$\Omega \gtrsim 1. \tag{6}$$

Inequalities Eqs. (2) and (4)–(6) now give the regime, where the simple Bessel function dependence of Eq. (1) can be used in case of an LR shunted junction.

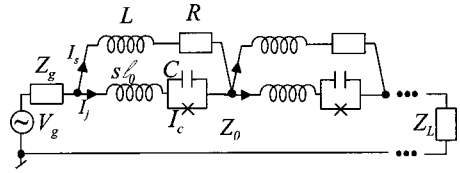

FIG. 2. The circuit equivalent of a JJA branch.

B. Microwave attenuation

Minimizing microwave attenuation in the array is essential, since all junctions need to be biased with sufficiently similar pump amplitude. Here we try to derive a simple analytic expression for the attenuation in circuit of Fig. 2. We assume that at pump frequency the current is mainly coupled capacitively through the junction, i.e., $1/2\pi fC \gg 2\pi fL_J$, where $L_J=\Phi_0/2\pi I_c$ is the Josephson inductance. We also assume that the transmission line inductance for the length of one junction is larger than the capacitive reactance, i.e., $s\ell_0 \gg 1/2\pi fC$, where s is the length occupied by one junction and ℓ_0 is the transmission line inductance per unit length. We further assume that the inductive reactance of the shunt circuit is larger than the shunt resistance, i.e., $2\pi fL \gg R$. The loss due to shunt resistors in a junction is $P_{\text{loss}}=(1/2)RI_s^2$, where I_s is the current flowing through the shunt resistor. The propagating power $P_{\text{prop}}=(1/2)Z_0I_j^2$, where I_j is the current flowing through the junction and Z_0 is the transmission line impedance. The ratio of current through the shunt I_s and the current through the junction I_j is approximately the inverse ratio of inductances, i.e., $I_s/I_j \approx s\ell_0/L$. Summing up, one can write the attenuation per junction in the form

$$\alpha=\frac{1}{2}\frac{P_{\text{loss}}}{P_{\text{prop}}}=\alpha_c\left(\frac{s\ell_0}{L}\right)^2, \tag{7}$$

where $\alpha_c=\frac{1}{2}R/Z_0$ describes the attenuation of the line composed of the Josephson junctions with pure resistive damping. The factor $(s\ell_0/L)^2$ indicates the improvement in transmission line attenuation due to the frequency dependent damping of the Josephson junction.

With the design parameters of our arrays $R=0.31\,\Omega$, $Z_0=2.6\,\Omega$, $L=4\,p$H, $l_0=14$ nH/m, $s=33\,\mu$m, Eq. (7) yields $\alpha=0.80\times10^{-4}$ Np per junction (0.007 dB per junction) in excellent agreement with the result obtained with the numerical model, where parasitic elements due to practical realization were also included and the approximations used here were not imposed.[10] It is noteworthy that $\alpha_c \approx 0.06$ Np per junction (0.5 dB per junction), i.e., inductance decreases the attenuation markedly.

C. ac calibration accuracy

A proposed setup for ac generation with a programmable JJA is introduced in Ref. 11, where the errors originating from different parts of the setup are considered. The accuracy limit set by the JJA itself is due to finite speed of switching between different constant voltage steps. To find an estimate for this, we assume that the switching transients are slow compared to Josephson and plasma oscillations. Therefore we assume that the state of the JJA moves from

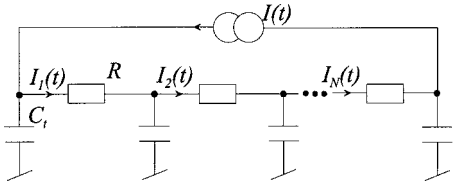

FIG. 3. The distributed RC_t circuit used in analyzing the device speed. $I(t)=0$ for $t<0$ and $I(t)=I_0$ for $t\geq 0$.

one step to another via the resistive branch of the $I-V$ curve. During the transient, the Josephson junctions and the transmission line look like a distributed RC_t circuit as shown in Fig. 3. The transmission line capacitance per junction is C_t. The bias current of ith junction obeys the following equation:

$$\frac{dI_i}{dt}=\frac{1}{RC_t}(I_{i+1}-2I_i+I_{i-1}). \tag{8}$$

If the difference of currents of subsequent junctions is assumed small, the above equation can be rewritten as[12]

$$\frac{\partial I(x,t)}{\partial t}=\frac{\Delta x^2}{RC_t}\frac{\partial^2 I(x,t)}{\partial x^2}, \tag{9}$$

where Δx is the distance between two junctions. This is a heat equation. If the transition is, say, from the zeroth step to another step, the initial and boundary conditions are $I(x,0)=0$ for $0<x<L$ and $I(0,t)=I(0,L)=I_0$, where L is the length of the array and I_0 is the bias current. The solution is

$$I(x,t)=I_0\left(1-\frac{1}{L}\sum_{n=0}^{\infty}\frac{4}{\pi(2n+1)}\sin\frac{(2n+1)\pi x}{L}\times\exp\left[-(2n+1)^2\frac{t}{\tau_{RC}}\right]\right), \tag{10}$$

where $\tau_{RC}=(RC_t/\pi^2)(L/\Delta x)^2$. The sum term describes the transient, and the slowest decaying term is $n=0$. Therefore the time constant is

$$\tau_{RC}=\frac{RC_t}{\pi^2}N^2, \tag{11}$$

where $N=L/\Delta x$ is the number of junctions.

To find out, how large an error in ac voltage generation this corresponds to, we assume binary,[5,6] or equivalent, bias setup, where the voltage consists of superposition of voltage pulses of the form shown in Fig. 4. For simplicity, we assume that the transients are exponentially shaped having a time constant τ_{RC} and that the rise time is the same for all transients. By Fourier transforming the generated signal and defining that the correct voltage is the first frequency component, we arrive to the relative error

$$\frac{\Delta V_1}{V_1}=2\pi^2(f_s\tau_{RC})^2, \tag{12}$$

where f_s is the frequency of generated ac signal. This is independent of the bit count or the exact shape of the generated signal. An issue is, of course, filtering out higher harmonics, but a method for doing this with high accuracy is presented in Ref. 11. For example, if one needs to generate 1 kHz signal with an accuracy of 0.1 ppm the array needs to have $\tau_{RC}\lesssim 70$ ns.

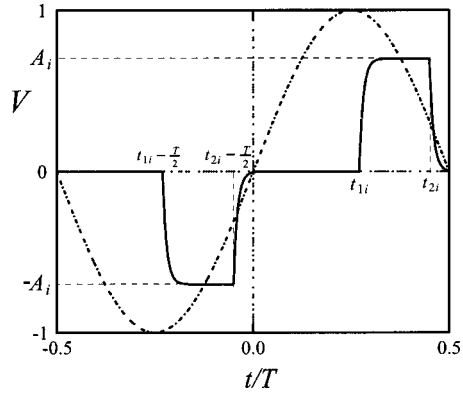

FIG. 4. The digitized sine wave generated with a JJA is assumed to be a superposition of pairs of pulses consisting of exponential edges. The amplitudes $A_i=nf/K_J$ are obtained with fundamental accuracy. The effects of transients, timing and filtering have to be analyzed in order to predict the error of the resulting rms value of the ac voltage.

D. Optimization of the array design

Here we describe a process, where the results of the three previous sections are utilized to find optimal parameters for a circuit design. The objective is to provide design values for a given output voltage so that the step amplitudes and the ac accuracy of the device are maximized using as low microwave power as possible. The criteria to be satisfied are those of Eqs. (2) and (4)–(6). We assume that the junctions are in a microstripline geometry (width w and height h), whose impedance can be written as

$$Z_0=\sqrt{\frac{\mu_0}{\epsilon_0\epsilon_r}}\frac{h}{w}, \tag{13}$$

i.e., the effect of fringe fields and the kinetic inductance is neglected. We further assume that the surface of the transmission line is completely consumed by the Josephson junctions, i.e., that the space needed for junction boundaries etc. is negligible. We also assume that there are N junctions of width w and length s divided into M branches, each of which has an own pump microwave input.

The output voltage is

$$U_{\text{out}}=nN\Phi_0 f, \tag{14}$$

where n is the step number.

The pump current needed to maximize the amplitude of a given voltage step is

$$I_n=2\pi k_n\Phi_0 f^2 C\approx 2\pi(1+n)\Phi_0 f^2 C, \tag{15}$$

where $k_n\approx 1+n$ is the argument, which maximizes the nth Bessel function. This follows from Eq. (1). The power propagating at the microstriplines is $P_{\text{in}}=\frac{1}{2}Z_0 I_n^2 M$,

$$P_{\text{in}}=M\rho(1+n)^2 hws^2, \tag{16}$$

where $\rho=2\sqrt{\mu_0/\epsilon_0\epsilon_r}\pi^2\Phi_0^2 f^4 c_s^2$, and $c_s=C/ws$ is the capacitance per unit area.

The critical current density j_c is maximized so that the constraint set by Eq. (2) is satisfied. This leads to $\Omega\sqrt{\beta_c}=3$ [or equivalently $\sqrt{j_c/c_s}=(f/3)\sqrt{2\pi\Phi_0}$]. For a given fabrication process this is done by selecting a proper tunnel barrier thickness. The critical current is given as $I_c=j_c ws$. The amplitude of the nth step I_{cn} is approximately $(4/\pi\sqrt[3]{n})I_c$, i.e.,

$$I_{cn}=4\frac{j_c ws}{\pi\sqrt[3]{n}}, \tag{17}$$

which follows from Eq. (1) and properties of Bessel functions.

To minimize the attenuation per junction [Eq. (7)], the inductance should be maximized under the constraint set by Eq. (5), which can also be expressed as $L=2R^2C$ in the limiting case. Using also the definition of Ω, Eq. (13), and $\ell_0\approx\mu_0(h/w)$, the attenuation can be given as

$$\alpha=\sqrt{\mu_0^3\epsilon_0\epsilon_r}\left(\frac{\Omega j_c}{2\Phi_0 f}\right)^3\frac{1}{c_s^2 h s^3}.$$

The attenuation depends on $\Omega=3/\sqrt{\beta_c}$ [see Eq. (2)], and thus β_c should be maximized. According to Eq. (4) $\beta_c=4$ and thus $\Omega=1.5$. The total attenuation of all junctions in a branch [see Eq. (7)] can now be written as

$$\alpha_{\mathrm{tot}}=\frac{N}{M}(\kappa h s^3+\alpha_d s), \tag{18}$$

where $\kappa=(3j_c/4\Phi_0 f)^3\sqrt{\mu_0^3\epsilon_0\epsilon_r}/c_s^2$ and the second term is added to account for the dielectric attenuation, which is α_d per unit length.

If the current at the entrance of a branch is I_n as given by Eq. (15), it will be $I_n\exp[-\alpha_{\mathrm{tot}}]$ at the end of the branch. Using the properties of Bessel functions and Eq. (1), it can be found that a tolerable variation in pump current along a branch is about $2\pi\Phi_0 f^2 C$, i.e., we must require that $I_n-I_n\exp[-\alpha_{\mathrm{tot}}]<2\pi\Phi_0 f^2 C$. Using Eq. (15) we can now write

$$\alpha_{\mathrm{tot}}\lesssim\ln\left(1+\frac{1}{n}\right). \tag{19}$$

The requirement for the attenuation becomes stricter as n increases. From Eqs. (18) and (19) it follows that

$$\frac{N}{M}(\kappa h s^3+\alpha_d s)\lesssim\ln\left(1+\frac{1}{n}\right). \tag{20}$$

If we assume that $n\geqslant 3$ then an approximation $\ln(1+1/n)\approx 1/n$ can be used.

The array speed can be given, since τ_{RC} in Eq. (11) is (using $C_t=\epsilon_0\epsilon_r ws/h$, $R=\Phi_0 f/j_c ws\Omega$ and $\Omega=1.5$)

$$\tau_{RC}=\gamma N^2\frac{1}{h}, \tag{21}$$

where $\gamma=(2/3\pi^2)\Phi_0 f\epsilon_0\epsilon_r/j_c$.

The Eqs. (14), (16), (17), and (21) yield the quantities of interest U_{out}, P_{in}, I_{cn}, and τ_{RC} as functions of the design parameters, i.e., dimensions w, s, and h, step number n, the number of junctions N, and the number of branches M. These have to be selected so that Eq. (20) is satisfied. The other parameters j_c, ρ, κ, and γ are constant for a given fabrication process and a pump frequency. One should also remember that dimensions w and s should be selected so that the self-induced magnetic fields do not suppress the critical current, i.e., w, $s\lesssim 2\lambda_J$, where λ_J is the Josephson penetration depth (see, e.g., Ref. 12).

To quantify the above results, for our process, values $j_c\approx 3\times 10^5\ \mathrm{A/m^2}$ and $c_s\approx 0.05\ \mathrm{F/m^2}$ and $\epsilon_r\approx 6$ apply. For $f=70\ \mathrm{GHz}$, this leads to $\rho\approx 7.8\times 10^{14}\ \mathrm{W/m^4}$, $\kappa\approx 1.5\times 10^{16}\ \mathrm{l/m^4}$, and $\gamma\approx 1.7\times 10^{-21}\ \mathrm{sm}$. The measured value of dielectric attenuation is $\alpha_d\approx 5.8\ \mathrm{Np/m}$ (see Sec. III). From $\lambda_J\approx 50\ \mu\mathrm{m}$ it follows that $w=100\ \mu\mathrm{m}$ can be used.

If we choose $U_{\mathrm{out}}=1\ \mathrm{V}$ and $n=3$, it follows that $N=2300$ [Eq. (14)]. If we require that $I_{cn}=700\ \mu\mathrm{A}$, it follows that $s=27\ \mu\mathrm{m}$ [Eq. (17)]. Choosing $M=2$ it follows from Eq. (20) that $h\lesssim 350\ \mathrm{nm}$. To minimize the ac error $h=350\ \mathrm{nm}$ is selected, from which it follows that $\tau_{RC}=26\ \mathrm{ns}$ [Eq. (21)]. The power propagating in the transmission lines is $P_{\mathrm{in}}\approx 0.6\ \mathrm{mW}$ [Eq. (16)], which should be easily available from a Gunn diode.

If we instead choose $U_{\mathrm{out}}=10\ \mathrm{V}$, $n=3$, $I_{cn}=300\ \mu\mathrm{A}$, $M=8$, similar reasoning leads to $N=23\,000$, $s=11\ \mu\mathrm{m}$, and $h=2.0\ \mu\mathrm{m}$. The input power is $P_{\mathrm{in}}=2.4\ \mathrm{mW}$ and $\tau_{RC}=450\ \mathrm{ns}$. Comparing the two examples demonstrates the decreasing speed and step amplitude as a function of increasing output voltage. At one volt level it is relatively easy to design an array able to generate 1 kHz ac voltage with a sub-ppm accuracy, whereas for a 10 V array this is significantly more difficult.

To further study interdependencies of speed, output voltage, step amplitudes, and power consumption, we assume now for simplicity that $\alpha_d=0$, i.e., that the attenuation is only due to shunt resistors. Then, based on Eq. (20), we can set

$$M=\left(\frac{U_{\mathrm{out}}}{\Phi_0 f}\right)\kappa h s^3,$$

where also Eq. (14) was used. Using Eqs. (14), (16), (17), and (21) one can now derive the relation

$$\tau_{RC}=\frac{\sqrt{6}(n+1)}{512\sqrt{\pi}n^{7/6}}(c_r\Phi_0 j_c\lambda_J)^{-2}\frac{(U_{\mathrm{out}}I_{cn})^{5/2}}{f\sqrt{P_{\mathrm{in}}}}, \tag{22}$$

where it has also been set at $w=2\lambda_J$ and defined as $c_r=(\epsilon_r\epsilon_0\mu_0)^{-1/2}$. We conclude that the speed of the optimized array is fundamentally dependent on the required output voltage U_{out}, the step amplitude I_{cn}, and the required microwave power P_{in} according to Eq. (22). In order to double the output voltage without affecting the speed, the microwave power has to be more than 30 times higher, which is difficult in practice. One way around the problem might be to use a higher pump frequency. Since τ_{RC} is proportional to $j_c^{-4}f^{-1}$, and according to Eq. (2) $j_c\propto f^2$, the time constant is proportional to $1/f^5$.

III. DESIGN, FABRICATION, AND EXPERIMENTS

The fabrication process is based on the VTT superconducting quantum interference device process with some modifications.[13] The main processing steps are as follows:

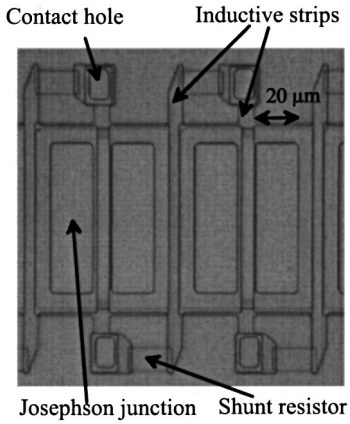

FIG. 5. Photographs of a piece of a transmission line.

(1) deposition and patterning of the first niobium layer to form the lower conductor in the microwave stripline. (2) Deposition of a 1 μm thick silicon oxide layer by the plasma enhanced chemical vapor deposition (PECVD) method. This insulator forms the stripline dielectric. (3) Deposition of the trilayer that forms the Josephson junctions. This multilayer structure has the following constitution: niobium–aluminum–aluminum oxide–niobium. The aluminum oxide forms the tunneling barrier which determines the critical current density of the Josephson junction. The area of the Josephson junction is delineated by anodizing the surrounding area. The layer formed by anodization is an insulator at low temperatures. This layer also forms the dielectrics of the capacitors. The lower niobium layer of the multilayer structure also forms the top conductor of the stripline. (4) Deposition and patterning of a 300 nm thick insulator layer (PECVD silicon oxide). (5) Deposition and patterning of the top niobium layer. This layer connects the upper electrode of the Josephson junction. (6) Deposition and patterning of the molybdenum layer. This forms the resistors. (7) Deposition and patterning of the passivation layer (PECVD silicon oxide).

The junction chains were a realization of the circuit in Fig. 2. A photograph of a piece of the chain is shown in Fig. 5. The inductance required for the microwave blockade is a narrow strip, which is in series with the shunt resistor.

Other circuit elements were designed in a conventional manner using standard microwave design methods. The 70 GHz pump is brought to the array chip via an *E*-type waveguide. The transition from the waveguide to the chip is provided by a finline taper, in which a design of PTB is used (see e.g., Ref. 14). After the transition there is a power distribution network, which divides the signal into branches. In the design there were 16 branches each having 154 or 218 junctions. The arrays can be binary biased with a four bit arrangement. Extra short circuits at low frequencies are inhibited by dc block capacitors. The series connection of branches at low frequencies is provided via low-pass filters.

Measured $I-V$ curves are shown in Fig. 6. The microwave power is selected so that the amplitude of the third constant voltage step is maximized. One can see, that the voltage steps appear flat within the given resolution. Larger resolution dc measurements have also shown that 1 V output voltage is reproducible within 1 nV with our arrays.[15] For

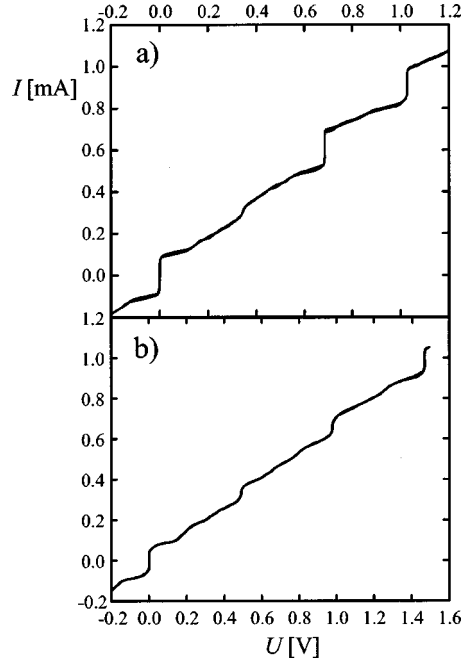

FIG. 6. Measured $I-V$ curves of: (a) 2310 and (b) 3270 junctions divided into 15 branches of equal length. The amplitude of the 70 GHz pump signal is chosen so that the amplitude of the third constant voltage step is approximately maximized. The components have critical currents of about 300 μA.

our current array design (3270 junctions) it follows from Eq. (12) that a signal of 1 kHz can be generated with an accuracy of about 0.1 ppm. However, it should be noticed that the our arrays are not yet optimal, so following the lines of Sec. II D, this could be improved.

The attenuation in a junction line was measured by measuring the amplitude of the superconducting step for the first and the last junctions in an array branch of 260 junctions (Fig. 7). A fit of the form $\Delta I_0 = 2I_c|J_0(B_i\sqrt{P_{\text{in}}})|$, where I_c is the critical current of the junction, P_{in} is the input power to the array, and B_i is a constant. By determining the constants B_i for the first and last junctions the attenuation can be calculated. The result was about 0.01 dB per junction in good agreement with the calculated result (0.007 dB, see Sec.

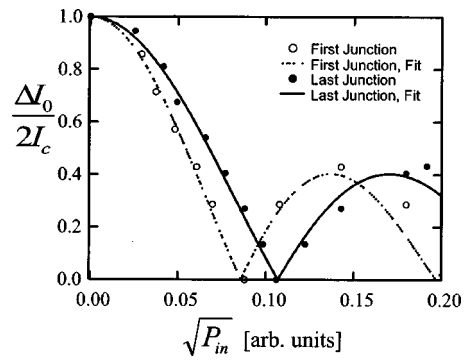

FIG. 7. The result of the attenuation measurement with an array branch having 260 junctions. Shown is the amplitude of the superconducting step as a function of the microwave amplitude at the input. The amplitude is measured for the first and last junctions of the array. Based on the fit of the zeroth Bessel function of the first kind, the attenuation is about 0.01 dB per junction.

II B). The attenuation was also experimentally found to be a significant factor in improving the voltage step quality. In Ref. 10 we studied an array design having much higher attenuation, and the resulting constant voltage steps were much more rounded, especially for the steps with index $n>1$.

In addition to the total attenuation of the transmission lines, the dielectric attenuation was measured with the method described in Ref. 16. In particular, different dielectric deposition processes were compared. The result was that the lowest attenuation (0.5 dB/cm) was obtained with the standard process (PECVD silicon oxide 50 nm at 120 °C+950 nm at 180 °C). This corresponds to the attenuation of about 0.002 dB per junction, so the main contribution comes from the shunt resistors in our current design.

ACKNOWLEDGMENTS

The authors wish to thank Panu Helistö, Mikko Kiviranta, and Jari Penttilä for constructive discussions. The project was partially funded by MIKES (Centre for Metrology and Accreditation).

[1] S. P. Benz, C. A. Hamilton, C. J. Burroughs, and T. E. Christian, Appl. Phys. Lett. **71**, 1866 (1997).
[2] V. Lacquaniti, S. Gonzini, S. Maggi, E. Monticone, R. Steni, and D. Andreone, IEEE Trans. Appl. Supercond. **9**, 4245 (1999).
[3] H. Schulze, R. Behr, F. Müller, and J. Niemeyer, Appl. Phys. Lett. **73**, 996 (1998).
[4] H. Schulze, F. Müller, R. Behr, J. Kohlmann, and J. Niemeyer, IEEE Trans. Appl. Supercond. **9**, 4241 (1999).
[5] C. A. Hamilton, C. J. Burroughs, S. P. Benz, and J. R. Kinard, IEEE Trans. Instrum. Meas. **46**, 224 (1997).
[6] C. J. Burroughs, S. P. Benz, T. E. Harvey, and C. A. Hamilton, IEEE Trans. Appl. Supercond. **9**, 4145 (1999).
[7] S. P. Benz and C. A. Hamilton, Appl. Phys. Lett. **68**, 3171 (1996).
[8] S. P. Benz, C. A. Hamilton, C. J. Burroughs, and T. E. Harvey, IEEE Trans. Instrum. Meas. **48**, 266 (1999).
[9] R. L. Kautz and R. Monaco, J. Appl. Phys. **57**, 875 (1985).
[10] J. Hassel, H. Seppä, L. Grönberg, and I. Suni, IEEE Trans. Instrum. Meas. **50**, 195 (2001).
[11] P. Helistö, J. Nissilä, K. Ojasalo, J. S. Penttilä, and H. Seppä, IEEE Trans. Instrum. Meas. (in press).
[12] T. C. Van Duzer, *Principles of Superconducting Devices and Circuits* (Prentice–Hall, Englewood Cliffs, NJ, 1999).
[13] H. Seppä, M. Kiviranta, A. Satrapinski, L. Grönberg, J. Salmi, and I. Suni, IEEE Trans. Appl. Supercond. **3**, 1816 (1993).
[14] F. Müller, R. Pöpel, J. Kohlmann, J. Niemeyer, W. Meier, T. Weimann, L. Grimm, F.-W. Dünschede, and P. Gutmann, IEEE Trans. Instrum. Meas. **46**, 229 (1997).
[15] R. Behr *et al.*, IEEE Trans. Instrm. Meas. (in press).
[16] H.-G. Meyer, G. Wende, L. Fritzsch, F. Thurm, M. Schubert, F. Müller, R. Behr, and J. Niemeyer, IEEE Trans. Appl. Supercond. **9**, 4150 (1999).

Reprinted with permission from the publisher.
In: Fast Josephson Arrays for Voltage and Impedance Metrology. Conference of Precision Electromegnetic Measurements. London, 27 June - 2 July 2004.
Conference Digest, pp. 154–155

FAST JOSEPHSON ARRAYS FOR VOLTAGE AND IMPEDANCE METROLOGY

Juha Hassel[1], Leif Grönberg[2], Panu Helistö[1] Heikki Seppä[1], Jaani Nissilä[3] and Antti Kemppinen[3]

[1]VTT Information Technology, Microsensing, P.O. Box 1207, 02044 VTT, Finland
[2]VTT Information Technology, Microelectronics, P.O. Box 1206, 02044 VTT, Finland
[3]MIKES (Centre For Metrology and Accreditation), P.O. Box 239, 00181 Helsinki, Finland

Abstract

We introduce an optimized Josephson double array generating two independent voltages up to 1.5V using only one microwave input. Such an array, combined with the quantum Hall resistance, can provide the basic traceability for an electricity metrology laboratory from DC voltage to capacitance. We describe the array and present preliminary experimental results from DC measurements. Extending the output voltage up to 10V is discussed.

Introduction

Conventional undamped Josephson array voltage standards (JAVS) have nowadays a well established position as the primary source of DC voltage utilizing Josephson-relation $V=Nf/K_J$ where f is the bias frequency, $K_J \approx 2e/h$ is the Josephson constant and N is an integer. Realization of AC voltage using quantum voltage standards has been a subject of wide interest recently [1-4], since it would provide a more direct link from constants of nature to RMS voltage than the conventional methods. Development of fast programmable Josephson arrays has made it possible to tune the output voltage rapidly enough to generate AC waveforms. Furthermore, using two independent AC sources with adjustable amplitudes and phases it is possible to construct a bridge for comparisons of arbitrary impedances. This would, for example, make it possible to create link from quantum Hall resistance to the capacitance. In this Paper we present the design and preliminary experimental results from a new programmable JAVS suitable for the purpose. The array can be driven with a single microwave source, and it generates two independent, floating output voltages.

Array design and fabrication

The arrays are fabricated using externally shunted Superconductor-Insulator-Superconductor -junctions and the standard VTT niobium trilayer process. The devices are designed using frequency dependent damping of the junctions[1] and they are optimised to maximise stability and speed, while power consumption is simultaneously minimised[2]. In the optimum, these parameters are tied together approximately by

$$\frac{tP^{1/2}}{U\Delta I_n} \propto f^{-5}, \qquad (1)$$

where τ is the risetime of the signal, P the input power, U the output voltage, ΔI_n the step width and f the pump frequency .

In addition to optimal array design it is crucial to have a fabrication process, which reproduces junction and shunt parameter values to a high level of accuracy. We improved the temperature control during junction oxidization to reduce critical current spread across the wafer. It is found especially crucial to have a sufficiently low variation in shunt resisance values within a chip [1]. In our case the criterion for shunt resistances is about $DR = (R_{max} - R_{min})/2R < 6\%$. Here R_{max} and R_{min} are the values of the largest and smallest resistances on the chip and R is the average value. The scatter of film thickness was reduced by using the sputter in a mode, where the sample stage oscillates during the deposition. Furthermore, experiments with test structures measuring the effect of both film thickness and litography indicated that we are

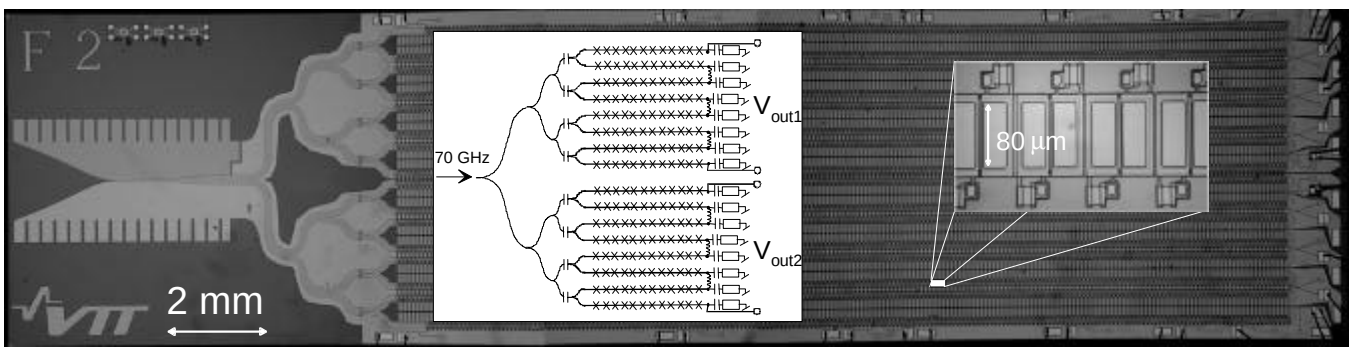

Fig. 1. A photograph of an array componet. The left inset shows a schematic of the two arrays as well as the microwave input and terminations. The right inset shows a magnification of a piece of junction chain with junctions (large rectangles) and shunts.

able to fabricate the required few thousand shunt resistors with *DR* as low as a few per cent.

The array is shown in Fig. 1. The fin-line taper provides transition from an E-band waveguide to the microstripline network, which delivers the power into two subarrays. Both subarrays have 3315 junctions in series divided into eight microwave branches. The maximum output voltages of the subarrays are about 0.5V, 1.0V and 1.5V for f » 70 GHz using the first, the second and the third voltage step (n = 1,2,3), respectively. The array bias is arranged in an 8 bit configuration. Furthermore a wiring of the voltage ratio 3124/2209 » $\sqrt{2}$ is provided for resistance-reactance calibrations. The critical current of the junctions is about 700 μA. The estimated time constant of the array is 100 ns, which enables generation of 1 kHz signal with a relative uncertainty of about 0.1 ppm. In our preliminary DC measurements we have obtained flat constant voltage steps up to n = 3 within measurement resolution of a few hundred nanovolts. An example IV plot at n = 2 is shown in Fig. 2. The calculated microwave power consumption of the array is 3.4 mW with n = 3 excluding the mismatch from the waveguide transition. From the experiment, the estimated total microwave power consumption was about 5 mW.

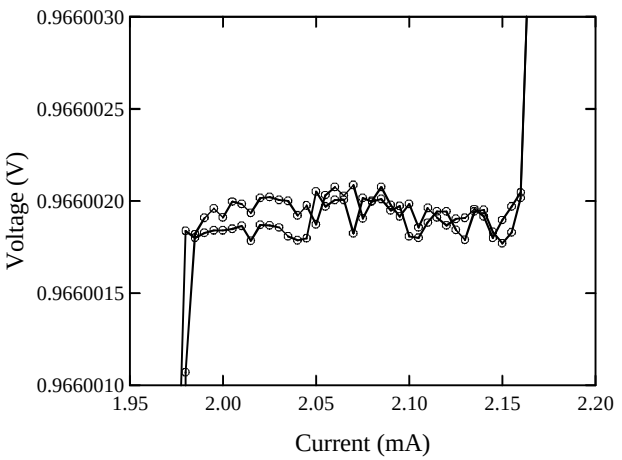

Fig 2 : Current-voltage plot of one half of the double-array chip at n = 2.

We are also currently developing 10V programmable JAVS components. First arrays have been fabricated and experimental results are expected soon.

AC and Impedance calibrations

A method to generate an accurate AC voltage with a fast Jospehson array is presented in [5]. The latest version of the electronics is described in [6]. In brief, the idea is to generate a square wave by switching between voltage steps $+n$ and $-n$ and to compare the first Fourier component to a reference source (e.g. a calibrator) using a lock-in amplifier as a null indicator.

Using the double array, a bridge circuit can be devised using a single microwave input. One possible bridge realisation is shown in Fig. 3. One array provides a stable current for the bridge. A tunable arm is used to provide a virtual ground. The second Josephson voltage is used to find the exact ratio of the two impedances. Fine-tuning the ratio can be done with frequency.

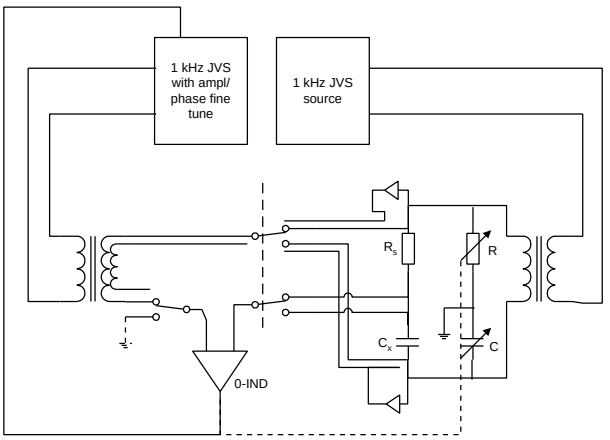

Fig 3 : Impedance bridge with two phase-locked AC Josephson voltage references.

References

[1] J. Hassel, H. Seppä, L. Grönberg, and I. Suni, "SIS Junctions with Frequency Dependent Damping for a Programmable Josephson Voltage Standard", *IEEE Trans. Instrum. Meas.*, Vol. 50, No.2, pp. 195-198, April 2001.

[2] J. Hassel, H. Seppä, L. Grönberg, and I. Suni, "Optimization of a Josephson Voltage Array Based on Frequency Dependently Damped Superconductor-Insulator-Superconductor Junctions", *Rev. Sci. Instrum.*, Vol. 74, No. 7, pp. 3510-3515, July 2003.

[3] C.J,. Burroughs, S.P. Benz, T.E. Harvey, and C.A. Hamilton, "1 Volt DC Progammable Josephson Voltage Standard", ", *IEEE Trans. Appl. Supercond.* Vol. 9, No. 2, June 1999

[4] H. Schulze, G. Müller, R. Behr, J. Kohlmann, J. Niemeyer, and D. Balashov, "SINIS Josephson Junctions for Programmable Josephson Voltage Standard Circuits", *IEEE Trans. Appl. Supercond.* Vol. 9, No. 2, June 1999

[5] P. Helistö, J. Nissilä, K. Ojasalo, J.S. Penttilä, and H. Seppä, "AC Voltage Standard Based on a Programmable SIS Array", *IEEE Trans. Instrum. Meas.* Vol. 52, No. 2, pp. 533-536, April 2003.

[6] J. Nissilä, K. Ojasalo, A. Kemppinen, A. Manninen, J. Hassel, P. Helistö, and H. Seppä, "Development of a Quantum AC Voltage Standard Based on Externally Shunted Josephson Arrays", this conference.

Reprinted with permission from the publisher.
In: IEEE Transactions on Applied Superconductivity 2001.
Vol. 11, No. 1, pp. 260–262.

PUBLICATION 4

Analysis of the Bloch Oscillating Transistor

Juha Hassel and Heikki Seppä

Abstract— **The Bloch-oscillating transistor (BOT) is a device where coherent Cooper-pair current in mesoscopic Josephson junctions can be controlled with single-electron tunneling from the base-electrode. We show computational results on the single-junction BOT (sj BOT). Also the double-junction BOT (dj BOT) is introduced. An approximate formula of the device noise temperature is also presented.**

Keywords— **Bloch oscillations, Single electron tunneling, Mesoscopic tunnel junctions**

I. Introduction

THE Bloch-oscillations in mesoscopic Josephson junctions are coherent charge oscillations, which are a manifestation of the band structure in the energy dispersion relation[1-4]. They occur if a junction is sufficiently free of dissipation. However, also in an undamped junction Zener-tunneling tends to drive the system to higher energy bands thus suppressing the oscillations and some dissipation is needed to return the junction to the lowest energy band[5]. In this paper we analyze properties of the Bloch-oscillating transistor (BOT)[6], where the dissipation for the junction is provided in a controlled way by a normal tunnel junction. The computational results for the single junction BOT (sj BOT) show that the characteristics are qualitatively similar to those of a Bipolar Junction Transistor. Furthermore, we present an idea of the double-junction BOT (dj BOT), which is probably easier to realize.

II. Model

Two circuit equivalents of the sj BOT are shown in Fig. 1. They are equivalent up to the definition of voltages. The junction #1 connects the normal conducting base electrode to the superconducting island. The junction #2 connects the superconducting island to the superconducting emitter electrode. Its Josephson coupling energy $E_J = \Phi_0 I_{cs}/2\pi$ is assumed to be of the same order as the charging energy $E_c = e^2/2C_2$. The impedance of the LR-circuit at the collector electrode is assumed large so that the charging effects have to be taken into account when computing single-electron tunnel rates of the junction #1 [7]. The large-impedance environment also guarantees that the quasicharge is a good variable describing the state of the junction #2.

The model used in simulations is presented in detail in [6]. The junction #2 is described with the theory of Bloch-oscillations[1]. The energy versus quasicharge Q_2 is shown in Fig. 2. A band structure is formed, where the magnitude of the gap between two lowest bands is

Manuscript received September 19th 2000

The Authors are with the VTT Automation, Measurement Technology, VTT Technical Research center of Finland, P.O. Box 02044 VTT, Finland (telephone and e-mail of the corresponding author +358-9-456-6771, Juha.Hassel@vtt.fi)

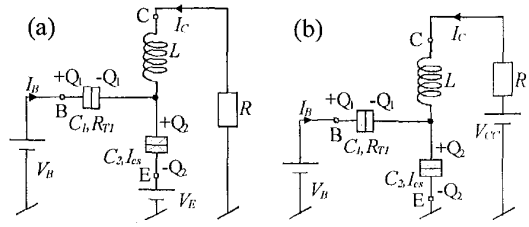

Fig. 1. The equivalent circuit of the sj BOT. The circuits in (a) and (b) are equivalent up to the definition of voltages.

the Josephson coupling energy E_J. Between higher bands the gap is assumed zero. If the junction is initially at the lowest energy band and charge is driven to or from the island via the collector, the quasicharge is increased until it reaches the value $|Q_2| = e$. At that point either a Cooper pair tunnels through the junction so that Q_2 changes from $+e$ to $-e$ or from $-e$ to $+e$, or Zener-tunneling occurs so that the charge continuously increases to $|Q_2| > e$. The probability of Zener-tunneling is $P^Z_{0\leftrightarrow 1} = \exp\left[-(\pi e^3/8\hbar I_C C)\,(E_J/E_C)^2\right]$[5]. We assume for the discussion that if $|Q_2| < e$ the junction is at the lowest (zeroth) energy band, if $e < |Q_2| < 2e$, it is at the first band etc.

It is assumed that no single electron tunneling [8] occurs through junction #2. This is justified if $e^2/2C_2 \lesssim 2\Delta$, where Δ is the superconducting gap, i.e. that the junction is biased below the gap at the voltage range of interest. The single electron tunnel-resistance R_{T1} is assumed constant. This is justified if the junction #1 is biased above the gap most of the time, which occurs if $e^2/2C_1 \gtrsim \Delta$. It is therefore preferable that $C_1 < C_2$. The tunnel rates are obtained using the Orthodox Theory with the local rule.

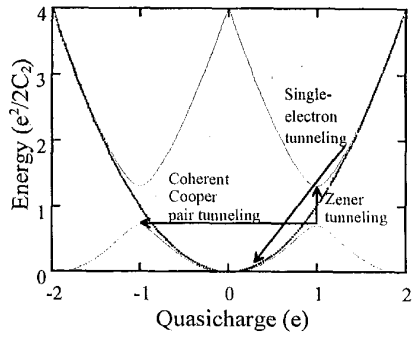

Fig. 2. The energy versus quasicharge in a mesoscopic Josephson junction. Different possible transitions are denoted with arrows.

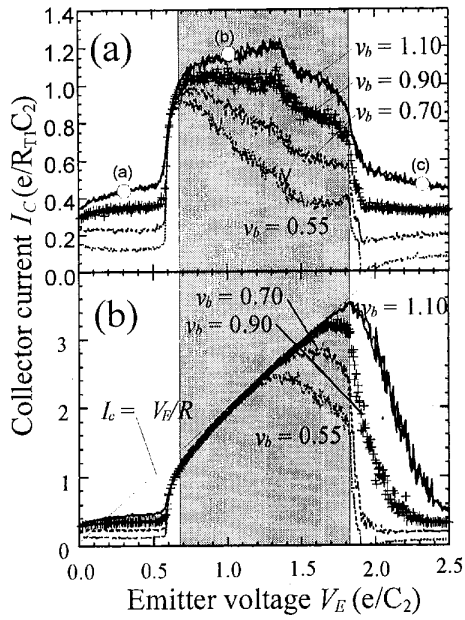

Fig. 3. The collector current as function of the emitter voltage for the connection of Fig. 1 (a). In (b) the Zener-tunneling is neglected.

III. Simulations

The parameter definitions and their values used in simulations are as shown in Table 1.

A set of simulated curves using the bias arrangement of Fig. 1(a) is shown in Fig. 3. The active region, where the Bloch-oscillations occur is shown in gray. The Figs. 3(a) and 3(b) are otherwise similar, but in the latter Zener-tunneling is neglected. In Fig. 3(b) it can be seen, that in the region where Bloch-oscillations occur without dissipation, the Josephson junction acts as a short circuit and the relation $I_C = V_E/R$ is satisfied. However, when Zener-tunneling is turned on (Fig. 3(a)), I_C becomes smaller.

The curves of Fig. 3(a) can be understood by looking at Fig. 4, where the quasicharge Q_2 is shown as a function of time at different bias points. In Figs. 4(a) and (c) the system never reaches the Brillioun zone boundary $|Q_2| = e$, so Bloch oscillations do not occur. In the active region (Fig. 4(b)) one sees Bloch-oscillations interrupted occasionally by Zener-tunneling, which takes the system to the first band $|Q_2| > e$. From there it is returned to the lowest band via single-electron tunneling, the probability of which can be tuned with the base voltage enabling collector current tuning.

TABLE I
Definitions and Values of the Dimensionless Parameters Used in Simulations

Parameter	Definition	Value
c_1	C_1/C_2	0.1
l	$LR_{T1}^2 C_2$	0.26
ε_J	$E_J/(e^2/2C_2)$	0.6
r	R/R_{T1}	0.5
α_t	$h/\pi^2 e^2 R_{T1}$	0.077

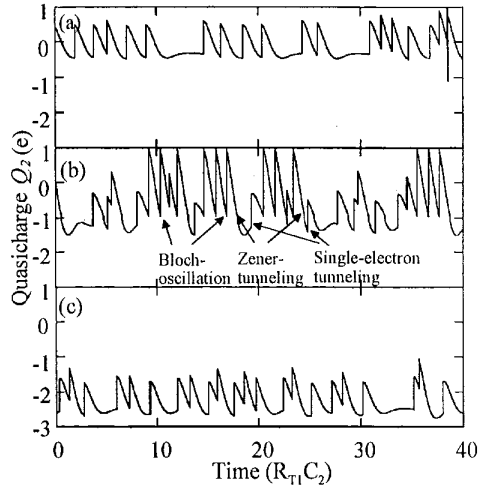

Fig. 4. The quasicharge versus time at bias points denoted in Fig. 3(a).

Fig. 5 shows the characteristics curves with the bias arrangement of Fig. 1(b). It can be seen that the collector current I_C has a plateau at about $V_{CC} \approx 1.8e/C_2$.At this point the BOT operates as an ideal current source. We have also shown that both current and power gain are obtained for a small signal connected at the base electrode[6].

IV. Noise

To approximately understand the noise properties of the BOT, we assume that voltage noise at the input is due to thermal noise from the tunnel resistance R_{T1}, i.e., $e_n = \sqrt{4k_B T R_{T1}}$. We assume that current noise is arising from the shot noise of the tunnel junction, i.e. $i_n = \sqrt{2eI_B} = \sqrt{2e^2 f_B}$, where f_B is the frequency of single-

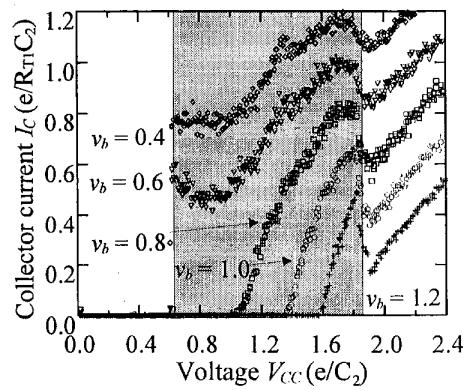

Fig. 5. The collector current as a function of the bias voltage for the circuit of Fig. 1(b).

electron tunneling. We have also assumed here that the subsequent tunnel events are not correlated. The noise temperature is then obtained as

$$T_n = \frac{e_n i_n}{2k_B} = \sqrt{\frac{2TR_{T1}e^2 f_B}{k_B}} \approx \sqrt{\frac{Thf_B}{k_B}} = \sqrt{TT_q}, \quad (1)$$

where the approximate equality assumes that the tunnel resistance R_{T1} is approximately the quantum resistance $h/2e^2$. In the last equality temperature $T_q = hf_B/k_B$ is defined. The noise temperature is smaller than the bath temperature if $T_q < T$.

The optimal input resistance to the device can be similarly estimated as

$$R_{opt} = \frac{e_n}{i_n} \approx 2R_q\sqrt{\frac{T}{T_q}}. \quad (2)$$

The value of f_B is needed for the optimization and it depends on several design parameters, which should be known before the numerical values of T_n and R_{opt} can be obtained.

V. Realization Issues

In the experimental realization of the sj BOT probably the most difficult issue is to implement the required large-impedance environment in order to keep the quasicharge a good variable and to preserve the charging effects essential for the device. For example, if the capacitance C_2 is taken to be 1 fF and the tunnel resistance 34 kΩ, the required inductance is 300 nH, which is very difficult to realize with contemporary technologies. Possible solutions might be the kinetic inductance of a nanotube, a narrow superconducting wire or the inductance of a series array of Josephson junctions. However, a possibility might also be the double junction BOT (dj BOT), shown in Fig. 6. Instead of providing the blockade by a linear circuit, an extra Josephson junction is introduced to the collector electrode. The collective Bloch-oscillations of the two junctions can now be tuned by single-electron tunneling from the base electrode, which according to our belief should result in dynamics similar to those of the sj BOT.

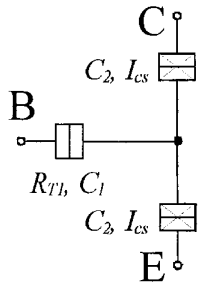

Fig. 6. The equivalent circuit of the double junction BOT.

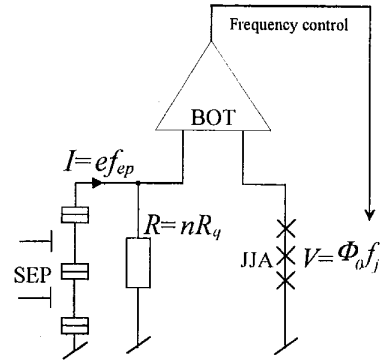

Fig. 7. A schematic of the measurement setup to provide a test bench for the metrological triangle.

VI. Applications

An active area of research today is the realization of the metrological triangle. To date there is no setup, which would serve as the test of its consistency to the level of 10^{-7} or better. One problem is to find a component serving as a preamplifier stage in a measurement similar to that of Fig. 7. There a resistor, whose value can be traced to the quantum resistance, is driven with a current from a single-electron pump (SEP). This is compared to a voltage obtained from a Josephson junction array (JJA). The measurement gives the value of the Klitzing constant.

VII. Conclusions

We have shown that the sj BOT has characteristics that resemble those of a Bipolar Junction Transistor. The realization issues were discussed, and the major difficulty in practice was found to be the large-impedance environment. Therefore an idea of the dj BOT was introduced. Intuitively, it should have properties similar to that of the sj BOT.

References

[1] K. K. Likharev and A. B. Zorin, "Theory of the Bloch oscillations in small Josephson junctions", *J. Low Temp. Phys.* vol. 59, pp. 347-382, Nov. 1985.

[2] L. S. Kuzmin, "Experimental evidence for the autonomous Bloch oscillation in single Josephson Junctions", *IEEE Trans. Appl. Supercond* vol. 3, pp. 1983-1986, Mar. 1993.

[3] A. B. Zorin, "Quantum-limited electrometer based on single Cooper pair tunneling", *Phys. Rev. Lett.* vol. 76, pp. 4408 Jun. 1996.

[4] S. V. Lotkhov, H. Zangerle, A. B. Zorin, T. Weimann., H. Scherer and J. Niemeyer, "Superconducting electrometer based on the resistively shunted Bloch transistor, *IEEE Trans. Appl. Supercond.* vol. 9, 3664-3667, Sep. 1998.

[5] U. Geigenmüller and G. Schön, "Single electron effects and Bloch Oscillations in normal and superconducting tunnel junctions", *Phys. B* vol. 152, pp. 186-202, Aug. 1988.

[6] H. Seppä and J. Hassel, "The Bloch-oscillating transistor", submitted for publication in *Appl. Phys. Lett.*

[7] G.-L. Inglold and H. Grabert, "Finite temperature current-voltage characteristics of ultrasmall Josephson junctions", *Europhys. Lett.* vol. 14, pp. 371-376, Feb. 1991.

[8] D. Averin and K. K. Likharev, "Coulomb Blockade of single-electron tunneling, and coherent oscillations in small tunnel junctions", *J. Low Temp. Phys.* vol. 62, pp. 345-373, Feb. 1985.

Reprinted with permission from the publisher.
In: Science 2003. Vol. 299, pp. 1045–1048.
http://www.sciencemag.org/cgi/content/abstract/299/5609/1045

Low-Noise Current Amplifier Based on Mesoscopic Josephson Junction

J. Delahaye,[1]* J. Hassel,[2] R. Lindell,[1] M. Sillanpää,[1] M. Paalanen,[1] H. Seppä,[2] P. Hakonen[1]†

We used the band structure of a mesoscopic Josephson junction to construct low-noise amplifiers. By taking advantage of the quantum dynamics of a Josephson junction, i.e., the interplay of interlevel transitions and the Coulomb blockade of Cooper pairs, we created transistor-like devices, Bloch oscillating transistors, with considerable current gain and high-input impedance. In these transistors, the correlated supercurrent of Cooper pairs is controlled by a small base current made up of single electrons. Our devices reached current and power gains on the order of 30 and 5, respectively. The noise temperature was estimated to be around 1 kelvin, but noise temperatures of less than 0.1 kelvin can be realistically achieved. These devices provide quantum-electronic building blocks that will be useful at low temperatures in low-noise circuit applications with an intermediate impedance level.

Charge quantization in nanoelectronic devices is expected to lead to a variety of novel components. The most important invention so far is the single-electron transistor (SET) (*1, 2*), which presents an unsurpassed charge sensitivity both in the normal and superconducting states (*3*). Fast SETs are good candidates for readout devices in solid-state quantum computers (*4*). Owing to its small input capacitance, a SET works extremely well with large source impedances, and various applications of SETs have been proposed accordingly (*5*).

Superconducting quantum interference devices (SQUIDs) reach extremely good sensitivity with small-impedance sources (*6*). They are the common choice for measurements trying to approach the standard quantum limit or even attempting to go beyond it. At intermediate impedance values (~1 megohm), both SETs and SQUIDs run into problems due to impedance mismatch that seriously degrades their performance in this regime.

We present an experimental demonstration of a Bloch oscillating transistor (BOT) that is a good device candidate for intermediate impedance levels. The principle of the device (*7*) takes advantage of the interlevel transition probabilities and relaxation phenomena in a quantum Josephson junction (JJ), whereby it is possible to construct a device in which a small current of single electrons is used to generate a substantially larger (super)current of Cooper pairs. In our experiments, a ratio of more than 30 has been reached between these two currents.

The quantum behavior of a superconducting junction is described by the Schrödinger equation (*8*)

$$\frac{d^2\psi}{d(\varphi/2)^2} + \left(\frac{E}{E_C} + \frac{E_J}{E_C}\cos\varphi\right)\psi = 0 \quad (1)$$

where ψ is the wave function describing the state of the JJ, E is energy, φ is the phase difference of the order parameter across the junction, $E_C = e^2/2C$ denotes the Coulomb energy set by the junction capacitance C, and the Josephson coupling energy $E_J = [(h/2\pi)/(2e)]I_C$ is given by the critical current I_C of the junction (h, Planck's constant; e, electronic charge). From this Mathieu equation, energy bands (Fig. 1) should be formed in a similar manner as that formed for electrons in a periodic potential (*9*). In the limit of small Josephson coupling, $E_J/E_C \ll 1$, the width of the lowest band is nearly equal to E_C, and the gap between the first and second bands is given by E_J. In the strongly superconducting case, $E_J/E_C \gg 1$, the bandwidth becomes exponentially small with $\exp[-(8E_J/E_C)^{1/2}]$, and the gap grows as $(8E_JE_C)^{1/2}$. This scenario is valid only if the quantum fluctuations of charge are suppressed by a resistance $R_C > R_Q = h/(2e)^2 \sim 6.5$ kilohms in the immediate vicinity of the junction (R_C, resistance of the environment; R_Q, quantum resistance); i.e., the lead capacitance is blocked off from the junction.

The basic quantum dynamics of a JJ involves Bloch oscillations and Zener tunneling (illustrated in Fig. 1, left). Bloch oscillations take place when the state of the junction adiabatically follows its ground state. Under the influence of a weak current bias, charge Q of the JJ runs along the band, which leads to Bloch reflection at the Brillouin zone boundary (indicated by the horizontal line in Fig. 1, left). This time-correlated tunneling of Cooper pairs is characterized by a frequency $f_B = I/2e$ in a current-biased JJ.

Zener tunneling occurs when the junction leaves its ground state at the Brillouin zone boundary by tunneling through the forbidden energy gap without a change of charge. As the bias current increases, the probability of crossing the band gap by Zener tunneling grows according to the formula ($E_J \ll E_C$)

$$P_{Zener} = \exp(-I_Z/I) \quad (2)$$

where the Zener breakdown current $I_Z = \{(\pi eE_J^2)/[8(h/2\pi)E_C]\}$ (*10*). Thus, at bias currents $I \sim [(\pi E_J)/(16E_C)]I_C$, the probability of Zener tunneling becomes substantial.

Relaxation downward from higher bands can be induced either by an intrinsic mechanism at rate $\Gamma_\downarrow$ or by an external quasiparticle injection Γ_{ext}. If $\Gamma_\downarrow \ll \Gamma_{ext}$, then external, active control of the junction dynamics can be achieved. $\Gamma_\downarrow$ is a strong function of the environmental impedance R_C, and it can be made small when $R_C \gg R_Q$ and when temperature T is small (*11*).

To go beyond the regime of Coulomb

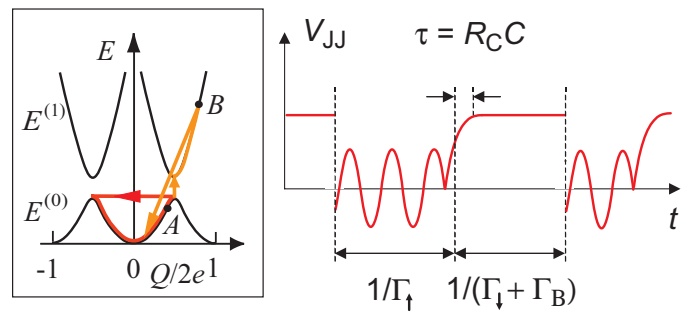

Fig. 1. Basic processes of a BOT in the charge space. (**Left**) Bloch oscillation on the lowest energy band $E^{(0)}$ is denoted by the closed red loop. Occasional Zener tunneling to the second band $E^{(1)}$ is marked by the vertical orange arrow, and the relaxation induced by external quasiparticle injection is indicated by the slanted orange arrow. On the lowest band, the largest possible voltage across the JJ is at point A, given by $V_{JJ}^{max} = dE^{(0)}/dQ|_{max}$; point B denotes the location where $V_{JJ} = V_{bias}$. (**Right**) The voltage of the Josephson junction (V_{JJ}) is displayed as a function of time. The upward and downward tunneling rates, $\Gamma_\uparrow$ and $\Gamma_\downarrow$, as well as the quasiparticle tunneling rate Γ_B are discussed in the text. A moving picture of the working cycle of the BOT can be found in Movie S1.

[1]Low Temperature Laboratory, Helsinki University of Technology, Post Office Box 2200, 02015 HUT, Finland. [2]Microsensing, VTT Information Technology, Post Office Box 1207, 02044 VTT, Finland.

*Present address: High Magnetic Field Laboratory, LCMI/CNRS BP 166, F-38042 Grenoble, France.
†To whom correspondence should be addressed. E-mail: pertti.hakonen@hut.fi

blockade of Cooper pairs (*12*) and to have a supercurrent I flowing in the JJ, the biasing voltage has to satisfy $V_{bias} > dE^{(0)}/dQ|_{max}$, the maximum slope of the lowest band (point A in Fig. 1, left). Then the junction will propagate along the lowest level and perform Bloch oscillations in a periodic manner at f_B. When the current increases, the probability of crossing the band gap by Zener tunneling grows. By properly selecting the ratio of E_J/E_C and the current I, one can tune the probability ratio P_{Zener}/P_{Bloch} so that the state of the junction will tunnel into the second band after a few Bloch oscillations (N on average).

If $V_{bias} < dE^{(1)}/dQ|_{max}$, the maximum slope of the second band, then the state of the JJ will become stationary on the higher band after Zener tunneling. If there is no intrinsic relaxation ($\Gamma_\downarrow \rightarrow 0$), the junction will not relax and it will remain stationary, i.e., Coulomb blockaded on the higher band (e.g., at point B in Fig. 1, left). Consequently, there will be no supercurrent in the JJ before relaxation takes place, owing to externally induced quasiparticle tunneling (indicated by the slanted orange arrow in Fig. 1, left). After relaxation, the junction will again resume the sequence of Bloch oscillations. In this way, a small current of injected quasiparticles results in a $2N$-amplified current of Cooper pairs. The voltage $V_{JJ}(t)$ over the JJ during the principal cycle of the BOT is illustrated in Fig. 1, right: $V_{JJ}(t)$ either varies sinusoidally at f_B or is fixed by V_{bias}. The transition from the former to the latter takes place over a time scale set by the R_CC time constant, whereas the opposite occurs within the electron tunneling time. The simplest realization of the BOT consists of a JJ, a normal metal tunnel junction (NIN), and a compact large resistance R_C (Fig. 2, top).

To estimate the current gain β of the BOT, we can incorporate the relaxation rate due to the base current I_B, $\Gamma_{ext} = \Gamma_B = I_B/e$, into the total downward transition rate [which becomes $\Gamma_\downarrow + \Gamma_B$ (Fig. 1, right)]. Assuming that the time constant for charge relaxation $\tau = R_CC$ can be neglected and that I_B flows only when the JJ is Coulomb blockaded, one may write for the BOT gain ($V_C > e/C$)

$$\beta = \frac{dI_C}{dI_B} = \frac{V_C}{eR_C}\,\frac{1}{\Gamma_\uparrow + \Gamma_\downarrow} \qquad (3)$$

Here I_C denotes the collector current and V_C is the total transport voltage. This equation predicts current gains on the order of 10 at $E_J/E_C = 0.7$ and $T = 0.1$ K. Further details can be found in (*13*).

We also performed more elaborate analysis of the BOT operation based on the application of $P(E)$ theory to the tunneling rates (*14*). The $P(E)$ theory takes into account probabilities of inelastic tunneling processes in a resistive environment where phase fluctuations are governed by R_C, and thereby, it allows us to simulate the operation of the BOT in a more reliable manner than was possible in the first simulations (*7*) based on the orthodox theory. By taking into account both the inelastic Cooper pair and quasiparticle tunneling, we obtained I-V curves similar to the measured ones. Contrary to Eq. 3, these simulations show that a small (on the order of 1 nA, strongly dependent on V_C) base current is needed to reach $\beta \sim 10$. According to our simulations, the maximum current gain takes place around $E_J/E_C \sim 1$, i.e., in a region where the approximations used ($E_J \ll E_C$) start to break down; hence, all the reported simulation results in this study should be considered as indicative only.

For technological reasons, our practical realization of the BOT is slightly different from the scheme shown in Fig. 2. Instead of the NIN junction for injecting quasiparticles, we used a superconductor-normal metal tunnel junction (SIN). This is a somewhat less desirable choice, but manufacturing such a device is nonetheless complicated because it requires a rather elaborate four-angle evaporation process (*15*). The sample structure consists of three elements: an Al-AlO_x-Al JJ [SQUID-like geometry for tunability (*15*)] with tunneling resistance $R_T^{JJ} \cong 5$ kilohms; a superconducting-normal Al-AlO_x-Cu tunnel junction with $R_T^{SIN} \cong 10$ kilohms; and a thin-film Cr resistor of $R_C \cong 50$ kilohms (20 μm long), located within a few μm of the two junctions. A scanning electron micrograph of a manufactured BOT device is displayed in Fig. 2, bottom.

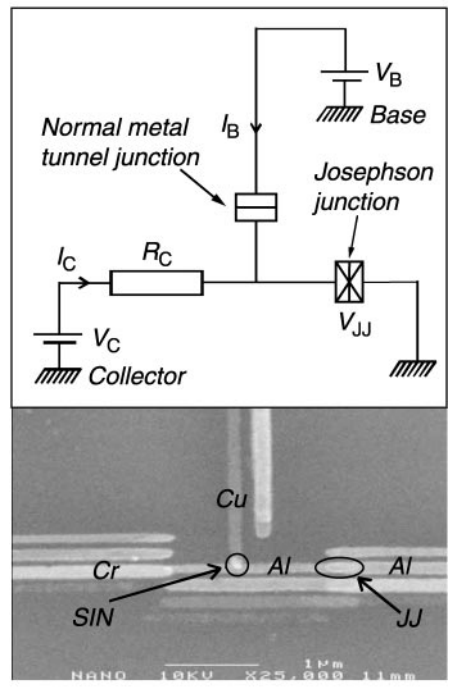

Fig. 2. (**Top**) Implementation of a Bloch oscillating transistor. R_C denotes the collector resistance; bias currents and the corresponding voltage sources are also marked. (**Bottom**) A scanning electron micrograph of a manufactured device in which the normal metal tunnel junction has been replaced by a SIN (Al-AlO_x-Cu) tunnel junction.

The measured I-V characteristics of a hysteretic BOT device, called H, are illustrated (Fig. 3) at a few values of base current I_B. The voltage V_C denotes the full voltage across the Cr resistor and the JJ. The base current to the SIN junction is injected by means of a 100-megohm bias resistor at room temperature, but this biasing effectively becomes a voltage bias owing to the line capacitance of the coaxial line inside the cryostat. The active region, where I_B has a large effect, is small and moves with increasing I_B. The I-V curves are slightly hysteretic with respect to the direction of the voltage ramp; of our three samples, only sample H (*15*) showed hysteresis. The hysteresis is related to the fact that a variable part of I_B causes only intraband transitions, not relaxation from the upper level.

There is a substantial asymmetry with respect to the polarity of V_C in the I-V curves of sample H (the region where $|V_C|$ is slightly below the hysteresis loop in Fig. 3). At $I_B = +0.8 \ldots +1.2$ nA, the maximum current-induced change at $V_C < 0$ is ~10 times that at $V_C > 0$. We consider this asymmetry as very strong proof that the underlying principle of the BOT operation is working: Relaxation due to quasiparticle tunneling can take place only under one polarity (*16*). If the device would work as a parametric amplifier owing to I_B-induced changes in the environmental impedance, then the behavior should be symmetric. The maximum current gain is

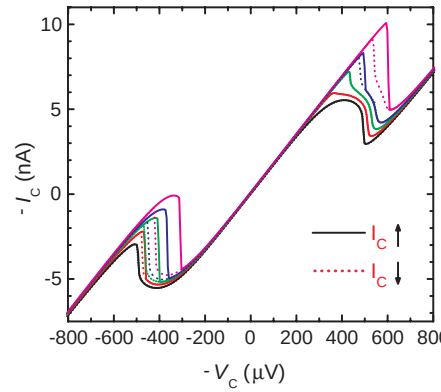

Fig. 3. Current-voltage characteristics for a hysteretic BOT device (sample H) at base current $I_B = 0$ (black), 0.4 nA (red), 0.8 nA (green), 1.2 nA (blue), and 2 nA (magenta). The parameters of the device are as follows: $E_J = 78$ μeV, $E_C = 50$ μeV, $R_C = 54$ kilohms, $R_T^{JJ} = 7.7$ kilohms, and $R_T^{SIN} = 5.8$ kilohms, where R_T^{JJ} and R_T^{SIN} refer to the resistances of the Josephson and SIN junctions, respectively. Up and down voltage sweeps are represented by the solid and dotted curves, respectively.

obtained at $I_B = 1$ nA, which is consistent with our simulations using $P(E)$ theory.

In the measured current gain at $I_B = 1$ nA on a nonhysteretic sample (NH) (Fig. 4), the gain is seen to peak rather strongly with respect to the transport voltage; the peaking of the current gain becomes more prominent with increasing values of β. This peaking reflects the strong dependence of Zener tunneling on the external current. However, negative feedback can always be used to enhance the operating region.

As a function of E_J/E_C, we find a maximum, $\beta \sim 35$, at an optimum ratio of $E_J/E_C = 3.4$. Such a large ratio for E_J/E_C means that higher bands of the junction are involved in the process: The lowest bands are too narrow to present a Coulomb blockade that is as large as that needed for the BOT operation. This factor has not yet been taken into account in our simulations. Above the optimum ratio, the gain drops quickly. At present, the rapid decrease of gain at large values of E_J/E_C is not understood, and it may be a weakness of our nonoptimized first devices.

The other main characteristics of a low-noise amplifier are the available power gain η, the bandwidth BW, the dynamic range A, the optimum input impedance Z_{opt}, and the noise temperature T_N. For the available power gain of sample NH, we obtained a value of $\eta = [(Z_{out})/(Z_{in})]\beta^2 = 5$ by measuring β, Z_{in}, and Z_{out}. This small value is due to an impedance conversion, i.e., the measured input impedance follows $Z_{in} \cong \beta R_C$, whereas at the output, $Z_{out} = -30$ kilohms at the optimum operating point. The bandwidth is expected to be limited well below $\min(1/R_C C, f_B/\beta) \sim 1$ GHz, set either by the RC time constant or the Bloch oscillation frequency. The bandwidth restricts the minimum value of I_B because, at least, $I_B > 2eBW$, according to the Nyquist sampling theorem. From the experimental curves in Fig. 4, we obtain for the dynamic range $A = 50$ pA at the largest current gains. At gains on the order of 10, $A = 250$ pA.

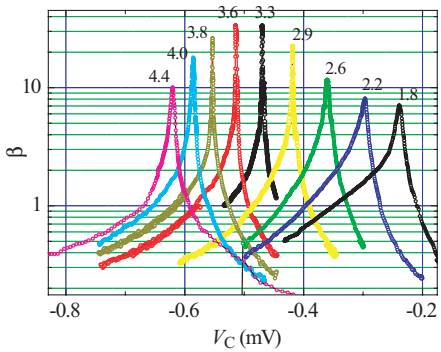

Fig. 4. Current gain measured for a nonhysteretic BOT (sample NH) when the ratio E_J/E_C is tuned over 1.8 to 4.4. The base current was fixed at $I_B = 1$ nA to maximize the current gain. The parameters of the device are as follows: $E_J^{max} = 150$ μeV, $E_C = 35$ μeV, $R_C = 67$ kilohms, $R_T^{IJ} = 4.3$ kilohms, and $R_T^{SIN} = 10$ kilohms. In this BOT, we also had a Cr resistor of 50 kilohms next to the SIN junction.

The noise properties of a BOT are rather complicated. This is mostly because the input and output noises are strongly correlated. Consequently, our noise analysis differs slightly from the standard modeling. A BOT has two principal noise sources: the shot noise due to I_B and the broadening of the Bloch oscillation peak caused by the current fluctuations in collector resistance R_C. Owing to charge relaxation through R_C, a BOT is insensitive to $1/f$ background charge fluctuations that severely hamper the operation of SETs.

The width of the Bloch oscillation peak is given by the equation (*8*)

$$\Gamma_B = (\pi/e)^2 k_B T/R_C \qquad (4)$$

This contribution spreads approximately over the frequency span of 2 GHz at $T = 100$ mK with $R_C = 67$ kilohms. Thus, even though the total power of the Bloch oscillation peak was as high as $(100\ \mu eV)^2$, it amounts only to voltage noise of 2 nV/(Hz)$^{1/2}$. Further away from f_B, its contribution becomes smaller, and its share can be neglected below 1 GHz; indeed, the Bloch peak is so weak and broad that it is barely visible in the Fourier power spectra of our simulated data.

The most detrimental noise contribution is the current fluctuation i_n due to the shot noise of I_B (*17*). Because it is inherent to the device owing to tunneling of electrons at the base, this noise component must be independent of the source impedance. In our noise model, the source independence is achieved with a correlated voltage noise generator, $e_n = Z_{in} i_n$, in the input circuit. Optimization with respect to the noise factor (*18*) results in $Z_{opt} = Z_{in}$ and $T_n = Z_{in} i_n^2/k_B = 2eI_B Z_{in}/k_B \sim eV_{in}/k_B$. Typical values for our present samples are $Z_{opt} = 300$ to 400 kilohms and $T_n = 1$ to 4 K, calculated for moderate current gains of $\beta = 4$ to 6 at $I_B = 0.2$ to 0.4 nA [$i_n \sim 8$ to 11 fA/(Hz)$^{1/2}$] (*19*). With $i_n = 10$ fA/(Hz)$^{1/2}$, the relative dynamic range becomes better than 80 dB/(Hz)$^{1/2}$.

T_n may be substantially smaller than the above estimate. According to our simulations, the base current consists of two parts: $I_B = I_{B1} + I_{B2}$, where I_{B1} induces interlevel transitions (relaxation), whereas I_{B2} causes transitions within only one band. The ratio I_{B1}/I_{B2} depends on the operating point and, typically, we find $I_{B2} > I_{B1}$ in our calculations. Because only I_{B1} produces current gain, we expect $T_n^{calc} \sim 2eI_{B1}Z_{in}/k_B \ll T_n$. In the hysteretic regime, which vanishes with growing resistance of the base tunnel junction, the ratio I_{B1}/I_{B2} has two stable values. Close to the hysteretic region, the devices have a large gain, because, in addition to the change of I_B, there will be an enhancement in output current owing to a change in I_{B1}/I_{B2}.

In principle, a BOT can be used as a voltage-triggered, single-shot detector at $I_B = 0$. In this mode, a pair of oppositely biased BOTs can be used as an "event trigger" detector for charge qubits (*20*). Unfortunately, only a very small coupling between the qubit and the BOT is tolerated if one wants to equal the decoherence times measured recently by Vion *et al.* (*21*).

The most likely application of the BOT will be a submillimeter-wave detector based on either a SIN (*22*) or a SIS (superconductor-insulator superconductor) tunnel junction (*23*). Based on a SQUID readout with a noise of 50 fA/(Hz)$^{1/2}$ (*24*), a SIN detector reaches a noise-equivalent power of 10^{-18} W/(Hz)$^{1/2}$. Similar noise characteristics are obtained with SIS detectors, for which SET readouts have been demonstrated to yield $i_n = 15$ fA/(Hz)$^{1/2}$ (*25*). Our noise estimates for BOTs compare well with these results, even though they are based on first, nonoptimal devices. It has been suggested (*25*) that single-photon counting could be implemented with a quantum-limited SET for readout. An optimized BOT might reach the same performance, but in this case, it might be better to use a BOT as a charge multiplier, i.e., in a mode where individual charge pulses in the output are resolved.

BOTs may also find their way into metrology, where the detection and comparison of small quantized currents generated by a single-electron tunneling current pump is an issue. Ultimately, the goal is to close the quantum triangle by combining Josephson voltage, quantum Hall resistance, and quantum current standards at the level of relative uncertainty of 10^{-8}. One approach is to use an amplifier based on a cryogenic current comparator and a SQUID to multiply the current generated by a SET pump. The equivalent current noise for such a setup has been demonstrated to be 4 fA/(Hz)$^{1/2}$ (*26*). With a BOT, one should reach comparable noise levels, with the further benefit of an on-chip integration of the readout element.

References and Notes

1. D. V. Averin, K. K. Likharev, *J. Low Temp. Phys.* **62**, 345 (1986).
2. T. A. Fulton, G. J. Dolan, *Phys. Rev. Lett.* **59**, 109 (1987).
3. A. Aassime, D. Gunnarsson, K. Bladh, P. Delsing, R. Schoelkopf, *Appl. Phys. Lett.* **79**, 4031 (2001).
4. M. H. Devoret, R. J. Schoelkopf, *Nature* **406**, 1039 (2000).
5. K. K. Likharev, *Proc. IEEE* **87**, 606 (1999).
6. J. Clarke, in *SQUID Sensors: Fundamentals, Fabrication, and Applications*, H. Weinstock, Ed. (Kluwer Academic, Amsterdam, 1996), pp. 1–62.
7. J. Hassel, H. Seppä, *IEEE Trans. Appl. Supercond.* **11**, 260 (2001).
8. D. Averin, K. K. Likharev, A. B. Zorin, *Sov. Phys. JETP* **61**, 407 (1985).
9. See, for example, G. Schön, A. D. Zaikin, *Phys. Rep.* **198**, 237 (1990).
10. A. D. Zaikin, I. N. Kosarev, *Phys. Lett. A* **131**, 125 (1988).

11. A. D. Zaikin, D. S. Golubev, *Phys. Lett. A* **164**, 337 (1992).
12. D. B. Haviland, L. S. Kuzmin, P. Delsing, T. Claeson, *Europhys. Lett.* **16**, 103 (1991).
13. J. Delahaye *et al.*, *Physica E*, in press.
14. G. L. Ingold, Yu. V. Nazarov, in *Single Charge Tunneling, Coulomb Blockade Phenomena in Nanostructures*, H. Grabert, M. Devoret, Eds. (Plenum, New York, 1992), pp. 21–107.
15. Materials and methods are available as supporting material on *Science* Online.
16. If quasiparticle tunneling occurs in the opposite direction, the tunneling brings the junction charge Q further away from the background charge Q_0, and the energy will increase according to $[1/(2C)](Q - Q_0)^2$. Consequently, the junction will make a transition to the third energy level.
17. The output current is made of charge pulses of size βe. Therefore, the output current noise is given by $[2(\beta e)I_{out}]^{1/2} = [2(\beta e)\beta I_B]^{1/2} = \beta[(2eI_B)^{1/2}]$, and this reduces to the shot noise of I_B at the input. This contains all of the noise, except possible leakage current contributions. The apparent switching voltage noise at the output is given simply by the instantaneous $R_C I_{out}(t)$.
18. A. van der Ziel, *Noise in Solid State Devices and Circuits* (Wiley, New York, 1986), chap. 3.
19. There is a small noise contribution from the output leakage current of ~1 nA. Using the measured transconductance $g_m \cong 1/R_C$ (valid when $\beta > 5$), we estimate a contribution of 0.4 K in T_n.
20. Yu. Makhlin, A. Schnirman, G. Schön, *Rev. Mod. Phys.* **73**, 357 (2001).
21. D. Vion *et al.*, *Science* **296**, 886 (2002).
22. M. Nahum, J. M. Martinis, *Appl. Phys. Lett.* **63**, 3075 (1993).
23. A. Peacock *et al.*, *Nature* **381**, 135 (1996).
24. See, for example, D. Golubev, L. Kuzmin, *J. Appl. Phys.* **89**, 6464 (2001).
25. R. J. Schoelkopf, S. H. Moseley, C. M. Stahle, P. Wahlgren, P. Delsing, *IEEE Trans. Appl. Supercond.* **9**, 2935 (1999).
26. Y. De Wilde, F. Gay, P. M. Piquemal, G. Génevès, *IEEE Trans. Instrum. Meas.* **50**, 231 (2001).

27. We acknowledge interesting discussions with M. Kiviranta, J. Pekola, J. Penttilä, A. Schakel, and A. D. Zaikin. This work was supported by the Academy of Finland and by the Large Scale Installation Program ULTI-3 of the European Union (HPRI-CT-1999-00050).

Supporting Online Material

www.sciencemag.org/cgi/content/full/299/5609/1045/DC1
Materials and Methods
Table S1
Reference
Movie S1

16 October 2002; accepted 20 December 2002

Reprinted with permission from the publisher.
In: Journal of Applied Physics 2004. Vol. 95, No. 12, pp. 8059–8062.

Control of Coulomb blockade in a mesoscopic Josephson junction using single electron tunneling

J. Hassel[a] and H. Seppä
VTT Information Technology, Microsensing, P.O. Box 1207, FIN-02044 VTT, Finland

J. Delahaye and P. Hakonen
Low Temperature Laboratory, Helsinki University of Technology, P.O. Box 2200, FIN-02015 HUT, Finland

(Received 2 February 2004; accepted 29 March 2004)

We study a circuit where a mesoscopic Josephson junction (JJ) is embedded in an environment consisting of a large bias resistor and a normal-insulator-superconductor (NIS) junction. The effective Coulomb blockade of the JJ can be controlled by the tunneling current through the NIS junction leading to transistor-like characteristics. We show using phase correlation theory and numerical simulations that substantial current gain with low current noise ($i_n \lesssim 1$ fA/$\sqrt{\text{Hz}}$) and noise temperature ($\lesssim 0.1$ K) can be achieved. Good agreement between our numerical simulations and experimental results is obtained. © *2004 American Institute of Physics.*
[DOI: 10.1063/1.1751231]

I. INTRODUCTION

Mesoscopic Josephson junctions (JJ) display interesting phenomena owing to the conjugate nature of phase and charge.[1] Coulomb effects cause delocalization of the macroscopic phase variable across the tunnel junction, which leads to the formation of energy bands.[2] As the bandwidth grows rapidly with the band index, a mesoscopic JJ makes it possible to construct devices where the operation is based on controlling the transitions between energy levels of the junction, thereby controlling the effective Coulomb blockade of the device.[3,4] The control is made using a small tunnel current of single electrons. Thus, the device is distinguished from the ordinary Coulomb blockade devices, like single electron transistors (SETs), where the current is adjusted by an external, capacitively coupled voltage.[5]

We have investigated the circuit where a mesoscopic Josephson junction (JJ) is embedded in an environment consisting of a large bias resistor and a normal-insulator-superconductor (NIS) junction. The JJ is biased in the regime where the system becomes a two-level system with two distinct Coulomb blockade strengths. The effective Coulomb blockade of the JJ is controlled by the tunneling current through the NIS junction, which leads to transistor-like characteristics. This device, called the Bloch oscillating transistor (BOT),[4] provides a low-noise current amplifier whose input impedance level makes it an intermediate device between the ultimate low temperature amplifiers, the superconducting quantum interference device and the SET.[6]

We present experimental results on the basic properties of BOTs, and compare them with computer simulations based on time dependent phase correlation theory for electron and Cooper pair tunneling. We show that this provides a way to model the devices quantitatively. Noise properties of the devices are discussed, the conclusion being that ultralow-noise current amplifiers (current noise $i_n \lesssim 1$ fA/$\sqrt{\text{Hz}}$ referred to input) can be built on the basis of controlled JJs. The simulated results are shown to be in a good agreement with our experimental findings.

II. PRINCIPLE OF OPERATION

Schematically our device is shown in Fig. 1 (left frame). A Josephson junction (JJ) connects a superconducting island to the emitter electrode (E). A normal-insulator-superconductor (NIS) junction connects the normal base electrode (B) to the island. Furthermore, a high-impedance, thin film resistor R_C connects the island to the collector electrode (C). When the isolation resistance $R_C \gg R_Q = h/4e^2$, charge fluctuations on the JJ are small and the dynamics of the junction consists purely of Bloch reflections at the Brillouin zone boundary, interrupted by occasional Zener tunneling between the bands.[7]

Fundamentally, the operation of a BOT is understood on the basis of the band structure of a Josephson junction. The energy versus (quasi) charge Q_I of a JJ is shown with a thick uniform curve in the right frame of Fig. 1. When the collector is voltage biased by V_C, the ''island'' charge Q_I tends to relax through R_C towards the value $Q_I = (C_{\text{JJ}} + C_{\text{NIS}})V_C - C_{\text{NIS}}V_B \approx C_\Sigma V_C$, where $C_\Sigma = C_{\text{JJ}} + C_{\text{NIS}}$. At $Q_I = e$, Cooper pair (CP) tunneling returns the system back to the state $Q_I = -e$. Repetition of this Bloch oscillation cycle produces a net current from the collector to the emitter. The competing process for the CP tunneling at $Q_I = e$ is Zener tunneling up to the second energy band, where Bloch oscillations do not occur and the current flow stops (Coulomb blockade voltage $\partial E/\partial Q_I > V_C$). From the second band the system may return back to the first one by single electron tunneling through the base junction. Thus, as a result of a single electron tunneling event through the NIS junction, a sequence of Cooper pair pulses is injected through the JJ, which leads to a current

[a]Author to whom correspondence should be addressed; electronic mail: juha.hassel@vtt.fi

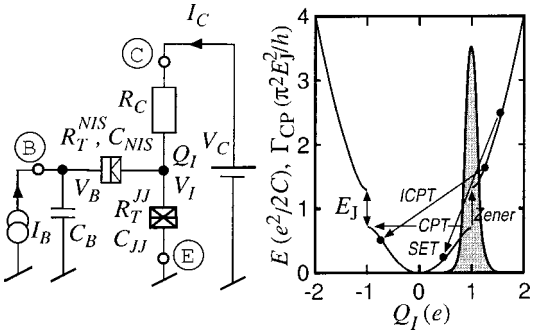

FIG. 1. Schematics of the circuit (left frame) for controlling the Coulomb blockade of Cooper pairs. The injector of single electron current, the superconductor-normal junction, is denoted by NIS while the Josephson junction is coined by JJ. Symbols for different biasing voltages and the resulting currents are also given in the figure. Q_I denotes the island charge that is governed by Eq. (1). See the caption of Table I for other parameters. The right frame illustrates the energy vs charge diagram used in the simulations. The distribution at the Brillouin zone boundary illustrates the charge fluctuations due to the resistive environment. Arrows indicate possible tunneling processes in the BOT: CPT—Cooper pair tunneling, ICPT—inelastic Cooper pair tunneling, SET—single electron tunneling, Zener—tunneling up to higher energy band. Γ_{CP} denotes the tunneling rate for both CPT and ICPT.

gain equaling the average number of electrons in the CP sequence. This kind of action is below referred to as regular BOT operation.

III. COMPUTATIONAL MODEL

The above picture is, however, an overidealization in most experimental cases. In a real situation all input electrons do not produce output current pulses, but rather cause intraband transitions. It is also hard to fabricate large enough thin film resistances to achieve coherent Bloch oscillations. Qualitatively, the picture of the two-level system still works, but the measured current gains are clearly less than the calculated values.[8] When R_C becomes relatively small, $\sim 10R_Q$, charge fluctuations grow and inelastic Cooper pair tunneling may take place clearly before the Brillouin zone boundary. This makes the dynamics more complicated and our present experiments and simulations are aimed at clarifying this question.

In our computational model the island charge as function of time is obtained by integrating the equation

$$\frac{dQ_I}{dt}=\frac{V_C-V_I}{R_C}-\left(\frac{dQ_I}{dt}\right)_{\mathrm{NIS}}-\left(\frac{dQ_I}{dt}\right)_{\mathrm{JJ}}, \tag{1}$$

where the first term represents the charge relaxation through the collector resistor, and the last two terms represent tunneling current in the NIS and JJ, respectively. $(dQ_I/dt)_{\mathrm{NIS}}$ contains only quasiparticle current while $(dQ_I/dt)_{\mathrm{JJ}}$ includes both quasiparticle and Cooper pair tunneling. The base junction is current biased, as in the experiments, but the gate capacitance $C_B\sim 1$ pF (see Fig. 1) converts it effectively into voltage bias V_B.[9]

To integrate Eq. (1) in the presence of finite Josephson coupling and electromagnetic environment, we compute the Cooper pair tunneling through the JJ (Γ_{CP}) and quasiparticle tunneling through both junctions ($\Gamma_{\mathrm{QP}}^{\mathrm{JJ}},\Gamma_{\mathrm{QP}}^{\mathrm{NIS}}$) using the phase-fluctuation $P(E)$ theory.[10,11] As a modification to the standard theory, we use time dependent voltages V_I and V_I-V_B across the JJ and NIS junctions, respectively. V_I is given by

$$V_I=(C_{\mathrm{NIS}}/C_\Sigma)V_B+Q_I/C_\Sigma. \tag{2}$$

A basically similar modeling approach has been employed by Kuzmin *et al.*[12] when investigating the role of Zener tunneling on the IV curves of ultrasmall Josephson junctions. The difference is that we include the effect of quantum fluctuations in our model on top of the thermal noise which was employed in Ref. 13 only.

According to the $P(E)$ theory, tunneling does not happen strictly at $Q_I=e$, but is rather represented with a finite distribution, which is schematically shown in Fig. 1. Within this picture, one can still use the concept of band structure, the interpretation being that values $Q_I\lesssim e$ correspond to the first band, and $Q_I\gtrsim e$ to the second band. The band gaps, where Zener tunneling takes place, are now reflected in the probabilities at which the junction may pass from the lower to the higher band (see below).

The most critical assumption is made while computing the Cooper pair tunneling rate, for which the lowest order theory is valid when $E_JP(2\,eV)\ll 1$.[11] For the samples analyzed in this article, $\max[P(2\,eV)]\approx 0.3/E_C$ and $\max(E_J)\approx 1.7E_C$, so that second order effects may be expected to be small. The Cooper pair tunneling rate can then be computed as

$$\Gamma_{\mathrm{CP}}(V_I)=\frac{\pi E_J^2}{2\hbar}P(2\ \ eV_I), \tag{3}$$

where the function $P(E)$ is defined as

$$P(E)=\frac{1}{2\pi\hbar}\int_{-\infty}^{\infty}dt\,\exp\left(J(t)+\frac{i}{\hbar}Et\right). \tag{4}$$

The phase correlation function $J(t)=\langle[\varphi(t)-\varphi(0)]\varphi(0)\rangle$, which takes into account the fluctuations of the phase $\varphi(t)$ on the junction. $J(t)$ is calculable from the real part of the environmental impedance.[11] Here we have also made the assumption that the effect of the environment is exclusively due to the collector resistance,[14] for which the $P(E)$ function was calculated numerically.

In the limit $R_C/R_Q\gg E_C/kT$, the CP tunneling rate as given by Eq. (3) becomes a Gaussian distribution centered around $V_I=e/C_\Sigma$.[11] If furthermore, $E_C/kT\gg 1$, the distribution narrows to a delta spike $\Gamma_{\mathrm{CP}}=(\pi E_J^2/2\hbar)\,\delta(2\ \mathrm{eV}-4E_c)$ which equals the equation obtained from the band model by neglecting the effect of the environment.[15] Hence, the basic features of the band model are embedded in the peaked tunneling probabilities. In a proper band model, however, the capacitance of the JJ entering Eq. (1) would be nonlinear and given by $(d^2E/dQ^2)^{-1}$. In our model, we take the capacitance as constant, which is valid in the limit $E_J\to 0$ only.

IV. COMPARISON WITH EXPERIMENTS

Our sample parameters are given in Table I. Details of sample manufacturing and experimental techniques can be found in Ref. 6. Measured and computed I_CV_C curves for

TABLE I. Parameters for our samples. Tunneling resistances (in kΩ) of the Josephson and NIS junctions are given by R_T^{JJ} and R_T^{NIS}, respectively. R_C denotes the environmental impedance of the Josephson junctions. The division of capacitance between the two junctions, C_{NIS} and C_{JJ}, are estimated on the basis of the measured resistances and geometrical dimensions. The last column indicates the minimum E_J^{min} and maximum E_J^{max} values of the Josephson energy in μeV.

	R_T^{JJ}	R_T^{NIS}	R_C	C_{NIS} (fF)	C_{JJ} (fF)	E_J^{min}/E_J^{max}
1	8.1	27.3	23	0.28	0.95	22/78
2	7.8	5.8	50	0.6	1.0	83/83

sample I with various E_J are shown in Fig. 2, each at several values of I_B. When $I_B=0$, a weak Coulomb blockade is visible at zero bias. The peak in current at nonzero voltages reflects Cooper pair tunneling processes, which are enhanced by single electron current through the base. The current gain β is found to be maximized in the region with negative slope: $\beta_{max}=3.2$ at $V<0$ ($I_B=3.3$ nA) and $\beta_{max}=3.0$ at $V>0$ ($I_B=2.5$ nA). From our simulations we get $\beta_{max}=2.8$ ($I_B=1.7$ nA) and 2.5 ($I_B=1.7$ nA), respectively. The relatively small maximum gains are caused by large current fluctuations owing to $R_C=23$ kΩ. Figure 3 displays I_CV_C curves for sample II with $E_J/E_C=1.7$. Both the measured data[6] and the simulated I_CV_C curves display hysteretic behavior. The computed curves in the regular BOT regime are seen to display growing hysteresis with increasing base current, in accordance with the measured data. Especially with large E_J, the current peak is at slightly lower voltages in the computed curves than in the measured data indicating that the computed probability of Zener tunneling is larger than in reality. This is a sign that our simplified picture of the energy band structure fails for large E_J.

The nonsymmetrical nature of the curves in Fig. 2 suggests that the mechanism for current gain is different at opposite biasing polarities. This is illustrated in the time traces of Q_I in Figs. 4(a) and 4(b). In the regular biasing case [$V_C<0$, Fig. 4(a)] single electron tunneling is seen to drive the system downwards from the upper band and, thus, it tries

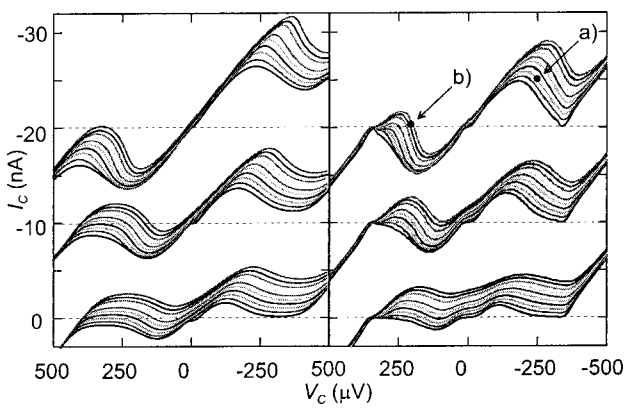

FIG. 2. Sets of I_CV_C curves measured (left) and computed (right) at $T=90$ mK on sample 1. Josephson coupling has been varied with $E_J/E_C=1.2$ at the topmost, $E_J/E_C=0.7$ at the middle, and $E_J/E_C=0.35$ at the lowest set. In each set the base currents $I_B=0$, 0.4, 0.8, 1.2, 1.6, 2.0, 2.4, 2.8, 3.2, and 3.6 nA (in order from bottom to top). The topmost set is offset by −20 nA and middle set by −10 nA for clarity.

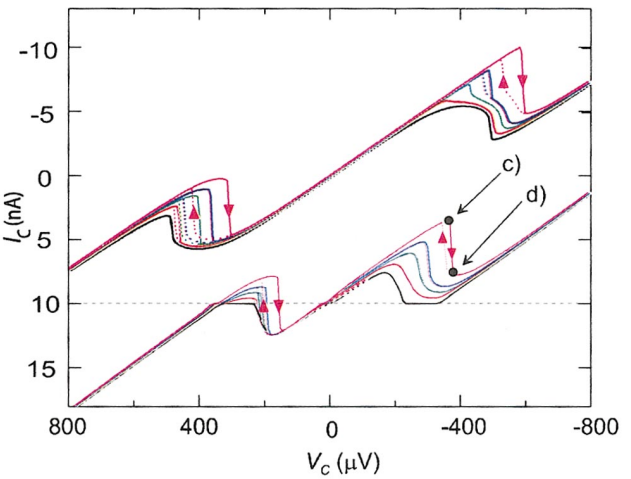

FIG. 3. (Color) I_CV_C curves for sample 2 with $E_J/E_C=1.7$ at base currents $I_B=0$, 0.4, 0.8, 1.2, and 2.0 nA. The upper set represents data measured at $T=100$ mK (see Ref. 6). The lower set is the result of simulation using the experimental parameters. It is offset by 10 nA for clarity.

to restore Bloch oscillations, i.e., the dynamics is essentially similar to the original BOT operation even though incoherent tunneling phenomena modifies it strongly. When $V_C>0$, on the contrary, I_B tends to drive the system into the second band, which leads to a suppression of 2e oscillations as seen in Fig. 4(b). The recovery of 2e oscillations now takes place through incoherent 2e tunneling, the tunneling probability of which is determined by the "tail" of $P(E)$ function.

Time domain plots of Q_I for the two hysteretic I_C branches (see Fig. 3) are shown in Figs. 4(c) and 4(d). On the upper branch [Fig. 4(c)] the dynamics is again regular BOT dynamics, essentially similar to that of Fig. 4(a). Now it is obvious that the system almost never relaxes to its stationary state, since the inverse of R_CC_Σ time constant is small compared to the tunneling rate Γ_{NIS}. Single electron tunneling

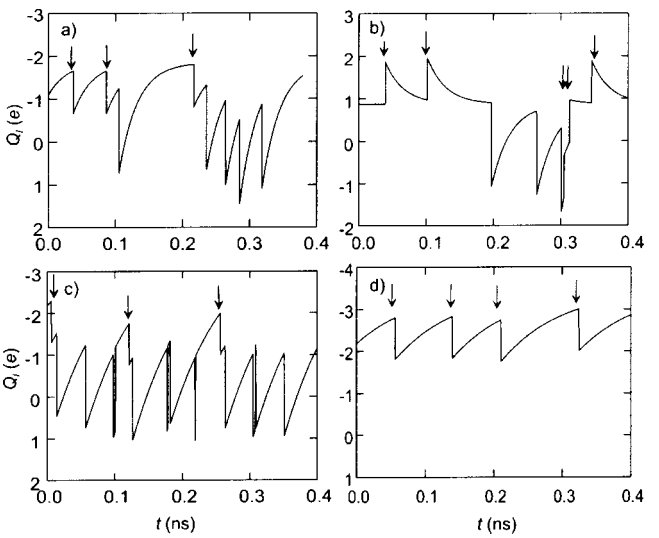

FIG. 4. Time traces of charge Q_I at the operating points denoted by solid circles in Figs. 2 and 3: (a) regular BOT operation, (b) inverted BOT operation, (c) regular BOT operation in the hysteretic region, and (d) operation in the hysteretic region with only intraband transitions induced by I_B. The arrows indicate single electron tunneling events.

still clearly enhances Cooper pair tunneling. At the lower branch, the system seldom returns to the lowest band, and the base current I_B mostly consists of tunneling events causing intraband transitions only. Therefore, Cooper pair tunneling is less likely and the collector current remains small. Two stable solutions can coexist since $I_B \propto (V_B - V_{JJ})$. Now, due to the current biased base electrode, V_B and V_{JJ} can each dynamically assume two different average values, while their difference remains the same leading to equal base currents in both cases.

In our simulations, the transition from nonhysteretic to hysteretic behavior can be crossed by increasing E_J. This is because increasing E_J enhances the stability of the type of solution presented in Fig. 4(c) by increasing the rate Γ_{CP} according to Eq. (3). Near the hysteresis point, the ratio of base tunneling currents, I_{B_1}/I_{B_2}, made of contributions causing either interband transitions (I_{B_1}) or intraband transitions (I_{B_2}) is found to vary steeply, for example, as a function of I_B. Consequently, a small change in the input current induces a large change in the output current, because of the conversion of base current between the types I_{B_1} and I_{B_2}. Large gain may then be obtained with ultralow noise. The output noise current is independent of source impedance if $C_B \gg C_\Sigma$. In this case the noise temperature can be written

$$T_N = Z_{\text{in}} \frac{i_{n_{\text{out}}}^2}{\beta^2}, \tag{5}$$

where Z_{in} denotes the input impedance and $I_{n_{\text{out}}}/\beta$ is the output current noise converted to the input. Near the hysteresis point, β may grow without limit, which makes it possible to reduce $T_N \to 0$. Note, however, that this takes place at the cost of input impedance $\sim \beta R_C$ and maximum acceptable input signal amplitude. Experimentally, we have found a sample with white noise of $i_n = 10\,\text{fA}/\sqrt{\text{Hz}}$ referred to the input. This implies a noise temperature T_N smaller by a factor of 5 compared to the shot noise approximation $i_n^2 = 2eI_B$. The result was measured on a sample having a Josephson coupling energy of order $4E_C$, i.e., slightly out of the validity range of our computational model. In our simulations, current noise values of order $1\,\text{fA}/\sqrt{\text{Hz}}$ and noise temperatures below 0.1 K have been reached using experimentally realizable parameters.

As mentioned in the beginning, our analysis is based on perturbation theory in E_J/E_C and the results are strictly valid in the limit $E_J \to 0$. Nevertheless, we believe that our simulations are principally valid at values of $E_J \simeq 1$. More serious problems occur when the width of the lowest band becomes exponentially narrow as for samples with $E_J/E_C \sim 4$.[6] In this case, the dynamics is dominated by transitions between higher bands, rather than the two lowest ones. As long as there are two major bands involved allowing one to use a two band approximation, our simulated results will be qualitatively correct.

V. CONCLUSION

In summary, we have shown that devices can be constructed using interlevel transitions, driven by single electron tunneling. The single electron current can be used either to drive the JJ into the blockade state, or out from the blockade. Both methods are seen to yield substantial current gain, though at slightly different values of bias voltage. Comparison of our experimental and theoretical results show that time-dependent $P(E)$ theory can be employed quite successfully to model the behavior of such devices. The essential features of BOT dynamics were found to be recovered even in the presence of relatively strong incoherent Cooper pair tunneling and the JJ could still be understood as a two-level system, whose switching is controlled by single charge tunneling. Furthermore, our simulations indicate that intraband transitions play a significant role in these three terminal devices. The devices may give substantial gain by conversion of base current between interlevel and intraband types. This leads to noise powers that are substantially less than the values obtained from the input shot noise approximation.

ACKNOWLEDGMENTS

The authors acknowledge fruitful discussions with R. Lindell, T. Heikkilä, F. Hekking, G.-L. Ingold, A. Niskanen, M. Paalanen, M. Sillanpää, M. Kiviranta, and A. Zaikin. This work was supported by the Academy of Finland and by the Large Scale Installation Program ULTI-3 of the European Union.

[1] See, e.g., M. Tinkham, *Introduction to Superconductivity*, 2nd ed. (McGraw–Hill, New York, 1996).
[2] D. Averin, K. K. Likharev, and A. B. Zorin, Sov. Phys. JETP **61**, 407 (1985); K. K. Likharev and A. B. Zorin, J. Low Temp. Phys. **59**, 348 (1985).
[3] H. Seppä and J. Hassel, cond-mat/0305263.
[4] J. Hassel and H. Seppä, IEEE Trans. Appl. Supercond. **11**, 260 (2001).
[5] For a recent review, see K. K. Likharev, Proc. IEEE **87**, 606 (1999).
[6] J. Delahaye, J. Hassel, R. Lindell, M. Sillanpää, M. Paalanen, H. Seppä, and P. Hakonen, Science **299**, 1045 (2003).
[7] A. D. Zaikin and I. N. Kosarev, Phys. Lett. A **131**, 125 (1988).
[8] J. Delahaye, J. Hassel, R. Lindell, M. Sillanpää, M. Paalanen, H. Seppä, and P. Hakonen, Physica E **18**, 15 (2003).
[9] V_B was calculated using the equation $dV_B/dt = 1/C_B[I_B + (Q_I dt)_{\text{NIS}}]$. It was assumed that $C_B \gg C_\Sigma$.
[10] M. H. Devoret, D. Esteve, H. Grabert, G.-L. Ingold, H. Pothier, and C. Urbina, Phys. Rev. Lett. **64**, 1824 (1990).
[11] G.-L. Ingold and Yu. V. Nazarov, in *Single Charge Tunneling*, edited by H. Grabert and M. H. Devoret (Plenum, New York, 1992), pp. 21–106.
[12] L. S. Kuzmin, Yu. A. Pashkin, D. S. Golubev, and A. D. Zaikin, Phys. Rev. B **54**, 10074 (1996).
[13] D. Golubev and A. D. Zaikin, Phys. Lett. A **164**, 337 (1992).
[14] That is, the fluctuation due to charge tunneling through both junctions has been neglected.
[15] G. Schön and A. D. Zaikin, Phys. Rep. **198**, 237 (1990).

Theory of the Bloch Oscillating Transistor

J. Hassel, and H. Seppä

VTT Information Technology, Microsensing,

P.O. Box 1207, FIN-02044 VTT

Abstract. The Bloch oscillating transistor (BOT) is a device, where single electron current through a normal tunnel junction enhances Cooper pair current in a mesoscopic Josephson junction leading to signal amplification. In this paper we develop a theory, where the BOT dynamics is described as a two-level system. The theory is used to predict current-voltage characteristics and small-signal response. The transition from stable operation into hysteretic regime is studied. By identifying the two-level switching noise as the main source of fluctuations, the expressions for equivalent noise sources and the noise temperature are derived. The validity of the model is tested by comparing the results with simulations and experiments.

PACS numbers: 74.78.Na, 85.25.Am, 85.35.Gv

I. INTRODUCTION

The Bloch oscillating transistor (BOT)[1–5] is based on tuning the probability of interlevel switching in a mesoscopic Josephson Junction (JJ). The equivalent circuit is shown in Fig. 1(a). The current I_C at the collector(C) -emitter(E) -circuit is controlled by the base current I_B leading to transistor-like operation. The physics is based on controlling the state of the JJ by means of quasiparticles tunneling through the normal tunnel junction connected to the base electrode (B).

The state diagram as function of the (quasi)charge Q_I is shown in Fig. 1(b)[6], where also the transitions are illustrated. It is assumed that the Josephson coupling energy E_J is smaller or of the same order as the charging energy $E_C = e^2/2C_\Sigma$, and that $R, R_{T1}, R_{T2} \gtrsim R_Q$. Here $C_\Sigma = C_1 + C_2$ is the total capacitance of the junctions, R is the collector resistor, and R_{T1} and R_{T2} are the tunnel resistances. The quantum resistance $R_Q = h/4e^2 \approx 6.5$ kΩ. We assume that C is biased at a point, where $V_C \gtrsim e/C_\Sigma$. The charge tends to relax through the collector resistor R_C towards $V_C C_\Sigma$. Here V_C is the collector voltage. If the system is initially at the lowest band ($|Q_I| < e$ in the extended band picture we are using), at $Q_I = e$ it is likely that a Cooper pair (CP) tunneling through the JJ returns the system back to $Q_I = -e$. Repeating this cycle, the Bloch Oscillation[6], leads to a net current through the

C-E circuit. We call the lowest band with allowed Cooper pair conduction the "first level".

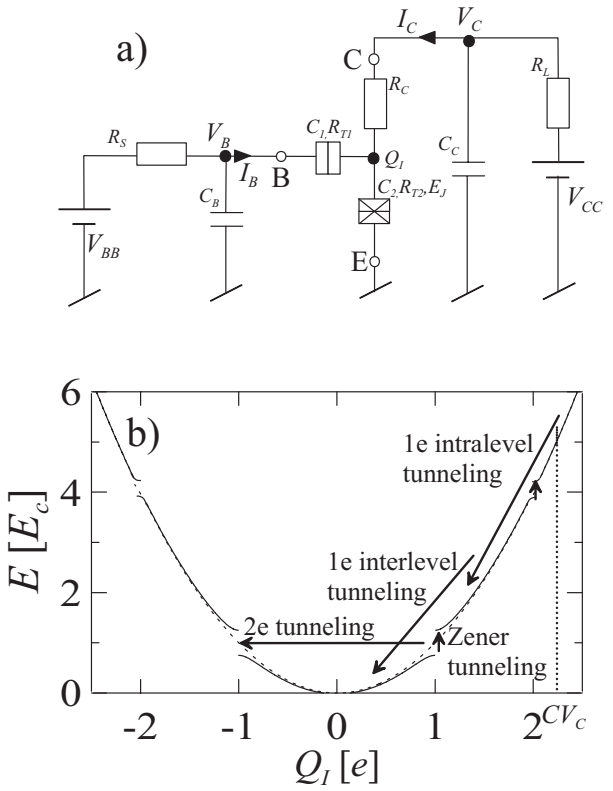

FIG. 1: *(a) Schematic circuit of a BOT connected to a source and a load. Source R_S is connected to the base electrode B and load R_L to the collector electrode C. The lead capacitances from the electrodes to the ground are C_B and C_C. The BOT itself consists of a Josephson Junction (JJ) connected to E, a normal tunnel junction connected to B and large $R_C \gg R_Q$ resistor connected to C. All three components are further connected to a superconducting node, which has small capacitance to the ground. (b) The state diagram of the JJ and the possible transitions.*

A competing process with the CP tunneling is the Zener tunneling[7], which provides a mechanism for an upwards transition. Zener tunneling takes the system to the upper bands ($|Q_I| > e$). Cooper pairs are allowed to tunnel only near the band gaps $|Q_I| = ne$, where n is an integer. However, in the limit of small E_J/E_C the Zener tunneling probability increases very rapidly as function of the band index n. Therefore CP tunneling is virtually blocked for $|Q_I| > e$. This enables us to treat the system as a two-level system. The "second level" consists of the higher bands with blocked CP tunneling. Downwards transitions are induced by one or more quasiparticles tunneling through the base junction (see Fig. 1(b)). Tuning the quasiparticle tunneling probability by changing base voltage or current leads to the control of average current through the C-E circuit, and thus to transistor-like characteristics.

The BOT was recently experimentally realized[3], and simulations showed that its properties can be quantitatively predicted with a computational model[5]. It is potentially useful in cryogenic applications such as readout circuits of radiation detectors, or measurement of small currents in quantum metrology. The aim of this article is to gain more insight into the BOT and to study the noise properties. To be able to do so, we derive an analytic theory, and study its applicability by comparing the results to computational and experimental data.

II. ANALYTIC THEORY

In the theory derived below, BOT is modelled as a mapping of voltages V_B and V_C into currents I_B and I_C. We assume that a single tunneling event will not affect the voltages. This is the case, since $C_B, C_C \gg C_\Sigma$ in a practical experimental setup.

We assume that $1 \ll E_C/kT \ll R_C/R_Q$ and $E_J \ll E_C$, which means that the Cooper pair tunneling rate reduces to a delta spike centered at $|Q_I| = e$ [8,9]. This recovers our interpretation of the two-level system. We also assume that $C_2 \gg C_1$ and neglect quasiparticle tunneling through the JJ. Below unnecessary subscripts for capacitances and charges are dropped, i.e. $C \equiv C_2 \equiv C_\Sigma$, $R \equiv R_C$, $R_T \equiv R_{T1}$ and $Q \equiv Q_I \equiv Q_2$. We analyze only the regime, where $V_C > e/C$ and $V_B' < 0$, since this is interesting for the amplifier operation. Here we have defined $V_B' = V_B - V_C$.

The collector and base currents are written as

$$I_C = \frac{1/\Gamma_\uparrow}{1/\Gamma_\uparrow + 1/\Gamma_\downarrow} I_S - I_B \tag{1}$$

$$I_B = -\frac{\langle N_e \rangle \, e}{1/\Gamma_\uparrow + 1/\Gamma_\downarrow}, \tag{2}$$

The transition rates between the two levels are $\Gamma_\uparrow$ and $\Gamma_\downarrow$. The "saturation current", i.e. current through the JJ at the first level, is $I_S = 2ef_B$, where f_B is the Bloch oscillations frequency. The number of electrons needed to induce a downwards transition is $\langle N_e \rangle$. Here we have neglected the possibility of single-electron tunneling, when the system is at the first level. This is justified, since typically the voltage $|V_1|$ is below the gap voltage in that case. The Eqs. (1) and (2) give general IV characteristics for the BOT.

Between tunneling events $dQ/dt = (V_C - Q/C)/R$. By integrating from $Q = -e$ to $Q = e$, i.e. over one Bloch period one gets f_B, and consequently

$$I_S = \frac{2V_Q}{R} \left[\ln \left(\frac{V_C/V_Q + 1}{V_C/V_Q - 1} \right) \right]^{-1}, \tag{3}$$

where we have defined $V_Q = e/C$.

The upwards tunneling rate (the Zener tunneling) can now be written as[10]

$$\Gamma_\uparrow = \frac{I_S}{2e\,\langle N\rangle}, \tag{4}$$

where

$$\langle N\rangle = \exp\left(\frac{I_z R}{V_C - V_Q}\right) - 1 \tag{5}$$

is the average number of Cooper pairs in one sequence of Bloch oscillations. One sequence here means the time between tunneling down to the first level and tunneling back to the second level. The Zener avalanche current is $I_z = \pi e E_J^2/8\hbar E_c$.

The downwards tunneling at low temperatures and for large R is exclusively due to single electron tunneling through the base junction. It is generally impossible to calculate exact analytic expressions for $\langle N_e\rangle$ and $\Gamma_\downarrow$. We proceed, however, by giving approximations in two limits. For $V_C < 2V_Q$ one electron always suffices to induce a downwards transition. Assuming further the low-temperature and large resistance limit of base electrode tunneling rates, and that the transient is short compared to the inverse of the tunneling rate, it follows[11]

$$\langle N_e\rangle = 1 \tag{6}$$

$$\Gamma_\downarrow = -\frac{1}{CR_T}\left(\frac{V_B'}{V_Q} + \frac{1}{2}\right). \tag{7}$$

If $V_C > 2V_Q$ the first electron tunneling through the base junction does not necessarily cause a transition to the first level, but some of but intralevel transitions occur instead. In this limit we have solved the problem numerically, and searched for a proper fitting function. The result is[11].

$$\begin{aligned}\langle N_e\rangle = {} & 0.04\left(\frac{R_T}{R}\right)^2 \\ & \times \exp\left(0.3\exp\left(1.8\frac{V_C}{V_Q} + 0.27\frac{V_C V_B'}{V_Q^2} - 0.2\frac{V_B'}{V_Q}\right)\right) + 1\end{aligned} \tag{8}$$

$$\begin{aligned}\Gamma_\downarrow^{-1} = {} & 1.2e\frac{R+R_T}{V_B'}\left(1 - \langle N_e\rangle\right) \\ & + RC\left(2.5\frac{R_T}{R} + 1.1\right)\left(\frac{V_Q}{V_B'}\right)^2.\end{aligned} \tag{9}$$

The fit is accurate, when $R_T \lesssim R$. The weaker dependence indicated by the unity term in Eq. (8) and $(2.5R_T/R + 1.1)\,(V_B'/V_Q)^2$ term in Eq. (9) dominate at $V_C \approx 2V_Q$ and large $|V_B'|$. In this case only one quasiparticle is needed to induce a downwards transition. This is possible, if the tunneling occurs during the transient immediately after the Zener tunneling, while still

$Q(t) < 2e$. The $\exp(0.3\exp(...))$-term dominates, when several tunneling events are needed to induce an interlevel transition. The very strong dependence is roughly explained as follows. Let us assume that $2V_Q < V_C < 3V_Q$ and the island charge is initially $Q \approx CV_C$ (see Fig. 1). Now at least two quasiparticles tunneling rapidly one after another are needed to induce a downwards transition. The quasiparticle tunneling probability is at its maximum, when $Q \approx CV_C$. However, after the first tunneling event Q drops down to $CV_C - e$ and therefore the probability also drops. Hence the probability for the second quasiparticle to tunnel before the charge relaxes back to $Q > 2e$ is small. The charge therefore tends to oscillate between $Q \approx CV_C$ and $Q \approx CV_C - e$ for a long time before the rather improbable event at $Q < 2e$ happens. This generates a large quantity of intralevel transitions thus increases $\langle N_e \rangle$ and decreases $\Gamma_\downarrow$.

III. COMPARING NUMERIC, ANALYTIC AND EXPERIMENTAL IV CURVES

In this Section we compare the results with the numerical model[5] based on the phase-correlation theory[8,9]. Earlier, it has been found to agree well with experimental results. Thus we believe that it provides evidence on the applicability of the analytic theory, though in the limit of large R, a simpler quasiclassical theory[6] should work as well. Also a direct comparison to experimental data is performed below.

In Fig. 2(a) we show a simulated set of $I_C - V_C$ curves (open circles), where the base is voltage biased. The base voltage V_B' is varied, while other parameters are $R = 1.5$ MΩ, $C = 0.2$ fF, $R_T = 12$ MΩ, $E_J/E_C = 0.1$, $T = 40$ mK and $\Delta = 1.5$ mV. Corresponding analytic curves (solid lines) are calculated from Eq. (1) using the approximation of Eqs. (6) and (7) when calculating $\langle N_e \rangle$ and $\Gamma_\downarrow$. The agreement is reasonably good. An error is caused by the finite temperature and the superconducting energy gap, when calculating the quasiparticle tunneling rate of the base junction. If the tunneling rates are computed numerically from the phase-correlation theory, the agreement is improved especially at low values of V_B' as denoted by the dashed lines in Fig. 2(a).

The remaining disagreement is related to the temperature dependence of Cooper pair tunneling probabilities. Even if E_C/kT is as high as about 120, incoherent Cooper pair tunneling enhances Cooper pair current at $V_C \approx V_Q = 800$ μV. The lower value of simulated I_C at larger values of V_C was found to be due to the fact that after a Cooper pair tunnels through the JJ, it can immediately tunnel into the opposite direction due to incoherent Cooper pair tunneling. This effectively suppresses $\langle N \rangle$, or equivalently enhances $\Gamma_\uparrow$. The effect is especially visible in Fig. 2(b), where a set of simulations with a current biased base electrode is performed for the same device. The simulated curves (solid circles) fall below the theoretical curves (lines) $I_C = (2\langle N \rangle + 1) I_B$ (see also Section IV), i.e. the current gain is suppressed. However, if we artificially forbid the "Cooper-pair back-tunneling" in the simulation (open squares in Fig. 2(b)) the agreement is clearly improved. This shows that

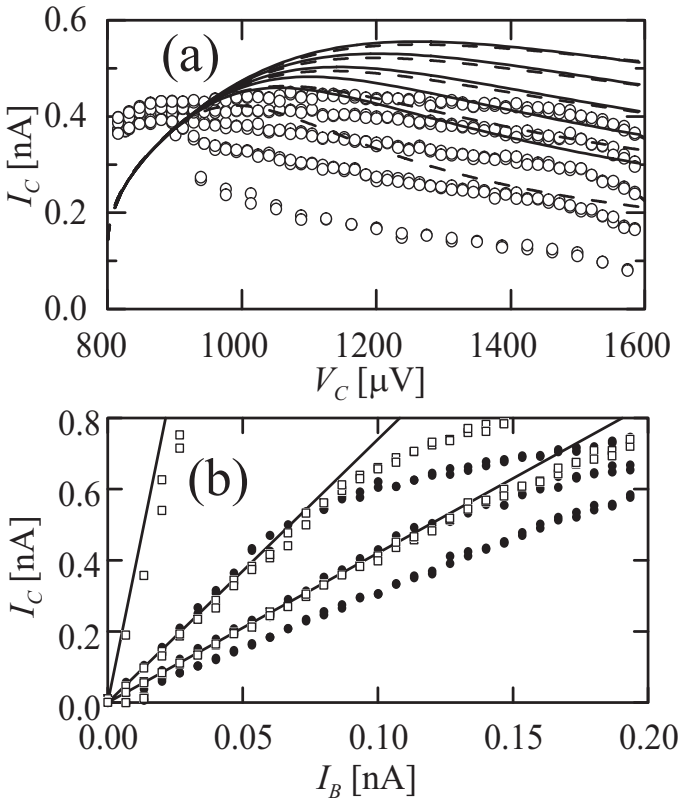

FIG. 2: *(a) Computed I_C-V_C plots with $R = 1.5$ $M\Omega$, $C = 0.2$ fF, $R_T = 12$ $M\Omega$, $E_J/E_C = 0.1$, $T = 40$ mK and $\Delta = 1.5$ mV (open circles). The base voltage has been varied as $V_B' = -2.5e/C$, -3.0e/C, -3.5e/C, -4.0e/C, -4.5e/C from down to top. Solid lines represent analytic values calculated from Eq. (1) together with approximations from Eqs. (6) and (7). Dashed lines are corrected analytic curves, which take base junction nonlinearity at the finite temperature into account. (b) Computed I_C-I_B plots for the same device (solid circles) at V_C =1.25e/C, 1.5e/C, 1.75e/C from up to down. The open squares shows the same simulation without "Cooper pair back-tunneling" and lines show analytic predictions.*

the effect indeed is the main factor suppressing the current gain in the point of operation governed by approximation given in Eqs. (6) and (7). Another mechanism due to spontaneous downwards transitions was discussed in Ref.[4], but it was found to be insignificant in this case.

As the tunnel resistance of the base electrode is decreased and the Josephson coupling increased in simulations and experiments citedel1,[5], the active bias region moves towards higher V_C indicating that the approximation of $\langle N_e \rangle$ and $\Gamma_\downarrow$ given in Eq:s (8) and (9) becomes relevant. In Fig. 3(a) a set of simulations with parameters similar to those considered above, with exceptions $R_T = 375$ kΩ, $E_J/E_C = 0.2$ and $\Delta = 0$ for the base junction (i.e. we have assumed that the base junction is a NIN junction here). At the upper set it is again shown a

set of simulated and analytic $I_C - V_C$ curves showing a reasonable agreement. The agreement is again further improved by forbidding the "Cooper-pair back-tunneling" in the simulation, which is shown in the lower set of curves.

Fig. 3(b) shows the situation for a dataset with decreaced E_C. The topmost set consists of analytic curves, where at $V_C \lesssim 2V_Q \approx 270$ μV approximation of Eqs. (6) and (7) and at $V_C \gtrsim 2V_Q$ approximation of Eqs. (8) and (9) is used. The two lower sets are simulated at $T = 20$ mK and $T = 300$ mK. Although again qualitatively similar, at $T = 20$ mK the main source of disagreement is the enhancement of $\Gamma_\uparrow$ at a finite temperature. At $T = 300$ mK the spike is spread, since at relatively large temperatures (now $E_C/kT \approx 2.6$) also $\Gamma_\downarrow$ is increased due to incoherent Cooper pair tunneling in a same sense as indicated in Ref.[4].

Fig. 4 shows a comparison of experimental (see Refs.[3] and[5] for detalis) and calculated IV curves. The experiment (Fig. 4(a)) was performed with a current biased base electrode, and the characteristic curves have also been solved for constant I_B in Fig. 4(b). The calculated data is discontinuous at $V_C = 2V_Q$, due to the different dynamics of downward transitions

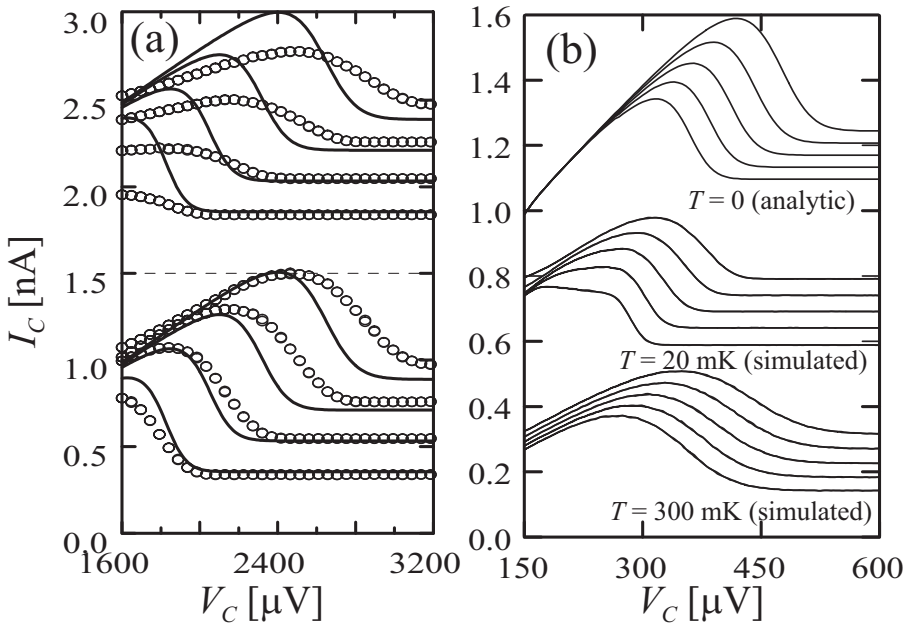

FIG. 3: *(a) Computed $I_C - V_C$ plots for a device otherwise similar to that of Fig. 3 except $R_T = 375$ kΩ, $E_J/E_C = 0.2$ and $\Delta = 0$ (an NIN base junction). The base voltages are $V_B' = -1.0e/C$, -1.5e/C, -2.0e/C, -2.5e/C from down to top (open circles) . Analytic IV curves (solid lines) are calculated from (1) together with approximations from Eqs. (8) and (9). The upper set (lifted by 1.5 nA for clarity) shows the result with the full simulation model, while the lower set shows the result without "Cooper pair back-tunneling". (b) Analytic and computed $I_C - V_C$ plots for a device having $R = 500$ kΩ, $C = 1.2$ fF, $R_T = 250$ kΩ, $\Delta = 200$ μV and $E_J/E_C = 0.3$. The two topmost sets have been lifted by 0.5 nA and 0.8 nA for clarity.*

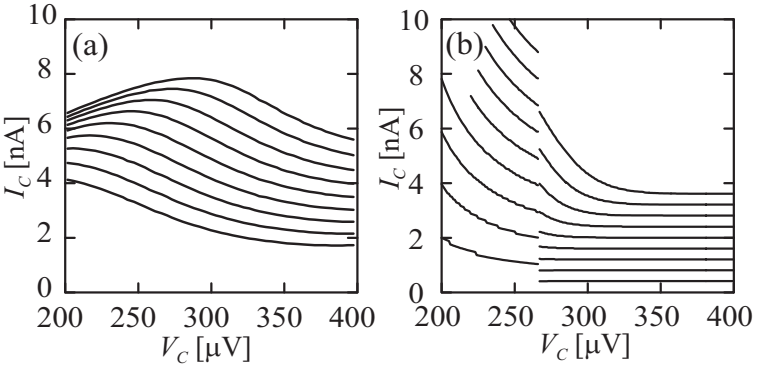

FIG. 4: *Comparison of (a) experimental[5] and (b) calculated data. The parameters are* $R \approx 23$ *kΩ,* $C \approx 1.2$ *fF* $R_T \approx 27.3$ *kΩ and* $E_J/E_C = 0.7$. *The base current is varied from -3.6 nA to -0.4 nA from up to down.*

as explained in Section II. The experimental data is not quite in the validity range of the theory, mainly due to the small value of $R \approx 23$ kΩ. Now $R/R_Q \approx 0.4E_C/k_B$. Thus the experimental data is partially washed out by fluctuations not included in the theory.

IV. LINEARIZED MODEL AND AMPLIFIER PROPERTIES

To analyze the BOT as an amplifier, we next linearize the model around a point of operation. The linearization is formally given as

$$\begin{bmatrix} i_C \\ i_B \end{bmatrix} = \begin{bmatrix} G_{out} & g_m \\ g_x & G_{in} \end{bmatrix} \begin{bmatrix} v_C \\ v_B \end{bmatrix}, \tag{10}$$

where i_C, i_B, v_C, v_B are the small-signal components of collector and base currents and voltages, i.e. small variations around the point of operation. The definitions of small-signal parameters are $G_{in} = (\partial I_B/\partial V_B)_{V_C}$, $g_m = (\partial I_C/\partial V_B)_{V_C}$, $g_x = (\partial I_B/\partial V_C)_{V_B}$ and $G_{out} = (\partial I_C/\partial V_C)_{V_B}$. By using the definitions and Eqs. (1) and (2) one now obtains the small-signal responce as function of device and bias parameters. Note that V_B is kept constant in the last two partial derivations. This is the natural choice, if the circuit shown in Fig. 1(a) is used. However, if the emitter is voltage biased instead of the collector, V_B' should be fixed instead. The choice does not have an effect on the analysis below, since we will be assuming small R_L, whence V_C is constant (see Fig. 1(a). This renders g_x and G_{out} redundant. In other words, we assume here that the BOT is read out with a current amplifier.

For some purposes it is also useful to define the current gain. $\beta = -(\partial I_C/\partial I_B)_{V_C} = -g_m/G_{in}$. By evaluating g_m and G_{in} from the definitions, this is given as

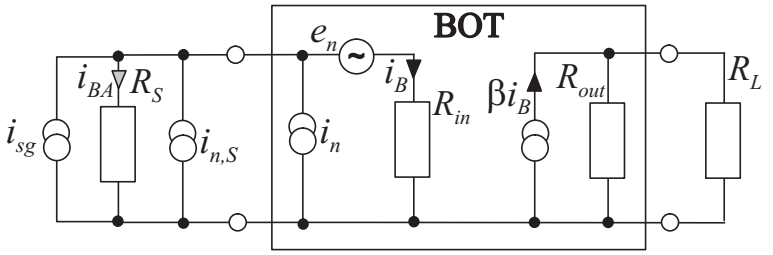

FIG. 5: *A graphical representation of the small signal model of the BOT in the limit of small R_L. The noise added by the BOT is represented with equivalent noise sources i_n end e_n.*

$$\beta = \frac{1}{e}\frac{I_S}{\Gamma_\uparrow \langle N_e \rangle (1-\beta_B)} + 1. \tag{11}$$

Here we have defined

$$\beta_B = -\frac{\Gamma_\downarrow (\Gamma_\uparrow + \Gamma_\downarrow)}{\Gamma_\uparrow \langle N_e \rangle} \left(\frac{\partial \langle N_e \rangle}{\partial V_B} / \frac{\partial \Gamma_\downarrow}{\partial V_B} \right) \tag{12}$$

In the approximation of Eq. (6) β_B is zero, since $\langle N_e \rangle$ is constant. Using Eqs. (8) and (9) instead makes values $\beta_B \approx 1$ possible. We call β_B the "hysteresis parameter" of the BOT.

The noise model for the BOT in the limit of small R_L is shown in Fig. 5. The signal and the noise from the source are described as current generators i_{sg} and $i_{n,S}$ in parallel with the source resistance R_S. The input and output impedances are $R_{in} = 1/G_{in}$ and $R_{out} = 1/G_{out}$. The current generator βi_B at the output accounts for the gain. The noise added by the BOT is represented in a standard fashion (see e.g.[13]) by equivalent voltage and current noise generators (e_n and i_n, respectively) at the input. According to Fig. 5 the output noise of the BOT excluding the contribution of the source ($i_{n,S} = 0$) at the output is

$$S_{i,out}^{1/2} = \frac{1}{R_{in}+R_S}\beta S_{en}^{1/2} + \frac{1/R_{in}}{1/R_{in}+1/R_S}\beta S_{in}^{1/2}, \tag{13}$$

where S_{en} and S_{in} are the spectral density functions corresponding to e_n and i_n, respectively. Note that e_n and i_n and are fully correlated with equal phases in our model. We next choose

$$S_{en}^{1/2} = \frac{2I_S}{-g_m}\sqrt{\frac{\Gamma_\downarrow \Gamma_\uparrow}{(\Gamma_\uparrow + \Gamma_\downarrow)^3}} \tag{14}$$

$$S_{in}^{1/2} = \frac{2I_S}{\beta}\sqrt{\frac{\Gamma_\downarrow \Gamma_\uparrow}{(\Gamma_\uparrow + \Gamma_\downarrow)^3}}. \tag{15}$$

Physically, the noise current at the output of the BOT $S_{i,out}$ is obtained by assuming that the dominant noise mechanism is the two-level switching noise due to collector current switching between values $I_C \approx 0$ and $I_C = I_S$. It can be shown, that with selections of Eqs. (14)

and (15), Eq. (13) produces the output noise in accordance to the theory of a two-level fluctuator(see e.g.[12]). Furthermore, the generators are independent of R_S. However, the backaction noise (i.e. the noise current i_{BA} through or voltage accross R_S) is not correctly predicted by the model.

The noise figure, defined as the ratio of total noise at the output divided by the noise contributed by the BOT, is $F = 1 + S_{i,out}\left[(\beta R_S)^2 (R_{in} + R_S)^2 S_{in,S}\right]^{-1}$, where $S_{in,S} = 4kT_0/R_S$ is the spectal density function of $i_{n,S}$ and T_0 is a reference temperature. One gets optimum impedance R_{opt} and corresponding minimum noise temperature T_n by minimizing F with respect to R_S and using the definiton $F = 1 + T_n/T_0$. It follows

$$R_{opt} = \sqrt{\frac{S_{en}}{S_{in}}} = |R_{in}| \tag{16}$$

$$T_n = \frac{1}{k_B}\sqrt{S_{en}S_{in}} = \frac{|R_{in}|\, S_{in}}{k_B}. \tag{17}$$

The correlation of the two sources shows in Eq. (17) in such a way that the prefactor is $1/k_B$ instead of $1/2k_B$, which is the case for uncorrelated sources. The difference stems from the fact that now the amplitudes of the two sources rather than the powers are summed.

If the approximation of Eqs. (6) and (7) is used to evaluate $\langle N_e \rangle$ and $\Gamma_\downarrow$ (whence also $\beta_B = 0$), one gets for some gain and noise parameters

$$\beta = 2\langle N \rangle + 1 \tag{18}$$

$$S_{in}^{1/2} = \sqrt{-\frac{4e}{R_T}\left(V_B' + \frac{V_Q}{2}\right)\left(1 + \frac{\Gamma_\downarrow}{\Gamma_\uparrow}\right)^{-3}} \tag{19}$$

$$R_{opt} = R_T\left(1 + \Gamma_\downarrow/\Gamma_\uparrow\right)^2 \tag{20}$$

$$T_n = -\frac{4e}{k_B}\left(V_B' + \frac{V_Q}{2}\right)\left(1 + \frac{\Gamma_\downarrow}{\Gamma_\uparrow}\right)^{-1}. \tag{21}$$

In this mode the BOT acts as a simple "charge multiplier", where one electron trigs $\langle N \rangle$ Cooper pairs, thus $\beta = 2\langle N \rangle + 1$. The current noise can also be expressed as $S_{in}^{1/2} = 2\sqrt{eI_B}\left(1 + \Gamma_\downarrow/\Gamma_\uparrow\right)^{-1}$. In the limit of small $\Gamma_\downarrow/\Gamma_\uparrow$ the Bloch oscillation sequences are short compared the total length of the "duty cycle" $1/\Gamma_\downarrow + 1/\Gamma_\uparrow$. Then the equivalent current noise can be understood to be simply the shot noise of the input current. In that case $S_{in}^{1/2} = 2\sqrt{eI_B}$. The prefactor 2 instead of more familiar $\sqrt{2}$ is due to the random length of charge pulses as opposed to the standard shot noise. With large $\Gamma_\downarrow/\Gamma_\uparrow$, or with long Cooper pair sequences, the noise drops. The impedance also increases because single electron tunneling is forbidden during the Bloch oscillations. One should remember, however, that this is strictly true only in the absence of base junction leakage current.

As noted above, the spectral noise density of the backaction noise current (i_{BA} in Fig. 5) in general differs from $S_{i,in}$. It can be shown, that for either $\Gamma_\uparrow/\Gamma_\downarrow \ll 1$ or $\Gamma_\uparrow/\Gamma_\downarrow \gg 1$, it is exactly that of the base current shot noise, i.e. $\sqrt{2eI_B}$. The maximum suppression of i_{BA} occurs at $\Gamma_\uparrow = \Gamma_\downarrow$, where the fano factor is 1/2. The reason for the difference in the equivalent current noise and the backaction noise is, that in the limit of large $\Gamma_\downarrow/\Gamma_\uparrow$ the output current noise becomes fully anticorrelated with i_{BA}. Thus i_{BA} does not directly determine the current resolution, or vice versa. To minimize the backaction noise, the device should be operated at a low base current. The low limit is here is set by spontaneous downwards transitions due to incoherent Cooper pair tunneling[4].

If the approximation from Eqs. (8) and (9) is used instead of Eqs. (6) and (7) for calculating $\Gamma_\downarrow$ and $\langle N_e \rangle$, the dominating terms are in many cases those dependent on β_B especially if $\beta_B \approx 1$. Here we give estimates of some gain and noise parameters. The derivation details and other parameters are shown in Ref.[11]. The hysteresis parameter is

$$\beta_B = 0.02 \left(\frac{R}{R_T}\right)^2 \exp\left(\frac{\pi e^2 R}{16\hbar}\left(\frac{E_J}{E_c}\right)^2\right), \tag{22}$$

while some other quantities of interest are

$$\beta \approx 1.2\,(1-\beta_B)^{-1} \tag{23}$$

$$S_{in}^{1/2} \approx \frac{12e}{\sqrt{RC}}\left(\frac{R_T}{R}\right)\beta^{-1} \tag{24}$$

$$R_{opt} \approx \frac{R}{2}\beta \tag{25}$$

$$T_n \approx \frac{50E_C}{k_B}\left(\frac{R_T}{R}\right)^2\beta^{-1} \tag{26}$$

As $\beta_B \to 1$ the current gain β diverges. However, the trade-off is that the optimum impedance R_{opt} also diverges. The fluctuation at the output does not depend on β_B, so the current noise $S_{in}^{1/2}$ and the noise temperature T_n decrease at the same time.

The physics in this limit can be understood as follows. With very large β_B the main effect of increasing V_B is increasing the number of electrons $\langle N_e \rangle$ needed to cause a downwards transition (see Eq. 12). This leads to decreasing I_B, i.e. negative input conductance. With very small β_B the only effect of increasing V_B is decreasing $\Gamma_\downarrow$. This leads to increasing I_B, i.e. positive input conductance[14]. At intermediate values, i.e. $\beta_B \approx 1$, the input conductance is close to zero. The effect is that a small change in I_B causes a large change in V_B. Consequently $\Gamma_\downarrow$, and thus also I_C change considerably. This leads to the enhancement of the current gain. Since the noise at the output is not enhanced comparably, this leads to decrease of the equivalent current noise and the noise temperature.

A set of simulated $I_C - I_B$ and $I_B - V_B$-plots with a varying Josephson coupling are shown in Figs. 6(a) and (b). The parameters were chosen so that the device is realizable

with Al-tunnel junctions (see the Caption of Fig. 6). Current biased base electrode was assumed. This shows how the current gain and the input impedance increase without limit, as β_B approaches unity. As β_B exceeds unity the curves become hysteretic. If the source resistance R_S is large, hysteresis is a manifestation of negative input conductance. Therefore a sufficient stability criterion for all source resistances is $\beta_B < 1$. For small source resistances the device is stable independently of β_B. The simulated IV curves become hysteretic at $E_J/E_C \approx 0.25$. According to Eq. (22) $E_J/E_C \approx 0.32$ leads to $\beta_B = 1$. It is also worthwhile to compare the stability criterion to experiments. In Ref.[5] the two samples have $\beta_B \approx 0.07$ and $\beta_B \approx 1500$ according to Eq. (22). The first one does not show hysteresis, whereas the second one does.

The current noise and the minimum noise temperature are shown as the function of the optimum resistance in Fig. 6(c) and (d). The computational noise data was obtained by performing a Fast Fourier Transform for the output current and averaging the low-frequency part. This together with computed small signal paramters gives the equivalent noise parameters. A correct form of dependencies, i.e. $S_{in}^{1/2} \propto R_{opt}^{-1}$ and $T_n \propto R_{opt}^{-1}$ are correctly reproduced as compared to Eqs. (24) - (26). Differences in absolute levels can partially be explained through the inaccuracy of the approximation. To some extent the differences can also be understood with reference to excess noise mechanisms discussed in Section V. However, correct forms of dependencies and the order of magnitude are correctly predicted by the theory.

V. SUMMARY AND DISCUSSION

We have developed an analytic of the BOT based on a two-level system. The two-level picture has some limitations. It excludes the effect of additional noise due to the finite band width of Bloch oscillations with finite R or T. It also excludes the additional noise of the leakage current (due to intraband transitions) through the collector resistance. Also the evaluation of transition rates at the limit of low T and large R introduces some error. The agreement with finite temperature data was, however, generally good suggesting that the approach is sufficient to yield quantitative predictions in the limit under discussion. Expressions for amplifier properties such as gain, stability, impedance levels and noise parameters were derived enabling amplifier optimization for a given purpose. It was shown that equivalent current noise spectral densities below 1 fA/$\sqrt{\text{Hz}}$ and noise levels below 0.1 K can be obtained with optimum impedance levels of order a few MΩ. According to finite-temperature simulations the noise temperature of the BOT can also be brought below its physical temperature.

Most other well-known mesoscopic amplifiers, e.g. single-electron transistor (SET)[15] or single Cooper pair transistor (SCPT)[16] are based on controlling a current flow by charging a gate electrode. The BOT is, on the other hand based on controlling the state of a JJ

by means of quasiparticle tunneling events. This makes it insensitive to bakcground charge fluctuations, whence 1/f noise is smaller. This makes it potentially better in low-frequency applications.

BOT was generally found to work in two modes. The first one is a simple quasiparticle - $\langle N \rangle$ Cooper pair converter. In the second mode intraband transitions play a role. These can be utilized to enhance amplification and suppress equivalent noise, but make the device potentially unstable. A stability criterion was derived and quantified by the hysteresis

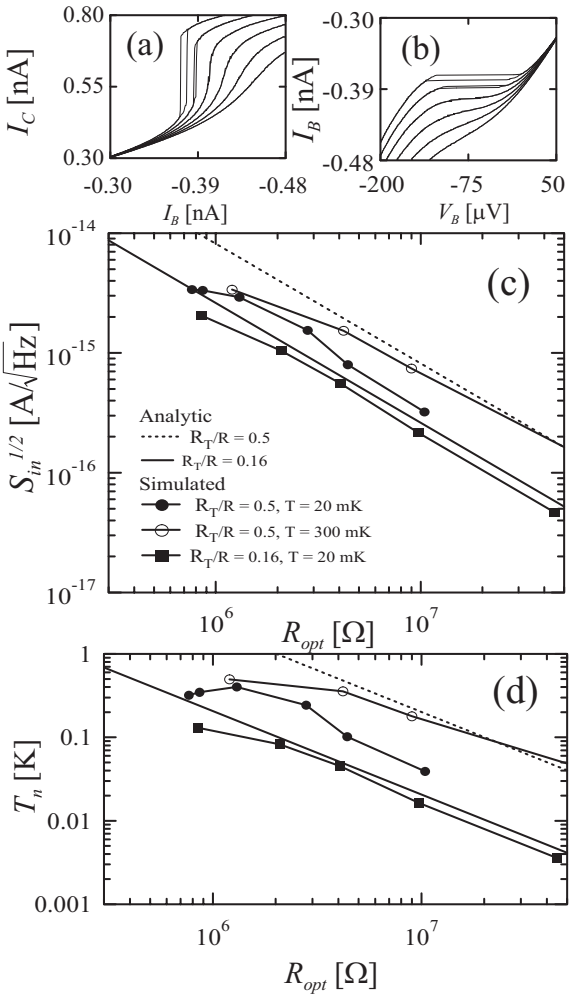

FIG. 6: *(a) and (b) Computed $I_C - V_C$ and $I_B - V_B$ curves ($R = 500$ $k\Omega$, $C = 1.2$ fF, $\Delta = 200$ μV, $T = 20$ mK and $R_T/R = 0.5$) The Josephson coupling E_J/E_C is varied from 0.18 to 0.28 (from left to right in (a) and down to up in (b)). (c) The current noise spectral density S_{in} referred to input and (d) the minimum noise temperature T_n as function of R_{opt}. Within each dataset E_J/E_C (or equivalently β_B) is varied. In (c) and (d) the parameters are as above with the exceptions of varying R_T/R and T as shown in the legend. The bias point in the simulations with $T = 20$ mK is $V_C = 3.5e/C$ and $V_C = 4.5e/C$ for those with $T = 300$ mK.*

parameter β_B.

Authors wish to acknowledge J. Delahaye, P. Hakonen and R. Lindell for their contribution. The work was supported by the Academy of Finland (project 103948).

---

[1] H. Seppä, and J. Hassel, cond-mat/0305263 (2003).

[2] J. Hassel, and H. Seppä. IEEE Trans. Appl. Supercond 11, 260 (2001).

[3] J. Delahaye, J. Hassel, R. Lindell, M. Sillanpää, M. Paalanen, H. Seppä, and P. Hakonen, Science 299, 1045 (2003).

[4] J. Delahaye, J. Hassel, R. Lindell, M. Sillanpää, M. Paalanen, H. Seppä, and P. Hakonen, Phys. E 18, 15 (2003).

[5] J. Hassel, J. Delahaye, H. Seppä, and P. Hakonen, J. Appl. Phys. 95, 8059 (2004).

[6] K.K. Likharev and A.B. Zorin, J. Low Temp. Phys. 59, 348 (1985).

[7] G. Schön, A.D. Zaikin, Phys. Rep. 198, 237 (1990).

[8] M.H. Devoret, D. Esteve, H. Grabert, G.-L. Ingold, H. Pothier and C. Urbina, Phys. Rev. Lett. 64, 1824 (1990).

[9] G.-L. Ingold and Yu. V. Nazarov, in Single Charge Tunneling, edited by H. Grabert and M.H. Devoret (Plenum Press, New York 1992), pp. 21-106.

[10] A.D. Zaikin and D.S. Golubev, Phys. Lett. A 164, 337 (1992).

[11] Derivation details, submitted to Electronic Auxillary Publications Service (EPAPS) (2004).

[12] Sh. Kogan, Electronic Noise and Fluctuations in Solids (Cambridge University Press 1996).

[13] J. Engberg, and T. Larsen, Noise Theory of Linear and Nonlinear Circuits (John Wiley & Sons 1995).

[14] Note that with our sign conventions ($V_B < 0$, $I_B < 0$) electrons are tunneling to the island, i.e. Increasing V_B decreases $\Gamma_\downarrow$, which increases I_B. On the other hand, increasing V_B increases $\langle N_e \rangle$, which decreases I_B.

[15] D. Averin, and K.K Likharev, J. Low Temp. Phys. 62, 345 (1986).

[16] A.B. Zorin, Phys. Rev. Lett. 76, 4408 (1996).

[17] F.N.H. Robinson, Noise and Fluctuations in electronic devices and circuits, Oxford university press (1974).

Theory of the Bloch Oscillating Transistor: Derivation details

Appendix A: Downwards tunneling probabilities

To calculate $\langle N_e \rangle$ and $\Gamma_\downarrow$ we first derive an approximation for the quasiparticle tunneling rate through the base junction as function of charge $\Gamma_{QP1}(Q)$. Neglecting the thermal rounding we get

$$\begin{aligned}\Gamma_{QP1}(t) &= \frac{1}{R_T C}\left(\frac{V_1}{V_Q} - \frac{1}{2}\right) \qquad (1)\\ &= \frac{1}{R_T C}\left(\frac{Q(t)}{e} - \frac{V_C + V_B'}{V_Q} - \frac{1}{2}\right), \text{ if } |V_1| > V_G\end{aligned}$$

$$\Gamma_{QP1}(t) = 0, \text{ if } |V_1| < V_G,$$

where the gap-voltage is V_G, i.e., we neglect the leakage current at the subgap voltages. In the most straightforward experimental realization the base junction is a NIS junction. In this case $V_G = \Delta + V_Q/2$ including the contribution of both superconducting and Coulomb gaps. In principle it is also possible to realize the base junction as a NIN junction, i.e. with suppressed superconductivity on the other electrode. Then the gap voltage is $V_G = V_Q/2$. In general, Γ_{QP1} is a function of time due to the time dependency of charge.

We next separate two different regimes to find analytic approximations for $\langle N_e \rangle$ and $\Gamma_\downarrow$. If $V_C < 2V_Q$ one electron always suffices to return the system to the first level, i.e., $\langle N_e \rangle = 1$. In this case the probability distribution of the first quasiparticle tunneling event after the Zener tunneling is

$$P(t) = \Gamma_{QP1}(t) \lim_{\Delta t \to 0} \prod_{j=1}^{t/\Delta t} \left(1 - \Gamma_{QP1}(j\Delta t)\right), \qquad (2)$$

which is the probability that an electron will tunnel at time t times the probability that it has not tunneled at earlier times. The charge in Eq. (1) before the first quasiparticle event obeys simple RC-relaxation, i.e.

$$Q(t) = CV_C\left(1 + \left(\frac{V_Q}{V_C} - 1\right)e^{-\frac{1}{RC}t}\right), \qquad (3)$$

where we assumed that Zener tunneling occurs at $t = 0$ (or equivalently that $Q(0) = e$). The average rate $\Gamma_\downarrow$ is the inverse of the weight of the distribution given by Eq. (2). Thus

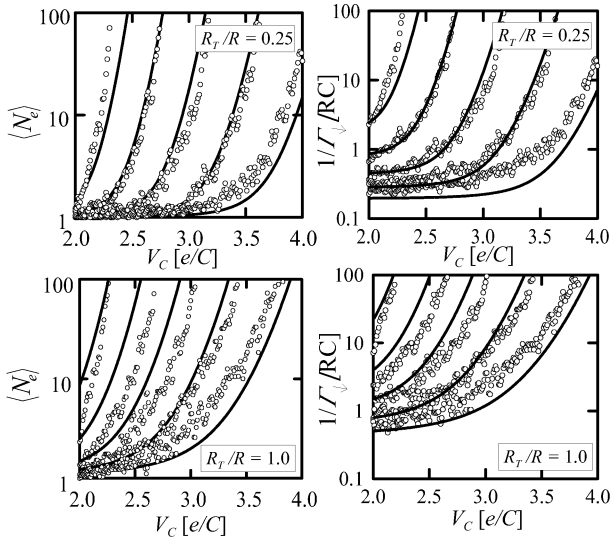

FIG. 1: Computed data for $\langle N_e \rangle$ and $\Gamma_\downarrow$ obtained by solving Eqs. (1) and (3) numerically (open circles). In each frame the base voltage is varied as $V_B' = -1.0e/C$, -1.5e/C, -2.0e/C, -2.5e/C, -3.0e/C from left to right. The lines correspond the fits, i.e. Eqs. (7) and (8).

$$\langle N_e \rangle = 1 \qquad (4)$$

$$\Gamma_\downarrow = \frac{1}{\int_0^\infty tP(t)\,dt}. \qquad (5)$$

In general, the downwards rate has to be evaluated numerically from (5). However, if we further assume that the transient in Eq. (3) is short, Eq. (2) reduces to a simple exponential distribution. This is equivalent to assuming that $Q(t) \approx CV_C$ at all times, and thus Eq. (1) also becomes time independent. Now simply $\Gamma_\downarrow = \Gamma_{QP1}$, and it follows

$$\Gamma_\downarrow = -\frac{1}{CR_T}\left(\frac{V_B'}{V_Q} + \frac{1}{2}\right). \qquad (6)$$

If $V_C > 2V_Q$ it is possible that the first electron tunneling through the base junction does not cause a transition to the first level, but some of the single quasiparticle events lead to intralevel transitions instead. To solve $\langle N_e \rangle$ and $\Gamma_\downarrow$ analytically from Eqs. (1) and (3) in this

case is unfortunately impossible. To find a sufficient approximation for our purposes, we have solved the problem numerically and searched for a proper fitting function. For simplicity we have assumed an NIN junction at the base electrode, i.e. $V_G = V_Q/2$ in Eq. (1). Some fits are shown in Fig. 1 and the result is

$$\langle N_e \rangle = 0.04 \left(\frac{R_T}{R}\right)^2 \times \exp\left(0.3 \exp\left(1.8\frac{V_C}{V_Q} + 0.27\frac{V_C V_B'}{V_Q^2} - 0.2\frac{V_B'}{V_Q}\right)\right) + 1 \tag{7}$$

$$\Gamma_\downarrow^{-1} = -\left(\frac{\partial I_C}{\partial I_B}\right)_{V_C} = 1.2e\frac{R+R_T}{V_B'}\left(1 - \langle N_e \rangle\right) + RC\left(2.5\frac{R_T}{R} + 1.1\right)\left(\frac{V_Q}{V_B'}\right)^2. \tag{8}$$

Appendix B: Hysteresis and noise parameters

In this Appendix we show the derivation of hysteresis and noise parameters in the limit $\beta_B \approx 1$. The starting points are the definitions

$$\beta_B = -\frac{\Gamma_\downarrow\left(\Gamma_\uparrow + \Gamma_\downarrow\right)}{\Gamma_\uparrow \langle N_e \rangle}\left(\frac{\partial \langle N_e \rangle}{\partial V_B} / \frac{\partial \Gamma_\downarrow}{\partial V_B}\right) \tag{9}$$

$$g_m = I_S \frac{\Gamma_\uparrow}{\left(\Gamma_\uparrow + \Gamma_\downarrow\right)^2}\frac{\partial \Gamma_\downarrow}{\partial V_B} + G_{in} \tag{10}$$

$$\beta = \frac{1}{e}\frac{I_S}{\Gamma_\uparrow \langle N_e \rangle \left(1 - \beta_B\right)} + 1 \tag{11}$$

$$S_{en}^{1/2} = \frac{2I_S}{-g_m}\sqrt{\frac{\Gamma_\downarrow \Gamma_\uparrow}{\left(\Gamma_\uparrow + \Gamma_\downarrow\right)^3}} \tag{12}$$

$$S_{in}^{1/2} = \frac{2I_S}{\beta}\sqrt{\frac{\Gamma_\downarrow \Gamma_\uparrow}{\left(\Gamma_\uparrow + \Gamma_\downarrow\right)^3}}, \tag{13}$$

$$R_{opt} = \sqrt{\frac{S_{en}}{S_{in}}} \tag{14}$$

$$T_n = \frac{1}{k_B}\sqrt{S_{en} S_{in}}. \tag{15}$$

The main task is to get sufficient estimates for I_S, $\Gamma_\downarrow$, $\Gamma_\uparrow$, $\langle N_e \rangle$, $\partial \langle N_e \rangle / \partial V_B$ and $\partial \Gamma_\downarrow / \partial V_B$ near an interesting point of operation. We note that for the approximation from Eqs. (7) and (8) used for $\langle N_e \rangle$ and $\Gamma_\downarrow$ to apply the collector voltage must satisfy $V_C \gtrsim 2V_Q$. For simplicity we assume that $V_C = 2V_Q$. When the system is at the second level, the voltage across the JJ is $V_2 \gtrsim V_Q$ and the collector current consists of the leakage current only, i.e. $I_C = -I_B$. Assuming that $V_2 = V_Q$ and that the base junction roughly acts as a linear resistor we get by analyzing the circuit of Fig. 1(a) and noting that by definition $V_B = V_B' + V_C$ the result $V_B' = -V_Q\left(1 + R_T/R\right)$, i.e. we have found estimates for the bias parameters. Using these and Eqs. (**??**), (**??**) and (7) we can readily write:

$$I_S \approx \frac{2e}{RC\ln 3} \tag{16}$$

$$\Gamma_\uparrow \approx \frac{1}{RC\ln 3}\exp\left(-\frac{\pi RC}{8\hbar}\frac{E_J^2}{E_c^2}E_C\right) \tag{17}$$

$$\langle N_e \rangle \approx 100\left(\frac{R_T}{R}\right)^2. \tag{18}$$

In the last Equation we have also utilized the assumption $R_T \lesssim R$.

To find an estimate for $\Gamma_\downarrow$ we can use physical intuition and insight learned from simulations. Since the operation is based on switching between the two states, the system spends roughly as much time in both states. Thus

$$\Gamma_\downarrow \approx \Gamma_\uparrow. \tag{19}$$

Although some error may be introduced by doing this, it is not too severe, since most properties depend more strongly on the derivative $\partial \Gamma_\downarrow / \partial V_B$, which will be calculated separately.

The derivative $\partial \langle N_e \rangle / \partial V_B$ is obtained by direct differentiation of Eq. (7), inserting the bias parameters V_B, V_C from above and applying the approximation $R_T \lesssim R$:

$$\frac{\partial \langle N_e \rangle}{\partial V_B} \approx \frac{270}{V_Q}\left(\frac{R_T}{R}\right)^2. \tag{20}$$

To obtain $\partial \Gamma_\downarrow / \partial V_B$ we first note that $\Gamma_\downarrow$ depends on V_B both through the explicit dependence in Eq. (8) and through $\langle N_e \rangle$. Since $\langle N_e \rangle$ depends very strongly on V_B we will approximate $\partial \Gamma_\downarrow / \partial V_B \approx \left(\partial \Gamma_\downarrow / \partial \langle N_e \rangle\right)\left(\partial \langle N_e \rangle / \partial V_B\right)$. By differentiation of Eq. (8), application of the bias parameters V_B and V_C from above and using Eq. (20) we get

$$\frac{\partial \Gamma_\downarrow}{\partial V_B} \approx 1.2e\Gamma_\downarrow^2 \frac{R+R_T}{V_B'}\frac{\partial \langle N_e \rangle}{\partial V_B}.$$

By using Eqs. (19) and (17) we now get

$$\frac{\partial \Gamma_\downarrow}{\partial V_B} \approx -\frac{290}{V_Q}\frac{1}{RC}\left(\frac{R_T}{R}\right)^2\left(\exp\left(-\frac{\pi RC}{8\hbar}\frac{E_J^2}{E_c^2}E_C\right)\right)^2. \tag{21}$$

By inserting Eqs. (16)-(21) into Eq. (9) we get the estimate

$$\beta_B = 0.02\left(\frac{R}{R_T}\right)^2 \exp\left(\frac{\pi e^2 R}{16\hbar}\left(\frac{E_J}{E_c}\right)^2\right), \tag{22}$$

The exponent (or $\langle N \rangle$) in Eqs. (17) and (21) affects on the device parameters mainly through β_B. For other purposes we may assume it roughly constant and solve it by setting $\beta_B = 1$ in Eq. (22), whence Eqs. (17) and (21) are simplified into

$$\Gamma_\uparrow \approx \frac{0.015}{RC}\left(\frac{R}{R_T}\right)^2 \tag{23}$$

$$\frac{\partial \Gamma_\downarrow}{\partial V_B} \approx -\frac{0.08}{V_Q}\frac{1}{RC}\left(\frac{R}{R_T}\right)^2. \tag{24}$$

The results

$$\beta \approx 1.2\,(1-\beta_B)^{-1} \tag{25}$$

$$g_m \approx -\frac{2}{R} \tag{26}$$

$$S_{in}^{1/2} \approx \frac{12e}{\sqrt{RC}}\left(\frac{R_T}{R}\right)\beta^{-1} \tag{27}$$

$$S_{en}^{1/2} \approx \frac{2e}{\sqrt{RC}}R_T \tag{28}$$

$$R_{opt} \approx \frac{R}{2}\beta \tag{29}$$

$$T_n \approx \frac{50E_C}{k_B}\left(\frac{R_T}{R}\right)^2\beta^{-1} \tag{30}$$

now follow by inserting Eqs. (16), (18), (19), (20), (23) and (24) into the definitions of interesting quantities, i.e. Eqs. (10), (11), (12), (13), (14) and (15).

Published by

Series title, number and report code of publication

VTT Publications 551
VTT–PUBS–551

Author(s)
Hassel, Juha

Title

Josephson junctions in charge and phase picture
Theory and applications

Abstract

Properties of weak links between two superconductors, or Josephson junctions, make them interesting for fundamental physics research. Since their discovery over four decades ago, they have provided a unique way to study the behavior of the superconducting quantum phase. More recently, ultra small, or mesoscopic, Josephson junctions with substantial single Cooper pair charging energy have gained interest due to their behavior as macroscopic quantum objects.

In addition to the theoretical interest, Josephson junctions can be used as active elements in circuit applications. Particularly, in this Thesis we study two different devices. We develop the required theoretical treatments, derive device properties, and compare the results with experimental data.

The first application is a Josephson voltage standard based on externally damped Superconductor - Insulator - Superconductor junctions. It consists of an array of large Josephson junctions connected in series and irradiated with a 70 GHz microwave signal. Phase locking the Josephson dynamics into the signal leads to the quantization of the voltage. This is utilized in metrology. We introduce a new circuit solution based on frequency dependent damping of the junctions. Optimization and some designs for practical arrays are presented. The purpose is to find such a design that the array is fast, has low power consumption and is as stable as possible. Arrays able to generate DC voltages of order 1 volt with metrological accuracy are demonstrated experimentally and their applicability in AC voltage calibrations is analyzed.

The second application is the Bloch Oscillating Transistor (BOT). The BOT is based on controlling the Cooper pair current in an ultra small Josephson junction by means of quasiparticles tunneling through a normal junction. As part of the thesis work, the principle of operation is first demonstrated computationally. The model is then refined to yield quantitative predictions of the characteristics. Finally, an analytic theory for the device is developed and the properties as an amplifier are derived.

Keywords

Josephson junctions, quantum metrology, mesoscopic tunnel junctions

Activity unit

VTT Information Technology, Tietotie 3, P.O.Box 1207, FIN–02044 VTT, Finland

ISBN			Project number
951–38–6418–9 (soft back ed.) 951–38–6419–7 (URL:http://www.vtt.fi/inf/pdf/)			
Date October 2004	Language English	Pages 38 p. + app. 40 p.	Price B
Name of project		Commissioned by	
Series title and ISSN VTT Publications 1235–0621 (soft back ed.) 1455–0849 (URL: http://www.vtt.fi/inf/pdf/)		Sold by VTT Information Service P.O.Box 2000, FIN–02044 VTT, Finland Phone internat. +358 9 456 4404 Fax +358 9 456 4374	

VTT PUBLICATIONS 551 Josephson junctions in charge and phase picture. Theory and applications Juha Hassel

Properties of weak links between two superconductors, or Josephson junctions, make them interesting for fundamental physics research. Since their discovery over four decades ago, they have provided a unique way to study the behavior of the superconducting quantum phase. More recently, ultra small, or mesoscopic, Josephson junctions with substantial single Cooper pair charging energy have gained interest due to their behavior as macroscopic quantum objects. In addition to the theoretical interest, Josephson junctions can be used as active elements in circuit applications. In this Thesis we study two different devices. The first application is a Josephson voltage standard based on externally damped Superconductor – Insulator – Superconductor junctions. Arrays able to generate DC voltages of order 1 volt with metrological accuracy are demonstrated experimentally and their applicability in AC voltage calibrations is analyzed. The second application is the Bloch oscillating transistor (BOT). The BOT is based on controlling the Cooper pair current in an ultra small Josephson junction by means of quasiparticles tunneling through a normal junction. As part of the thesis work, the principle of operation is first demonstrated computationally. The model is then refined to yield quantitative predictions of the characteristics. Finally, an analytic theory for the device is developed and the properties as an amplifier are derived.

Tätä julkaisua myy
VTT TIETOPALVELU
PL 2000
02044 VTT
Puh. (09) 456 4404
Faksi (09) 456 4374

Denna publikation säljs av
VTT INFORMATIONSTJÄNST
PB 2000
02044 VTT
Tel. (09) 456 4404
Fax (09) 456 4374

This publication is available from
VTT INFORMATION SERVICE
P.O.Box 2000
FIN–02044 VTT, Finland
Phone internat. +358 9 456 4404
Fax +358 9 456 4374

ISBN 951–38–6418–9 (soft back ed.)
ISSN 1235–0621 (soft back ed.)

ISBN 951–38–6419–7 (URL: http://www.vtt.fi/inf/pdf/)
ISSN 1455–0849 (URL: http://www.vtt.fi/inf/pdf/)